

AMERICAN UNIVERSITY OF BEIRUT

DEGRADATION OF SULFAMETHOXAZOLE BY PERSULFATE
ASSISTED MICROMETRIC Fe⁰ IN AQUEOUS SOLUTION:
ASSESSMENT OF BIMETALLIC AND TRIMETALLIC IRON-
BASED SYSTEMS

by
GHADA SAMIR AYOUB

A thesis
submitted in partial fulfillment of the requirements
for the degree of Master of Science
to the Department of Chemistry
of the Faculty of Arts and Sciences
at the American University of Beirut

Beirut, Lebanon
May 2014

AMERICAN UNIVERSITY OF BEIRUT

DEGRADATION OF SULFAMETHOXAZOLE BY PERSULFATE
ASSISTED MICROMETRIC Fe^0 IN AQUEOUS SOLUTION:
ASSESSMENT OF BIMETALLIC AND TRIMETALLIC IRON-
BASED SYSTEMS

by
GHADA SAMIR AYOUB

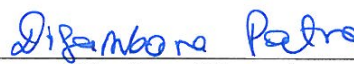
Approved by:

Dr. Antoine Ghauch, Associate Professor
Department of Chemistry




Advisor

Dr. Digambara Patra, Associate Professor
Department of Chemistry



Member of Committee

Dr. Mahmoud Al Hindi, Assistant Professor
Department of Mechanical Engineering



Member of Committee

Date of thesis defense: April 29, 2014

ACKNOWLEDGMENTS

Accomplishing the Masters' program at AUB is certainly a serious and demanding endeavor, which I wouldn't have completed without my advisor Prof. Antoine Ghauch. I'd like to express my deep appreciation and gratitude for his deep patience, guidance, understanding, and most importantly for his friendship during my graduate studies at AUB. His mentorship was paramount in providing a well-rounded experience consistent my long-term career goals. He encouraged me to not only grow as an experimentalist and a chemist but also as an instructor and an independent thinker. I'm also grateful to my advisor for giving me the opportunity to spend two and half months at the University of California Berkeley within the framework of PEER grant.

Sincere appreciation is also expressed to the committee members Prof. Digambara Patra and Prof. Mahmoud Al-Hindi for their or their input, valuable discussions, suggestions, and accessibility.

I would like to thank my professors who made my learning experience, throughout the past two years, unique, Dr Ghoul, Dr Bouhadir, Dr Ghaddar, Dr. Patra, and Dr. Karam. I am also grateful to the personnel in the Central Research Science Labortory (KAS CRSL) especially the engineer Joan Youness for his endless help. I'd like to thank Mr. Issam Azar the administrative assistant for his help and care.

Special thanks to my colleagues in research group Al-Mouthanna Tuqan and particularly Sahar Naim for her help, support, and motivation every time I'm depressed. I'm certainly lucky to meet the best colleagues in the chemistry department whose deep love, help, and encouragement made me stronger and more successful as easily as I did Rasha, Tharallah, Abdallah, Remi, Malak, Fatima, Ali, Nancy, Lubna, Lamis, Tarek, May, Ghinwa, and all the new graduates.

Finally, and most importantly, I would like to thank my Mom whose support, encouragement, quiet patience and unwavering love were undeniably the bedrock upon which the past few years of my life have been built. Her tolerance of my occasional vulgar moods is a testament in itself of her unyielding devotion and love. I'm grateful for my brother, sister, and for their faith in me and allowing me to be as ambitious as I wanted. It was under their watchful eye that I gained so much drive and an ability to tackle challenges head on.

AN ABSTRACT OF THE THESIS OF

Ghada Samir Ayoub for Master of Science
Major: Chemistry

Title: Degradation of sulfamethoxazole by persulfate assisted micrometric Fe⁰ in aqueous solution: Assessment of bimetallic and trimetallic iron-based systems.

Persulfate (PS) chemical activation using micrometric Fe⁰ particles (MIPs) was tested on sulfamethoxazole (SMX) solution (39.5 μM). MIPs load (0.89-17.85 mM), PS content (0.4-1.0 mM), pH (5.50-8.30) and alkalinity (bicarbonate) were the main parameters investigated for the improvement of SMX degradation. Optimum conditions for the enhancement of the reaction stoichiometric efficiency (RSE = 5.2%) were developed. The HPLC-MS supported results confirmed that in the absence of PS, SMX was converted into its reduced form through cleavage of the isoxazole N-O bond. The resulting unstable radical anion yielded a stable end-product identified as b-aminoenone after acceptance of electrons originated from the MIPs surface oxide. However, in the presence of PS, results did not show the presence of b-aminoenone. This suggested that PS activation into sulfate radicals (SRs) was responsible for the rapid degradation of SMX and its transformation product as well. Different water matrices were evaluated in order to understand the role that can play dissolved ions on the reaction degradation rate. Successive experiments (n = 3) of 1 h each conducted on remaining Fe⁰ showed complete SMX degradation. The mineralization extent of SMX under the experimental conditions reached 37% making from Fe⁰/PS system an excellent source of SRs able to sustain oxidation reactions in aqueous media of slightly acidic pH. This work was extended to investigate the potential of different iron-based systems to activate persulfate (PS) into sulfate radicals (SRs) through catalytic electron transfer reactions. SRs in their turn are then used to degrade sulfamethoxazole (SMX) in water. PS activators like Fe²⁺, Fe⁰, AgFe and CoFe (bimetallics), AgCoFe and CoAgFe (trimetallics) were tested on SMX solution (39.5 μM) spiked with PS (1.0 mM). Results on SMX degradation showed better kinetics and efficiency in case of non-plated iron particles used compared to bimetallic and trimetallic systems as well as Fe²⁺ at early stage of the reaction. Direct and sequential addition of Fe²⁺ resulted in better reaction stoichiometric efficiency (RSE); however, did not yield full SMX degradation in contrast to metallic particles. Bimetallic and trimetallic systems showed higher RSE than Fe⁰ initially due to less PS consumption while maintaining moderate SMX degradation rate. Smooth corrosion is responsible for the progressive release of iron corrosion products for SRs production. However, in case of improved corrosion, generated SRs are quenched by an excess of iron-based activators which

negatively affected the RSE. This work demonstrated the potential of iron-based systems to sustain PS longer in solution without the production of heavy sludge or formation of transformation products that can burden the treatment process.

CONTENTS

ACKNOWLEDGMENTS.....	v
ABSTRACT.....	vi
LIST OF ILLUSTRATIONS.....	xi
LIST OF TABLES.....	xv
LIST OF SCHEMES.....	xvi
LIST OF ABBREVIATIONS.....	xvii
Chapter	
I. INTRODUCTION.....	1
A. Literature review.....	3
1. Pharmaceutical Compounds.....	3
2. Sources.....	6
3. Fate of the Pharmaceuticals in the Environment.....	6
4. Characteristics of Selected Compound “SMX”.....	8
5. Early Treatment Methods-Fe ⁰ and Amended Fe ⁰	9
6. Treatment Methods – Advanced Oxidation Processes (AOP’s).....	11
7. Chemistry of Persulfate.....	13
8. Experiences with Different Activation Aids.....	15
a. Heat Activated Persulfate.....	15
b. Chemical Activation of PS via Fe ⁰ and Modified Fe ⁰	17
B. Objectives.....	22
II. MATERIALS AND METHODS.....	24

A. Chemicals.....	24
B. Metallic Particle Preparation.....	25
C. Experimental Setup.....	26
D. Chemical Analysis.....	30
III. DEGRADATION OF SULFAMETHOXAZOLE BY PERSULFATE ASSISTED MICROMETRIC Fe^0 IN AQUEOUS SOLUTION.....	32
A. Results and Discussion.....	32
1. Characterization of Fe^0 Particles in Different Systems.....	32
2. Direct vs Sequential Addition of Fe^{2+} and Fe^0	35
3. Effect of Iron Surface and Phosphate Buffer on the Degradation of SMX.....	39
4. Iron Load Effect on SMX Degradation.....	41
5. Effect of PS Content on SMX Degradation.....	45
6. Mineralization of SMX in $nwFe^0$ /SMX/PS System.....	50
B. Water Matrix Effect on SMX Degradation in Successive Degradation Cycles.....	50
1. Case 1 (Tap Water).....	51
2. Case 2 (DI Water).....	53
3. Case 3 (Underground Water, UGW).....	56
C. Effect of Iron Ageing on SMX Degradation and its Transformation Product.....	58
1. SMX Case in $nwFe$ /SMX/PS System.....	58
2. SMX Transformation Product Case in $nwFe^0$ /SMX/PS System.....	61
D. Identification of Transformation Product, Structure Elucidation and Proposed Reaction Pathway.....	62
IV. ASSESSMENT OF BIMETALLIC AND TRIMETALLIC IRON-BASED SYSTEMS FOR PERSULFATE ACTIVATION: APPLICATION TO SULFAMETHOXAZOLE DEGRADATION.....	72
A. Results and Discussion.....	72

1. Characterization of Fe ⁰ Plated Particles in Different Systems.....	72
a. Bimetallic Systems (CoFe and AgFe).....	72
b. Trimetallic Systems (AgCoFe and CoAgFe).....	76
B. Effect of Plated Systems on SMX Degradation.....	80
1. Bimetallic Systems.....	80
a. CoFe and AgFe vs Fe ⁰	80
2. Trimetallic Systems.....	88
a. AgCoFe and CoAgFe vs Fe ⁰	88
C. Effect of Agitation on SMX Degradation: Non Disturbed Systems.....	91
1. Fe ⁰ vs CoFe and AgFe.....	91
2. Fe ⁰ vs AgCoFe and CoAgFe.....	94
D. Transformation Products.....	96
V. CONCLUSION.....	99

BIBLIOGRAPHY.....	102
-------------------	-----

Appendix

I. RESEARCH CONTRIBUTIONS.....	112
II. REFERRED PUBLICATIONS (I) DEGRADATION OF SULFAMETHOXAZOLE BY PERSULFATE ASSISTED MICROMETRIC Fe ⁰ IN AQUEOUS SOLUTION.....	113
III. REFERRED PUBLICATIONS (II) SUBMICROMETRIC IRON PARTICLES FOR THE REMOVAL OF PHARMACEUTICALS IN WATER: APPLICATION TO B- LACTAM ANTIBIOTICS.....	114

ILLUSTRATIONS

Figure	Page
<p>Fig. 1. SMX (a) and PS (b) degradation under the influence of direct and sequential Fe²⁺ spiking compared to Fe⁰ powder additive in PS/H₂O systems. Experimental conditions: [SMX]₀ = 39.5 μM, [PS]₀ = 1.0 mM, [Fe²⁺] = [Fe⁰] = 2.23 mM; m (Fe⁰) = 2.5 mg, Error bars represent uncertainty at 95% confidence level.</p>	36
<p>Fig. 2. Effect of direct vs sequential addition of Fe²⁺ compared to Fe⁰ in PS/SMX solution on average % RSE over 30 min of reaction. Experimental conditions: [SMX]₀ = 39.5 μM, [Fe²⁺] = [Fe⁰] = 2.23 mM, m (Fe⁰) = 2.5 mg, pHi = 5.63.....</p>	38
<p>Fig. 3. Influence of MIPs surface and PB on the oxidation of SMX by PS. (a) MIPs used as received (nwFe for non-washed Fe), (b) acid-washed MIPs (wFe for acid-washed Fe). Experimental conditions: [Fe⁰] = 17.85 mM, [PS]₀ = 1.0 mM, [SMX]₀ = 39.5 μM, [PB] = 1 mM. Solid lines are only used to connect data. Error bars represent uncertainties at a 95% confidence interval.....</p>	40
<p>Fig. 4. (a)Influence of iron load on the oxidation yield of SMX in deionized water. (b) PS consumption at 10, 20 and 30 min of the reaction. (c) Concentration of total dissolved iron species into the reactor at 10, 20 and 30 min of the reaction. Experimental conditions: [Fe⁰] = 0.89-17.85 mM, [PS]₀ = 1.0 mM and [SMX]₀ = 39.5 μM. Solid lines are only used to connect data. Error bars represent uncertainties at a 95% confidence interval.....</p>	43
<p>Fig. 5. (a) Influence of PS additives on the oxidative treatment of SMX in deionized water. (b) Time course of PS during the reaction. (c) The RSE relative to each PS concentration in Fig. 5a calculated at different reaction times (5-60 min). (d) Concentration of iron species (equivalent Fe²⁺) at after 10, 20 and 30 min of the reaction. Experimental conditions: [nwFe⁰] = 2.23 mM, [PS]₀ = 0.40-1.00 mM, [SMX]₀ = 39.5 μM. Solid lines are used to connect data. Error bars represent uncertainties at 95% confidence interval.....</p>	47
<p>Fig. 6. (a)SMX degradation and (b) PS remaining after repetitive oxidation cycles in tap water matrix. Experimental conditions: [nwFe⁰] = 2.23 mM, [PS]₀ = 1.0 mM, [SMX]₀ = 39.5 μM. Solid lines are not fitting functions, they are only used to connect data. Error bars represent uncertainties at 95% confidence interval.....</p>	51
<p>Fig. 7. (a) SMX degradation and (b) PS remaining after repetitive oxidation cycles in DI water matrix. Experimental conditions: [nwFe⁰] = 2.23 mM, [PS]₀ = 1.0 mM, [SMX]₀ = 39.5 μM. Solid lines are not fitting functions, they are only used to connect data. Error bars represent uncertainties at 95% confidence interval.....</p>	54

- Fig. 8.** SMX degradation after repetitive oxidation cycles in an UGW matrix. Experimental conditions: $[\text{nwFe}^0] = 2.23 \text{ mM}$, $[\text{PS}]_0 = 1.0 \text{ mM}$, $[\text{SMX}]_0 = 39.5 \text{ }\mu\text{M}$. Solid lines are not fitting functions, they are only used to connect data. Error bars represent uncertainties at 95% confidence interval. 56
- Fig. 9.** Time course of SMX in Fe^0 and Fe^0/PS systems. Zone A is a PS free system. Zone B corresponds to PS-spiked systems. System **1** is made of the resulting solution at 120 min of reaction time to which 170 μL of PS is added with $[\text{PS}]_0 = 1 \text{ mM}$. System **2** is similar however after magnetic filtration of the resulting solution at 120 min of reaction time and addition of 1.6 mg of nwFe^0 so as to obtain $[\text{Fe}^0] = 2.23 \text{ mM}$. System **3** is similar to system **2** however without any Fe^0 addition. 59
- Fig. 10.** Time course of SMX and its transformation product during treatment in $\text{Fe}^0/\text{SMX}/\text{PS}$ system. Zone A corresponds to wFe^0/SMX system. Zone B corresponds to $\text{uFe}^0/\text{SMX}/\text{PS}$ (u: used) system in which PS was added to the resulting solution of Zone A; Zone C corresponds to SMX by-product/PS system in which the resulting solution of Zone B was magnetically filtered, spiked with PS and supplied or not with nwFe^0 . Experimental conditions: Zone A $[\text{nwFe}^0] = 5 \text{ g L}^{-1}$, $[\text{SMX}]_0 = 39.5 \text{ }\mu\text{M}$; Zone B: $[\text{PS}]_0 = 1.0 \text{ mM}$; Zone C: $[\text{nwFe}^0] = 0.1 \text{ g L}^{-1}$ for the upper curve, $[\text{nwFe}^0] = 0 \text{ g L}^{-1}$ for the lower curve, $[\text{PS}]_0 = 1.0 \text{ mM}$ 62
- Fig. 11.** LC-MS total ion chromatograms of SMX solution (20 mL) treated with nwFe^0 and PS. (a) nwFe^0/SMX system, $[\text{Fe}^0] = 89.2 \text{ mM}$, $[\text{SMX}]_0 = 39.5 \text{ }\mu\text{M}$. The inset is the MS spectrum of SMX obtained in (+) ESI. (b) $\text{uFe}^0/\text{SMX}/\text{PS}$ system: the resulting solution was spiked with 170 μL PS at 120 min. The inset is the MS spectrum of SMX transformation product obtained in (+)ESI and eluted at 5.8 min. (c) $\text{nwFe}^0/\text{SMX}/\text{PS}$ system: the resulting solution (17 mL) was magnetically filtered, spiked with 128 μL PS and supplied with 1.6 mg of nwFe^0 (2.23 mM). 65
- Fig. 12.** (a) MS, (b) MS/MS and (c) MS^3 spectra of SMX transformation product (positive ionization). 67
- Fig. 13.** (a) MS, (b) MS/MS and (c) MS^3 spectra of SMX transformation product (negative ionization). 68
- Fig. 14.** UV/Vis absorbance spectra of SMX and its transformation product showing bathochromic shift from 262 nm to 270 nm. 69
- Fig. 15.** Secondary electron images of (a) CoFe and (b) AgFe in addition to their corresponding X-ray spectra (c) and (d) collected within the circled area. Iron particles are plated with 1.3 μmole of Ag and 3.60 μmoles of Co. 73
- Fig. 16.** SEM images of CoFe (a) and AgFe (d) bimetallic systems as presented in Fig. 15. The corresponding X-ray maps of (b) Co ($\text{K}\alpha_1$), (c) Fe ($\text{K}\alpha_1$) and (e) Ag ($\text{K}\alpha_1$) obtained from the two bimetallic systems CoFe and AgFe over the entire shown

surface area (a, d). Areas of relatively high Fe concentrations are shown as bright regions in (c) and (f). In (b) less bright spots indicate areas of Co deposition whereas in (e) brighter spots indicate deposition of Ag at the surface of iron particles..... 75

Fig. 17. Secondary electron images of (a) AgCoFe and (b) CoAgFe in addition to their corresponding X-ray spectra (c) and (d) collected within the squared area. Iron particles are plated with 1.3 μ mole of Ag and 3.60 μ moles of Co..... 76

Fig. 18. SEM images of AgCoFe (a) and CoAgFe (d) trimetallic systems as presented in Fig. 17. The corresponding X-ray maps of (b) Ag ($K\alpha_1$), (c) Co ($K\alpha_1$) and (d) Fe ($K\alpha_1$) obtained from the two trimetallic systems AgCoFe and CoAgFe over the entire shown surface area (a, e). Areas of relatively high Fe concentrations are shown as bright regions in (d) and (h). In (c), (f) and (g) less bright spots indicate areas of Co and primary Ag deposition whereas in (b) brighter spots indicate deposition of Ag at the surface of iron particles as second deposited metal after Co..... 79

Fig. 19. Effect of bimetallic systems (CoFe and AgFe) and Fe^0 on SMX degradation in PS-free solutions. Experimental conditions: $[SMX]_0 = 39.5 \mu M$, $m(Fe^0) = m(AgFe) = m(CoFe) = 2.5 \text{ mg}$ (2.23 mM), $pH_i = 5.63$. Error bars represent uncertainty at 95% confidence level..... 80

Fig. 20. Effect of bimetallic systems (CoFe and AgFe) and non-plated Fe^0 on SMX degradation in PS / H_2O systems. Inset: Concentration of total dissolved iron species in bimetallics (AgFe and CoFe) and mono-metallic Fe^0 at 10, 20, and 60 min. Experimental conditions: $[SMX]_0 = 39.5 \mu M$, $[PS]_0 = 1 \text{ mM}$, $m(Fe^0) = m(AgFe) = m(CoFe) = 2.5 \text{ mg}$ (2.23 mM). Error bars represent uncertainty at 95% confidence level. 82

Fig. 21. Effect of plated (AgFe and CoFe 5:100) and non-plated Fe^0 on PS activation. Inset: Influence of bimetallics (AgFe and CoFe) systems on the % RSE calculated at different reaction times (10, 20, and 60 min). Experimental conditions: $[SPS]_0 = 1 \text{ mM}$, $[SMX]_0 = 39.5 \mu M$, $m(Fe^0) = m(AgFe) = m(CoFe) = 2.5 \text{ mg}$ (2.23 mM). Error bars represent uncertainty at 95% confidence level. 84

Fig. 22. Effect of transition metal ions Co^{2+} , Fe^{2+} , and Ag^+ on SMX degradation in PS / H_2O free systems. Experimental conditions: $[SMX]_0 = 39.5 \mu M$, $[Fe^{2+}]$, $[Co^{2+}] = [Ag^+] = 2.23 \text{ mM}$, $pH_i = 5.63$. Error bars represent uncertainty at 95% confidence level..... 86

Fig. 23. Effect of trimetallic systems (AgCoFe and CoAgFe) and non-plated Fe^0 on SMX degradation in PS / H_2O systems. Inset: Concentration of total dissolved iron species in trimetallic systems (AgCoFe and CoAgFe) and mono-metallic Fe^0 systems at 10, 20, and 60 min. Experimental conditions: $[SMX]_0 = 39.5 \mu M$, $[PS]_0$

= 1.0 mM, $m(\text{Fe}^0) = m(\text{AgCoFe}) = m(\text{CoAgFe}) = 2.5 \text{ mg}$ (2.23 mM). Error bars represent uncertainty at 95% confidence level. 88

Fig. 24. Effect of plated (AgCoFe and CoAgFe) and non-plated Fe^0 on PS activation. Inset: Influence of trimetallics (AgCoFe and CoAgFe) systems on the %RSE calculated at different reaction times (10, 20, and 30 min). Experimental conditions: $[\text{PS}]_0 = 1.0 \text{ mM}$, $[\text{SMX}]_0 = 39.5 \text{ }\mu\text{M}$, $m(\text{Fe}^0) = m(\text{AgCoFe}) = m(\text{CoAgFe}) = 2.5 \text{ mg}$ (2.23 mM). Error bars represent uncertainty at 95% confidence level. 90

Fig. 25. Effect of bimetallic systems (CoFe and AgFe) and non-plated Fe^0 on (a) SMX degradation and (b) PS consumption in PS / H_2O systems under non-disturbed conditions. The inset shows the calculated average % RSE at 60 min reaction time. Experimental conditions: $[\text{SMX}]_0 = 39.5 \text{ }\mu\text{M}$, $[\text{PS}]_0 = 1 \text{ mM}$, $m(\text{Fe}^0) = m(\text{AgFe}) = m(\text{CoFe}) = 2.5 \text{ mg}$ (2.23 mM). Error bars represent uncertainty at 95% confidence level. 92

Fig. 26. Effect of trimetallic systems (AgCoFe and CoAgFe) and non-plated Fe^0 on (a) SMX degradation and (b) PS consumption in PS / H_2O systems under non-disturbed conditions. The inset shows the calculated average %RSE at 60 min reaction time. Experimental conditions: $[\text{SMX}]_0 = 39.5 \text{ }\mu\text{M}$, $[\text{PS}]_0 = 1.0 \text{ mM}$, $m(\text{Fe}^0) = m(\text{AgCoFe}) = m(\text{CoAgFe}) = 2.5 \text{ mg}$ (2.23 mM). Error bars represent uncertainty at 95% confidence level. 94

Fig. 27. Reactivity of plated and non-plated iron-based systems: vertical bars display the ratio of k_{obs} measured for each of the amended Fe^0 systems to the k_{obs} values measured for the standalone Fe^0 system ($K_{obs}(\text{amended Fe}) / K_{obs}(\text{Fe})$). 96

Fig. 28. Trace chromatograms of SMX treated in Fe^0/PS systems with different Fe^0 loads. Inset is the UV-Vis absorption spectra of SMX and its derivative in Fe^0/PS systems during the first 10 min of the reaction. Experimental conditions: $[\text{SMX}]_0 = 39.5 \text{ }\mu\text{M}$, $[\text{PS}]_0 = 1.0 \text{ mM}$, $m(\text{Fe}^0) = 2.5$ and 100 mg. 97

Fig. 29. Trace chromatograms of SMX treated in Fe^0/PS systems with different Fe^0 loads. Inset is the UV-Vis absorption spectra of SMX and its derivative in Fe^0/PS systems during the first 10 min of the reaction. Experimental conditions: $[\text{SMX}]_0 = 39.5 \text{ }\mu\text{M}$, $[\text{PS}]_0 = 1.0 \text{ mM}$, $m(\text{Fe}^0) = 2.5$ and 100 mg. 98

TABLES

Table	Page
Table 1. Most frequently detected pharmaceuticals in wastewaters and their concentrations [16-19].	5
Table 2. Standard electrode potentials of some water constituents, oxidative reagent and transition metals relevant for the oxidative degradation of SMX in PS systems. Electrode potentials are arranged in decreasing order of E^0 .	10
Table 3. Laboratory and bench scale studies with heat activated PS.	16
Table 4. Masses of the weighed salts ^a used for the synthesis of bimetallic ^b and trimetallic ^c systems.	26
Table 5. SEM/EDX of iron particles after reaction in different Fe0/H2O systems over 2h. Experimental conditions: [Fe0]0 = 17.85 mM or 1 g/L, [SMX]0 = 39.5 μ M, [PS]0 = 1.0 mM, [PB] = 1.0 mM.	33
Table 6. MS and chromatographic characteristics of SMX and its transformation product after reaction in Fe0/SMX/PS system.	64
Table 7. Structural interpretation of LC-MS/MS and LC-MS3 fragmentation data obtained for SMX and its transformation product in Fe0/SMX/PS system.	70
Table 8. Observed first order (K_{obs}) kinetics rate constants of SMX degradation in PS solutions activated by different iron-based systems.	87

SCHEMES

Scheme	Page
Scheme 1. 2D and 3D structures of SMX Molecule.....	8
Scheme 2. Proposed degradation mechanism of SMX in (a) Fe ⁰ /H ₂ O and (b) Fe ⁰ /PS/H ₂ O systems at room temperature.....	66

ABBREVIATIONS

AMU: Atomic mass unit

AOPs: Advanced oxidation processes

APMs: Active pharmaceutical molecules

DI: Deionized water

DWT: Drinking water treatment

EDX: Energy dispersive X-ray spectroscopy

ESH: Electrode standard hydrogen

FR: Fenton reagent

HOs: Hydroxyl radicals

HPLC: High performance liquid chromatography

ICPs: Iron corrosion products

ISCO: In-situ chemical oxidation

k: rate constant

KV: Kilo volt

MCPs: Metal corrosion products

MIPs: Micrometric iron particles

MS: Mass Spectrometry

nw: non-washed

Obs: observed

pHi: initial pH

pH_f: Final pH

PMS: Peroxymonosulfate

ppb: part per billion

PS: Persulfate

PTFE: poly (tetrafluoroethylene)

RSE: Reaction stoichiometric efficiency

R_t: Retention time.

SEM: Scanning electron microscopy

SMX: Sulfamethoxazole

SRs: Sulfate radicals

TOC: Total organic carbon

UGW: Underground water

UV: Ultra violet

Vis: Visible

w: washed

WWTPs: Waste water treatment plants

ZVM: Zero Valent metal

CHAPTER I

INTRODUCTION

Water is our natural heritage, our miracle of life, it is the essence of life. With about 70% of the earth's surface is covered with water, it undeniably becomes one of our greatest resources. It is vital element for both domestic as well as industrial processes. However, our increasingly technological society has become indifferent to water. During the last three decades, the pollution of the aquatic environment has become an indispensable issue. Far from being pure, modern drinking water around the world contains many toxic chemicals and bacterial contaminants. These contaminants have been released into the environment with unforeseen consequences. This group, classified as so-called emerging contaminants, which is composed of products that are utilized in our daily life. For instance, this group include surfactants, pharmaceuticals and personal care products (PPCPs) such as shampoos and lotions [1, 2], as well as gasoline additives, fire retardants, plasticizers, etc. Moreover, other contaminants may originate from industrial and sewage wastes, mining activities, marine dumping, accidental oil leakage, burning of fossil fuels, chemical fertilizers and pesticides, radioactive wastes, leakage from landfills, hospital effluents, and other organic and inorganic contaminants [3]. Although, some of them are not persistent, they can still cause negative effects to living organisms, due to the continuous introduction into the pristine environment. Pharmaceuticals may reach the water resources not only from the production facilities and hospitals, but also from

improper household disposal. However, it has been noticed that pharmaceuticals and personal care products (PPCPs) which include pharmaceutical drugs, cosmetic ingredients, food supplements, and ingredients in other consumer products are persistent in drinking water potable reuse and pristine water [4]. Although, they are present in very low concentrations, in the lower ppb range, they can cause a serious risk to humans on the long term exposure such as abnormal physiological effects, reproductive impairment, increasing cancer incidences, and development of antibiotic resistant bacteria [5]. Conventional waste water treatment plants (WWTP) including precipitation, coagulation and filtration [6] have failed to remove effectively these recalcitrant contaminants from drinking water treatment (DWT) facility [4] as these wastewater treatment facilities were not designed to remove pharmaceuticals [7, 8]. Thus they initiated the utilization of emerging chemical oxidation water treatment processes such as advanced oxidation processes (AOPs) based on the generation of reactive radicals such as hydroxyl and sulfate radicals which react rapidly with organic contaminants. In general, AOPs are much faster (low residence time) and more powerful (mineralization) than conventional reactions. As a rule of thumb, AOPs are very effective in transforming organic compounds; whereas, conventional reactions are effective against inorganic contaminants [9-11].

A. Literature review

1. Pharmaceutical Compounds

Until the 1990's, some specific contaminants were in the interest and awareness of the public and the government. As these pharmaceuticals reach the soil, surface water, ground, and drinking water after being excreted from humans or animals via urine or feces, through the sewage system and into the effluent of wastewater treatment plants [12]. In addition to their metabolic excretion, pharmaceuticals disposed through agriculture, industry, medical treatment and common households also contribute to the presence of pharmaceuticals in water. Pharmaceuticals could be aromatics, halogenated aromatics, polyaromatics, pesticides, heavy metals (lead and mercury) and their derivatives. However, in the current era, the release of so-called emerging contaminants has become an environmental problem too. **Table 1** classifies a group of common pharmaceuticals that are present in the environment based on their therapeutic activity. The latter include antibiotics, analgesics, anti-inflammatory drugs, anti-epileptics, beta blockings, anti-depressing drugs, natural and synthetic hormones, lipid regulators, etc. [13].

The hazards imposed by these pharmaceuticals arise because they retain their chemical structure for a considerable period enough to perform their therapeutic work; and because they are continuously added they could remain in the environment for a long time and thus their existence impose threat whether in low or high concentrations [14, 15]. This problem has raised concern to researchers to tackle this issue and remove those compounds from water resources which include veterinary pharmaceuticals, personal care products, surfactants and surfactant residues, plasticizers and various industrial additives

[7, 8]. Most xenobiotic, as pharmaceuticals, occur in the environment at very low concentration, but they exhibit harmful effects on the living organism [31] due to their biological accumulative [32] properties in the long term exposure.

Table 1. Most frequently detected pharmaceuticals in wastewaters and their concentrations [16-19].

Therapeutic Use		Type and Name of Pharmaceutical
Antibiotics		Sulfonamides: SMX (0.02-0.58 $\mu\text{g L}^{-1}$) fluoroquinolones: ofloxacin (6-52 ng L^{-1}) bacteriostatic: trimethoprim (0.11-0.37 $\mu\text{g L}^{-1}$) Penicillin G (<0.025 $\mu\text{g L}^{-1}$)
Analgesic/Antipyretics	Analgesic/Antipyretic Non-steroidal anti-inflammatory drugs (NSAIDs)	Acetaminophen (10-23.33 $\mu\text{g L}^{-1}$) Diclofenac (0.01-510 $\mu\text{g L}^{-1}$), Naproxen (0.5-7.84 $\mu\text{g L}^{-1}$) Ibuprofen (0.49-990 $\mu\text{g L}^{-1}$) ketoprofen (0.13-3 $\mu\text{g L}^{-1}$) Carbamazepine (0.1-1.68 $\mu\text{g L}^{-1}$)
CNS (Central Nervous System) drugs	Antiepileptics	
Cardiovascular drugs	CNS stimulant Beta blockers	Caffeine (3.2-11.44 $\mu\text{g L}^{-1}$) Propranolol (0.05 $\mu\text{g L}^{-1}$), atenolol (10-730 ng L^{-1}), metoprolol (10-390 ng L^{-1})
	Cholesterol and Triglyceride reducers	Clofibrac acid (0.47-170 $\mu\text{g L}^{-1}$), gemfibrozil (0.3-3 $\mu\text{g L}^{-1}$) fezafibrate (0.1-7.6 $\mu\text{g L}^{-1}$)
Endocrinology treatments	Steroid hormones	17 α -ethinyloestradiol (1 ng L^{-1}), estrone, 17 β - estradiol, estriol (usually < 10 ng L^{-1})
Diagnostic aid-absorbable organic	Iodinated X-ray contrast media	Iopromide (0.026-7.5 $\mu\text{g L}^{-1}$), iomeprol (1.6 $\mu\text{g L}^{-1}$)

2. Sources

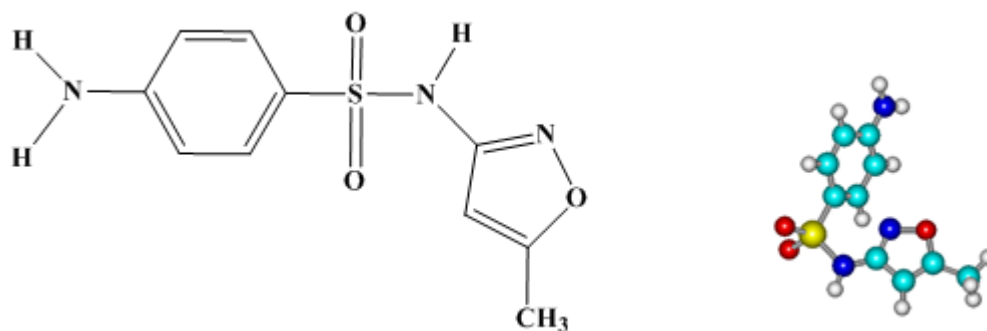
The pollution of the environment by pharmaceuticals is due to the improper discharge of the unused and expired medicines also from the effluents of the waste water treatment plants (WWTPs). Actually, pharmaceuticals are excreted without any structural change from human bodies [34-36] or in the form of their metabolites. In case of veterinary use, the main difference is that pharmaceutical compounds can be directly discharged onto the soil and into waters.

3. Fate of the Pharmaceuticals in the Environment

The behavior of pharmaceutical compounds and their metabolites in the aquatic environment depends on their interaction with either compounds present in nature (sediments, organic matters, and microorganism) or those added during the water treatment (active sludge, activated carbon, ion exchange resins, coagulants, disinfectants etc.). For instance, the formation of complexes or precipitates promotes elimination. The strong interaction with dissolved organic matter can increase their mobility in the environment. The physico-chemical (pH, salinity, oxygen content) and biological characteristics (microorganisms) of these compounds also have an important impact on the fate of the pharmaceuticals. Furthermore, the detectable concentrations in the environment depend on their pharmacokinetic behavior (half-life, metabolism etc.). Certain pharmaceuticals are slightly soluble in water; their partition and adsorption coefficient are high, showing that these compounds have a capacity for adsorption on solid particles and on organic matter. These properties permit their bioaccumulation [16-21]. The relation between the

bioaccumulation and the effect of these products means a threat to the proper functioning of aquatic ecosystems, as well as to the human health. For all these reasons, methods of treatment should be developed to remove these recalcitrant contaminants present in water sources. Some of the pharmaceuticals also can ultimately be mineralized to carbon dioxide and water under certain circumstance. Others don't degrade readily because of their lipophilicity and they are partially retained in the water. Or they can metabolizes to a more hydrophilic molecule that can pass easily through the wastewater treatment plant and ends up in the receiving waters. The latter group of pharmaceuticals are the most persistent in the environment. The release of such pharmaceuticals into the environment may impose toxicity virtually on any level of the biological hierarchy, i.e. cells, organs, organisms, population, ecosystem, or the ecosphere. Beside their toxicity, certain class of pharmaceuticals like antibiotics may cause a long term and irreversible change to the microorganism genome, making them resistant in their presence even in minute concentrations. From the aforesaid observations, it is contingent that the presence of pharmaceuticals in the pristine water cause a serious of environmental problems as these compounds (a) are utterly resistant to biological degradation processes and often escape intact from conventional treatment plants (b) may impose serious toxic and other effects to humans and other living organism and (c) exist in small concentrations, thus requiring more sophisticated and arduous analytical tools for their precise determination. For these negative consequences caused by the pharmaceuticals in water, we are interested particularly in the degradation of sulfamethaxazole (SMX) a recalcitrant organic compound present in water.

4. Characteristics of Selected Compound “SMX”



Scheme 1. 2D and 3D structures of SMX Molecule

Sulfamethoxazole is an antibiotic compound commonly used to treat and prevent diseases in animals, as well as promote growth and weight loss in livestock [22]. However, due to the extensive consumption, disposal, and excretion, these active pharmaceutical compounds (APMs) and in particular SMX have reached the water system; thus, posing serious health effects. In addition, recent studies have highlighted the role that livestock manure may play in contaminating surface and underground water after application, even at the ng and μg levels [23]. Such low concentration levels might allow antimicrobial agents altering microbial community structure yielding antibiotic resistance in environmental microbial populations [24-26]. Moreover, SMX is of great concern in the aquatic environment due to the development of antibacterial resistances. Because APMs are generally difficult to destroy through conventional biological means in wastewater treatment plants, removal methods have been developed with the aim of restoring water

quality. This is significant to avoid further pollution of the environment and enable safe reuse of such water, thereby decreasing fresh water consumption.

5. Early Treatment Methods-Fe⁰ and Amended Fe⁰

For the last two decades, Fe⁰ has been extensively used for water decontamination. Microscale iron particles and amended iron particles Me⁰Fe⁰ (where Me⁰ is the metal to be plated on the surface of Fe⁰) have been shown to be very efficient for the aqueous removal of several organic [27, 28] and inorganic compounds [9-11] by the release of iron corrosion products (ICPs). Fe⁰ has been considered for a long time a reducing agent based on the electrode potential of the couple Fe²⁺/Fe⁰ ($E^0 = -0.44$ V /ESH) (**Table 2**). The extent of contaminant removal is directly dependent on the availability of solid iron corrosion products (iron hydroxides and oxides). Because the oxide scale is always present on the Fe⁰ surface (at pH > 4.5), the continuance of the corrosion process and thus that of the contaminant removal depends on the porosity of the oxide scale [29] which have a complex composition. It has been demonstrated that Fe⁰ is an ideal medium for the continuous production of adsorbents for contaminant removal [30-36]. They are typically formed upon the oxidative dissolution of Fe⁰ which generates iron (II/III) oxyhydroxide phases [37, 38].

Table 2. Standard electrode potentials of some water constituents, oxidative reagent and transition metals relevant for the oxidative degradation of SMX in PS systems. Electrode potentials are arranged in decreasing order of E^0 .

Couple	Electrochemical reaction	$E^0(V)$
$S_2O_8^{2-} / SO_4^{2-}$	$S_2O_8^{2-} + 2e^- \rightarrow 2SO_4^{2-}$	2.01
Co^{3+} / Co^{2+}	$Co^{3+} + 1e^- \rightarrow Co^{2+}$	1.92
Ag^{3+} / Ag^+	$Ag^{3+} + 2e^- \rightarrow Ag^+$	1.90
O_2 / H_2O	$\frac{1}{2}O_2 + 2H^+ + 2e^- \rightarrow H_2O$	1.229
Ag^+ / Ag^0	$Ag^+ + 1e^- \rightarrow Ag^0$	0.799
Fe^{3+} / Fe^{2+}	$Fe^{3+} + 1e^- \rightarrow Fe^{2+}$	0.732
H^+ / H_2	$2H^+ + 2e^- \rightarrow H_2$	0.00
Co^{2+} / Co^0	$Co^{2+} + 2e^- \rightarrow Co^0$	-0.282
Fe^{2+} / Fe^0	$Fe^{2+} + 2e^- \rightarrow Fe^0$	-0.44

Four mechanisms have been proposed for the removal process of the contaminants: (1) contaminant adsorption on Fe^0 surface or at the surface of their corrosion products [39-41], (2) contaminant co-precipitation with metal corrosion products (MCPs) [42-44], (3) contaminant oxidation within the oxide layer [45, 46], and (4) contaminant reduction including catalytic hydrodehalogenation [47, 48]. The plating process performed by depositing a more electropositive metallic element on the surface of iron particles is known so far to increase Fe^0 corrosion through the formation of a galvanic couple [48, 49]. These mechanisms require the use of high iron loads (40 g L^{-1}) which might be a disadvantage due to the formation of lot of sludge that needs to be correctly disposed.

Accordingly, an alternative has been recently proposed [50] reducing thereby iron loads (by almost a factor of 1000 e.g. 50 mg L⁻¹ instead of 40 g L⁻¹) while feeding the medium with an oxidant such as hydrogen peroxide (Fenton's process) (**Eq. 1**) [39-42]) or persulfate (PS) which are able to generate sulfate radicals (SRs) (**Eq. 2**) and hydroxyl radicals (HRs) (**Eq. 1**). Fe⁰ has been shown to improve the activation of PS through the release of ICPs (e.g. Fe²⁺ and nascent iron oxides) during the corrosion process [50, 51].



6. Treatment Methods- Advanced Oxidation Processes (AOPs)

AOPs have proven to be the most effective technology in the degradation of pharmaceuticals. They are based on the generation of very reactive radicals, such as hydroxyl radicals, which are able to react with most organic and inorganic compounds and initiate their degradation. Reactive radicals are generated after the addition of oxidizing agents commonly known as the *in-situ* chemical oxidation (ISCO) technique such as ozone [52] and KMnO₄ [53]. Although, O₃ and KMnO₄ have shown good performances in wastewater remediation, they exhibited some disadvantages. As an illustration, water disinfection using ozone [52] was halted due to the low solubility of O₃ in water, disinfection using potassium permanganate was also stopped due to its failure to produce colorless effluents (persistence of the pink or brown coloration) after disinfection. In

addition to that, the reactivity of KMnO_4 is limited only to unsaturated compounds [54, 55].

AOPs also include the Fenton process for pharmaceutical removal. H_2O_2 has a strong oxidation potential ($E^0 = 1.78 \text{ V}$) and it non-selectively attacks most of the organic contaminants. Furthermore, H_2O_2 chemically activated by Fe^{2+} forms a homogeneous system involving the coupling of iron Fe^{2+} with hydrogen peroxide (H_2O_2) for the formation of HO \cdot radicals ($E^0 = 2.90 \text{ V}$), also known as Fenton Reagent (FR) according to **Eq.1**. The latter enhance significantly the oxidative transformation of contaminants [56]. However, FR has a major limitation including narrow functional pH in the acidic range, iron precipitation, slow kinetics of ferrous ion regeneration and the requirement of high concentration of iron (stoichiometric ratios) for the system to be efficient [57]. Furthermore, FR is too reactive to effectively handle the oxidants in subsurface environments [58]. For instance, most of the H_2O_2 would be rapidly consumed during transportation through the soil and aquifer before reaching the contaminants due to its high reactivity. Fenton-like reactions ($\text{Fe}^{3+} / \text{H}_2\text{O}_2$ with and without UV-light radiation) and UV / H_2O_2 , sonolysis [59], electron beam and γ - radiation, and TiO_2 photocatalysis are different modes for the oxidant activation. However, all the previously mentioned oxidants for in/ex situ remediation of water has been stopped as these methods are expensive and energy demanding as well as catalyst consuming and may yield unstable and / or stable metabolites. For all these reasons, there was a necessity for the use of an alternative oxidant that is more powerful, efficient, producing benign byproducts, and economical at

the same time. Here started the interest in the chemistry of sulfur-oxygen radicals SO_n^- (n = 3, 4, 5).

7. Chemistry of Persulfate

The interest in the chemistry of sulfur oxygen radicals was strengthened after the process of conversion of sulfur dioxide $SO_2(g)$ to acid rain H_2SO_4 was understood [60]. Many studies have been done to examine the pathway that generate $SO_5^{\bullet-}$ radicals as well as their redox potentials and the most feasible oxidation mechanism [61]. In situ chemical oxidation (ISCO) is an effective technology for the removal of organic contaminants from soil and underground water. Peroxydisulfate $S_2O_8^{2-}$ referred to as simply persulfate is the newest chemical oxidant to receive wide use. Persulfate usually occurs in the form of potassium, sodium, or ammonium salts. The most preferred form for ISCO is sodium persulfate as it has the highest water solubility and the most benign residual products. Sodium persulfate ($S_2O_8^{2-}$) is the strongest oxidant identified [62] with the redox potential ($E^0 = 2.01$ V) and it is highly aqueous soluble and relatively stable at room temperature [54]. $S_2O_8^{2-}$ was investigated to degrade organic molecules such as SMX, azo-dyes, trichloroethylene [63-65]. Reactions of persulfate with organic pollutants are very slow at ambient temperature. Nonetheless, persulfate is usually activated by UV light [66], heat [62], high pH, or transition metals (e.g. Fe^{2+} , Ag^+ , Co^{2+} etc.) to form sulfate radicals $SO_4^{\bullet-}$ which has a greater redox potential ($E^0 = 2.6$ V) than that of persulfate, but slightly lower than that of OH^{\bullet} ($E^0 = 2.9$ V). The $SO_4^{\bullet-}$ reactive intermediate is called *activated persulfate*. Whereas, the term *non-activated* persulfate refers to the use of persulfate ion

without any aid or activator (**Eq. 3**). Due to this diverse reactivity, persulfate today is widely applied in industrial processes such as polymerization and metal surface oxidation etc.[67]. Sulfate radicals are highly reactive species with a short lifespan, and can oxidize a variety of organic molecules much like the hydroxyl radicals, although the mechanism for the reaction is significantly different. In most cases, sulfate radicals abstract an electron from the organic molecule forming an organic radical cation as seen in **Eq. 4** [68], whereas, the hydroxyl radicals add to C=C or abstract a hydrogen from C-H bond [69]. The sulfate radical is an electrophilic reagent. This means that when an electron with donating group such as amino (-NH₂), hydroxyl (-OH), or alkoxy (-OR) are present on an aromatic molecule, the rate of the reaction with the $SO_4^{\bullet-}$ will increase; whereas, electron withdrawing groups such as nitro (-NO₂) or carbonyl (C=O) substituents will decrease the rate of the reaction [69].



As it has been demonstrated so far, reaction rates are not of solitary importance in terms of predicting contaminant degradability. Like other reactions involving radicals, such as hydroxyl radicals modeling or predictions of the chemistry of sulfate radicals are based on a competition kinetics approach. For instance sulfate radical can react with several inorganic species such as chloride, bicarbonate, and carbonate anions [70-73]. As reported by Liang, these anions are abundant in soil and groundwater systems and may compete

with the target contaminants for sulfate radicals (scavenging reactions) which could decrease the efficiency of the oxidative treatment. In this dissertation all the reactions are done in deionized water (DI) to avoid this common ion effect. Moreover, the pH of all the starting solutions is less than 6 in which no bicarbonate anions are present.

8. Experiences with Different Activation Aids

a. Heat Activated Persulfate

Table 3 summarizes several bench scale studies using heat activated persulfate. Ghauch et al. studied the oxidative removal of bisoprolol by the thermal activation of persulfate in phosphate buffer of pH 7 and at different temperatures. It was revealed that bisoprolol was completely degraded at 60°C. As for the reaction kinetics, bisoprolol followed a pseudo first order for 1-4 half-lives and the resulting rate constants from 40-70°C fit the Arrhenius equation [74]. Moreover, Ghauch et al. also demonstrated ibuprofen removal by the heat activated PS. Results showed that the ibuprofen was completely removed at 60°C and at a neutral pH [75]. Huang et al. [76, 77] studied the kinetics of heat assisted persulfate oxidation of methyl tert butyl ether (MTBE) in aqueous solution at various pH, temperature, and oxidant concentration. It was reported that increased temperature resulted in faster reaction rate. Another study performed by Waldemer et al. [73] and Huang et al. [78] showed that the degradation of some resistant contaminants requires a higher activation temperature at the same persulfate dose. Researchers have investigated persulfate reactivity at several temperatures and found that the temperature and reaction rate obey the Arrhenius equation [76, 77, 79, 80], and thus the degree of

impact on the rate of oxidation for each target organic compound depends on thermodynamic properties unique to each compound. Persulfate decomposition rate increases at higher temperatures, which result in an overall smaller contaminant removal at increased temperatures due to the faster persulfate depletion. Additionally, the inhibition of contaminant oxidation by other factors such as low pH can be more pronounced at higher temperature [79]. Both high temperatures and low pH result in increased rate of radical generation, a synergy that may favor radical-to-radical reactions instead of radical-to-contaminant reactions. Furthermore, scavenging reactions can also be accelerated at elevated temperatures.

Table 3. Laboratory and bench scale studies with heat activated PS.

Setup	Target Contaminants	Parameters assessed	Results (% removal)	Reference
40-70°C	Bisoprolol	Activation Energy, [PS], Activation temperature, pH, inorganic additives, half-life, and rate constant	50-60°C and pH = 7.0 contributed to full removal	Ghauch et al. 2012
50-70°C	Ibuprofen	[PS], Activation temperature, ionic strength, pH	At 60°C and pH = 7.0 full degradation	Ghauch et al. 2012
20-40°C aqueous (Aq.)	59 VOCs in a mixture	Activation temperature, [PS], complex vs simple mixtures, pH	At 40°C 37/49 VOCs > 90% halogenated ethanes, < 20%	Huang et al., 2005
40-60°C Aq. and soil	TCE 1,1,1-TCA	Activation temperature, kinetics, [PS], naturally occurring Fe	0-100% at 60°C	Liang et al., 2003
20-40°C aqueous (Aq.)	DCB	Activation temperature, [PS], pH, kinetics.	64-100 % removal	Bougie and Dube, 2007
40-50°C Aq.	MTBE	Activation temperature, [PS], pH, ionic strength	10% at 20°C, 87% at 40°C	Huang et al., 2002

20-40°C Aq.	PCE, TCE, cis and trans DCE	Kinetics, activation temperature, chloride, bicarbonate	55-93% for PCE	Waldmer et al., 2007
70°C Soil	16 PAH	PAH structure, PAH, Bioavailability	PS oxidation and biodegradation removed the same PAH fraction. 2-3-ring PAHs: 0-80% 4-ring PAHs: 0-75% 5-6 ring PAHs: 0-50%	Cuyppers et al., 2000

b. Chemical Activation of PS via Fe⁰ and Modified Fe⁰

In this dissertation, we have used commercial iron for PS activation, it is promising candidate for in-situ remediation because it is relatively non-toxic. Iron is present in high concentrations in soil and sediments and can be introduced into water and subsurface if necessary. In a real situation, the injected PS can, upon activation, progressively release SRs to oxidize water micro-contaminants [62-65]. PS anion (S₂O₈²⁻) is a strong oxidant, highly soluble in water [54] and can be activated to produce powerful SRs (**Eq. 2**) responsible indirectly for the generation of highly oxidative HRs (**Eq. 5**) in water under natural conditions [81, 82]. Activating PS has an advantage because of the production of SRs with greater standard potential (E⁰ = 2.6 V) than PS (E⁰ = 2.1 V) and H₂O₂ (E⁰ = 1.76 V) as well at neutral pH.

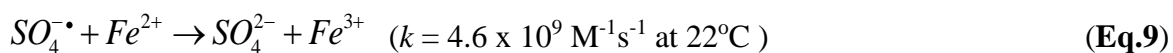


Activation can occur upon photolysis [83], microwaves [84], heat [85], electron beam [86], ultra-sonication [87], and upon its reaction with a metal ion. The latter can be

obtained directly in solution by feeding the medium with the corresponding salt (Eq. 2) or by introducing into the solution the corresponding zero-valent metal (ZVM). The ZVM get corroded in an aqueous medium and produces ions for PS activation (**Eqs. 6-8**).



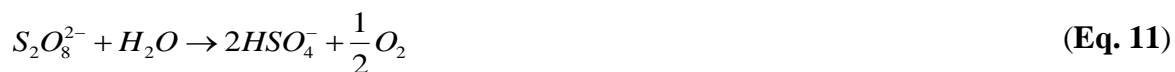
However, ions production should be limited in time and concentration since Fe^{2+} is involved in both radical generation (**Eq. 2**) and radical scavenging (**Eq. 9**), thus it is essential to optimize the metal concentration in order to achieve effective activation without quenching. Finding the optimum Fe^0/PS ratio to the reaction of sulfate radicals with excess iron instead of the target contaminants has been a big challenge. For instance, it should be considered that if excess quantities of Fe^{2+} are present in solution, the $SO_4^{\bullet-}$ reacts with Fe^{2+} (**Eq. 9**) which results in the reduction in the extent of Fe^{2+} activation due to the higher reaction rate constant between $SO_4^{\bullet-}$ and Fe^{2+} . Also, one should not neglect the direct reaction between Fe^0 and PS (**Eq. 10**). This reaction could have two serious drawbacks: (1) rapid consumption of PS, (2) an improved Fe^0 corrosion that releases quickly and abundantly Fe^{2+} in the medium thereby increasing radical quenching processes.





Accordingly, smooth Fe^{2+} releasing is mandatory. This can be optimized by using zero valent iron as a source of Fe^0 particles produced through Fe^0 corrosion in Fe^0/H_2O systems (**Eqs. 6-8**) [50]. In this case, Fe^{2+} can be progressively released into the solution under natural experimental conditions where dissolved oxygen as well as the pH and species like bicarbonate could not significantly disturb mild iron corrosion [65, 88-90] (**Eqs. 6-8**).

Furthermore, it is important to notice that the resulting pH of the solution is more directed by PS activation rather than iron corrosion. In fact, PS activation yields the formation of bisulfate (HSO_4^-) having acidic properties ($pK_a = 1.92$) (**Eqs. 11, 12**) while Fe^0 corrosion produces hydroxyl species (**Eqs. 7, 8**) HO \cdot s which non-selectively attack and degrade organic compounds [81, 82]. Thus, the higher selectivity of $SO_4^{\cdot-}$ could make $S_2O_8^{2-}$ based remedial technology more attractive than H_2O_2 based technologies because HO \cdot s is often scavenged by water constituents necessitating the use of greater mass of oxidant for remediation.



Being in an acidic medium favors the dissolution of iron oxides and the liberation of Fe^{3+} that can adsorb at the surface of iron particles to produce Fe^{2+} activator again (Eq. 13) in a catalytic way.



However, based on previous published work [91-93], sustaining iron corrosion could be enhanced through the deposition of an additional metal on the surface of iron particles creating thereby bimetallic and trimetallic systems [94-96]. These systems might possess additional properties to enhance the activation of PS into SRs in a sustainable way based on their new intrinsic properties. For example, problems such as (i) the loss of reactivity due to the formation of surface scale and (ii) the loss of hydraulic permeability due to the progressive occupation of the iron pores by ICPs such as iron hydroxides and oxides [97] could be solved. Subsequently the presence of an additional metal at trace level next to Fe^0 might improve the intrinsic properties of the metallic systems toward PS activation. It is also worth it to substitute sequential Fe^{2+} addition because addition of Fe^{2+} has shown to rapidly deplete PS in solution and that can be a burden for long term remediation processes based on PS technology [89].

In order to better understand the reactivity of sulfate radicals, the percent of the reaction stoichiometric efficiency (%RSE) which is equivalent to the ratio of the number of moles of sulfamethoxazole degraded over the number of moles of PS consumed (% RSE = Δ

[Sulfamethoxazole]/ Δ [PS] x 100) was calculated. The % RSE was only 5.2% in case of persulfate activated by Fe⁰ [50].

In order to improve the reactivity of Fe⁰ and increase the %RSE, efforts have been directed toward the usage of plated iron particles by chemically depositing some more electropositive metals (e.g. Co and Ag) on Fe⁰[91-96, 98]. It has been demonstrated by Dionysiou [61] that cobalt Co²⁺ had activated peroxymonosulfate (PMS) through an electron transfer mechanism from cobalt Co²⁺ for the generation of sulfate radicals (**Eqs. 14,15**). The advantage of this transition metal is the reverse electron transfer from Co³⁺ to Co²⁺ which is thermodynamically feasible (0.82 V) (**Eqs. 16,17**).



In addition to that, Ag⁺ was used also as activator for PS and as a source of SRs (**Eq. 18**). However, it was demonstrated that Co²⁺ is a more efficient catalyst than Ag⁺ since the SRs generated by Ag⁺ have comparable chances to react with organic compounds as well as Ag⁺. It has been noted too that Ag⁺ is more efficient scavenger of SRs than Co²⁺ (**Eq. 18**).



To our knowledge, this is the first time that such bimetallic (AgFe and CoFe) and trimetallic (AgCoFe and CoAgFe) systems are used to activate PS. We have investigated throughout this work (i) the impact of metal molecularity, plating order (in the case of trimetallic systems) and metal load on SMX removal and PS activation, (ii) the % reaction stoichiometric efficiency (RSE) calculated for bimetallic and trimetallic systems in comparison to non-plated Fe⁰, and (iii) the nature and presence or absence of transformation products formed during the oxidation process.

B. Objectives

In recent years, the presence of pharmaceuticals in the aquatic environment has been growing. After their use, the non-metabolized products are transferred into sewage treatment plants. Oxidation processes can be a solution for the complete elimination of these emerging pollutants. This contribution has reported the use of micrometric iron particles (MIPs) assisted PS for the degradation of recalcitrant active pharmaceutical molecules APMs like SMX. In the third chapter of this dissertation several parameters have been studied affecting SMX (39.5 μM) degradation in Fe⁰/H₂O systems which are (i) the PS load effect (0.4-1.0 mM), (ii) the MIPs content (0.89-17.85 mM), (iii) pH (5.5-8.3), and (iv) alkalinity (bicarbonate). We aim to develop the optimum conditions for the enhancement of the reaction stoichiometric efficiency (% RSE) of the carried reactions. HPLC-MS analysis was also performed to follow the SMX reaction pathway as well as its transformation product. Moreover, different water matrices were studied in order to

understand the role that dissolved ions play on the reaction degradation rate. Three successive experiments of 1 h each were conducted on remaining Fe^0 to follow SMX degradation and PS remaining toward complete mineralization.

Accordingly, a smooth Fe^{2+} releasing to activate persulfate (PS) into sulfate radicals (SRs) through catalytic electron transfer was conducted. SRs are then used to degrade sulfamethoxazole (SMX) in water. PS activators like Fe^{2+} , Fe^0 , AgFe and CoFe (bimetallics), AgCoFe and CoAgFe (trimetallics) were tested on SMX solution ($39.5 \mu\text{M}$) spiked with PS (1.0 mM) in order to improve the % RSE obtained in the case of Fe^0/PS systems, which reached 5.2%. Direct and sequential addition of Fe^{2+} were also performed in comparison with Fe^0 in order to optimize the conditions for the highest RSE. This work attests the potential of iron-based systems to sustain PS longer in solution without the production of heavy sludge or formation of transformation products that can burden the treatment process.

CHAPTER II

MATERIALS AND METHODS

A. Chemicals

SMX was obtained from Sigma Aldrich (USA), sodium persulfate (PS) ($\text{Na}_2\text{S}_2\text{O}_8$, 99%) from Chem-Lab (Belgium). Potassium iodide (KI) (puriss, 99-100.5%) and iron particles (puriss 99.5%, fine powder, and $< 150 \mu\text{m}$) were purchased from Riedel-de-Haen (Germany). Sodium dihydrogen phosphate dihydrate ($\text{NaH}_2\text{PO}_4 \cdot 2\text{H}_2\text{O}$, $>99\%$), hydrated tri-sodium phosphate $\text{Na}_3\text{PO}_4 \cdot 12\text{H}_2\text{O}$, phosphoric acid (H_3PO_4). Di-sodium hydrogen phosphate anhydrous (Na_2HPO_4) was purchased from Merck (Germany). Reagents for iron complexation to form “ferroin” complex (o-phenantroline, hydroxylamine and tri-sodium citrate) were acquired from Prolabo (France).

The metallic activators of SPS (Cobalt (II) chloride hexahydrate ($\text{CoCl}_2 \cdot 6\text{H}_2\text{O}$) and silver nitrate (AgNO_3)) were acquired from Sigma Aldrich (USA). Iron (II) chloride tetrahydrate ($\text{FeCl}_2 \cdot 4\text{H}_2\text{O}$), used for the quantification of total iron in solution instead of iron (II) sulfate (FeSO_4), (to avoid sulfate common ion effect) was also obtained from Sigma Aldrich. Ammonium acetate ($\text{C}_2\text{H}_7\text{NO}_2$, $> 98\%$, puriss ACS reagent), sodium hydrogen carbonate (NaHCO_3) and hydrochloric acid (HCl) were from Fluka (Netherlands). HPLC solvent (methanol) is of HPLC grade and purchased from Sigma. Millipore deionized water (DI) was used throughout this research project.

B. Metallic Particle Preparation

The process of successful plating is based on the electrochemical reaction which occurs between an oxidant of higher E^0 and a reductant of lower E^0 summarized in Table 2. To optimize the plating process, several parameters should be considered including temperature, electrolyte, and pH. For instance, in our lab, plating is done after washing the commercial iron with 1 M HCl (10 min) in order to assure the removal of aged iron oxides on Fe^0 surface; thus, rendering the Fe^0 particles accessible for the plating of transition metals. Hence after, the iron was rinsed with 500 mL deoxygenated DI water then dried into the freezer dryer (Labconco) over 2 h before use. Bimetallic systems were prepared according to the following redox reaction:



Where Me is the metal to be plated and “n” is its valence. Adequate amount of $CoCl_2 \cdot 6H_2O$ and $AgNO_3$ metal precursors were weighed on the microbalance (Mettler Toledo XS3DU) as summarized in **Table 4** according to their molecularities. In case of bimetallic systems, adequate amounts of the salt was dissolved in 10 mL DI and finally mixed with 1 g of Fe^0 particles. The vial was then placed on a vortex mixer with an orbital shaker device specifically designed for such experiments [91]. After 10 min of mixing, the Pyrex vial containing the plated solution was settled on a magnet to avoid any loss from the activated iron, and the supernatant solution was withdrawn using a 1 mL syringe and then discarded;

whereas, the remaining iron was placed on the freezer drier for a period of 2 h to ascertain complete humidity removal.

Table 4. Masses of the weighed salts^a used for the synthesis of bimetallic^b and trimetallic^c systems.

Metallic System	CoFe		AgFe		AgCoFe		CoAgFe	
Molecularity	5:100	1:100	5:100	1:100	5:5:100	1:1:100	5:5:100	1:1:100
Mass (mg)	212.4	42.5	150.8	30.2	138.4	26.7	44.2	39.4

^aCoCl₂·6 H₂O and AgNO₃

^bAgFe and CoFe

^cAgCoFe and CoAgFe

For the synthesis of trimetallic systems e.g. CoAgFe adequate amount of CoCl₂·6H₂O was added to the previously freeze dried bimetallic system AgFe so as to obtain the corresponding molecularity (1:1:100 and 5:5:100). The same procedure was followed for the preparation of AgCoFe trimetallic system starting by cobalt plating followed by silver deposition. 2.5 mg of the four plated bimetallic and trimetallic systems were used for the degradation experiments of SMX in PS spiked solutions. For reproducibility purposes, three aliquots of 2.5 mg of the metallic systems were randomly taken from the 1,000 mg previously prepared.

C. Experimental Setup

The SMX solution was prepared by adding 20 (±0.1) mg of SMX at room temperature (C₁₀H₁₁N₃O₃S; M.W. 253.05 g mol⁻¹ pK_{a1} = 1.7 and pK_{a2} = 5.6) to deionized

water (DI) (capped 1 L volumetric flask) to make a 79 μM stock solution [99]. For some experiments, DI water was replaced by tap, underground, and hydrogen carbonate enriched DI water. The resulting solution was then stirred overnight until complete SMX dissolution then filtered through a 0.45 μm filter to remove any non-dissolved particles. Sodium persulfate (PS) was prepared by adding 2.381 g of PS at room temperature (M.W. 238.1 g mol^{-1}) to a 100.0 mL volumetric flask. Phosphate buffer (PB) stock solution 200 mM was prepared by mixing 6.6860 g Na_2HPO_4 with 6.3396 g NaH_2PO_4 in 200 mL DI water in order to conduct experiments at pH 7.00. The resulting solution was placed under sonication for 5 min in order to assure complete dissolution. Micrometric iron particles (MIPs) were acid washed with 15 mL of 1.0 M HCl solution for 10 min then rinsed with 500 mL of deoxygenated DI water in order to remove any ions. The vial was then placed on the freezer drier (Labconco) for 2 h until complete dryness. Adequate volume (10 mL) of the prepared SMX solution is added to a 20 mL vial followed by adding sufficient volume of DI water in order to get the desired concentration of each reactant. For instance, $[\text{SMX}]_0 = 39.5 \mu\text{M}$ (10 mg L^{-1}) in all cases; $[\text{PS}]_0 = 0.4\text{-}1.0 \text{ mM}$ and $\text{PB} = 1.0 \text{ mM}$. Henceforth, adequate amount of the MIPs (1-20 mg of Fe^0) whether acid washed or not is added to several 20 mL Pyrex reactor vials at room temperature. All the reactors are done in duplicate for reproducibility purposes on a vortex shaker with fixed moderate speed intensity. The vortex used had a sample holder, which could accommodate up to 8 vials simultaneously. High vortex speeds will augment friction between MIPs, yielding more cracks in iron oxides at the MIPs surface area. Upon sampling, the reactor is placed on a magnet in order to immobilize the iron particles at the bottom of the vial and thus reduce

the loss of any MIPs. Then by the assistance of 1.0 mL BD syringe, aliquots (0.5 mL) of the solution is withdrawn directly from the solution and filtered via 0.22 μm PTFE acrodisk filter (Jaytee Biosciences Ltd., UK) into 2.0 mL HPLC vial. To ascertain the inactivity of the sulfate radicals in the HPLC vials before placing them on the thermostated HPLC autosampler at 4⁰C for analysis, the vials were chilled in an ice bath until the end of the reaction. For recycling experiments conducted with used MIPs (uFe) in PS/Fe systems, after the first cycle issued for 1 h, the treated solution was completely withdrawn from the reactor using a syringe. MIPs were kept immobilized at the bottom of the reactor using a magnet. A subsequent cycle was undertaken by adding 19.8 mL of fresh SMX solution (39.5 μM) and 200 μL of fresh persulfate (1.0 mM) as well. Aliquots (0.5 mL) were taken every 10 min for PS and SMX analysis over 1 h. A third cycle was also conducted over 1 h exactly the same as the second cycle. Three different recycling experiments were conducted by changing the water matrix. In the first recycling experiment, tap water was used instead of DI (acidified and not acidified). The second case of the recycling experiments were performed with bicarbonate (acidified and not acidified). The third set of recycling experiments were done by using underground water (UGW) (with and without acid) in order to mimic the natural conditions of natural water and soil.

For bi and trimetallic systems prepared, 2.5 mg of MIPs were weighed from 1000 mg of plated Fe⁰ and added into 20 mL reactor vial previously containing SMX (39.5 μM) and 1.0 Mm PS. In case of iron (II) salt usage (FeCl₂·4H₂O), SMX/PS solutions were directly and/or sequentially spiked with an appropriate volume of Fe²⁺ salt so as to obtain the desired concentration in all reactors (2.23 mM). Those (in triplicate) are then

positioned on the vortex shaker with a very moderate and constant mixing speed assuring homogeneous agitation and distribution of iron particles into the solution. For total iron analysis, two methods for quantification were used. The first one is through the utilization of o-phenantroline at a wavelength of 510 nm for “ferroin” maximum absorbance and the second method is by using Atomic Absorption Spectrometry. In case of using the first method, 0.5 mL of sample was withdrawn from the reactor followed by adding 100 μ L of concentrated HCl to assure complete dissolution of oxides. Henceforth, 100 μ L, 200 μ L, and 300 μ L of citrate, hydroquinone, and o-phenantroline were added, respectively. The resultant solution was diluted up to 10 mL and placed in the dark for 30 min to assure complete complexation reaction between iron and phenantroline for further analysis using UV/Vis spectrometry. A calibration curve (0.5, 1, 2, 3, 4, and 5 ppm) was used to quantify total iron in solution. The second method of iron quantification is based on using the AAS, in this case the reactor vial was placed on a magnet (when iron particles are used) and 5 mL aliquots were withdrawn using a micropipette and transferred into another 15 mL tube. 1.0 mL of concentrated HCl was added to the tube to ascertain the complete dissolution of iron oxides. The resultant solution was diluted up to 10 mL and placed in the refrigerator for further analysis using AAS. A calibration curve (2-50 ppm) was used to quantify total iron in solution. The pH was measured at the beginning and at the end of each experiment using a pH/Ion meter (Thermo Orion, USA) equipped with an ultra-combination pH electrode (Ross). Control tests were conducted in parallel in the absence of PS and SMX for each experiment. Data presented are averaged value of 4 replicate samples (duplicate experiments and duplicate analyses). The final results are given as $\text{mean}(\pm ts/\sqrt{n})$ where t

is the student value at 95% confidence interval, “s” the standard deviation and “n” the number of replicates.

D. Chemical Analysis

The quantification of SMX was performed on an Agilent 1100 Series LC/MS system consisting of a quaternary pump, a vacuum degasser, an autosampler, a thermostated column compartment and a diode array detector (DAD) coupled to an ion trap mass spectrometer detector (MSD). The liquid chromatography column was a C₁₈ reversed phase column (5 μm; 4.6 i.d. x 250 mm long) coupled to a security guard column HS C₁₈ (5 μm; 4.0 i.d. x 20 mm long) (Discovery, Supleco, USA) all maintained at 30°C during analysis. Additional details on this equipment have been previously described [74, 75, 91, 100]. The mobile phase consisted of 50:50 (v/v) 10 mM ammonium acetate and methanol under isocratic mode. The flow rate and injection volume were 0.5 mLmin⁻¹ and 25 μL respectively. The system was controlled by the LC/MSD Chem Station software version A.09.03. Under those conditions, SMX is eluted at 6.5 min and has maximum absorbance at 265 nm. The persulfate anions were determined at $\lambda_{\max} = 352$ nm using a Nanodrop 2000c UV-VIS Spectrophotometer (Thermo Scientific) after running a calibration curve (1, 0.5, 0.25, 0.1, 0.05 mM of PS) obtained by complexing PS with KI [101]. Then the concentration of PS in the sample is determined by substituting the absorbance in the equation obtained after drawing the calibration curve. Total iron was quantified via two methods which both revealed the same results. The first method iron quantification was via (i) using o-phenantroline at a wavelength of 510 nm for “ferroin”

maximum absorbance and the second method by using (ii) a calibration curve (2-50 mg L⁻¹) on an Atomic Absorption Spectrometer equipped with an iron hollow cathode lamp with Deuterium correction (Thermo labsystems Solaar). Iron based systems were characterized by a Scanning Electron Microscope (SEM). Surface morphology and elemental composition were studied by the mean of a Tescan Mira 3 LMU (Czech Republic). This SEM is equipped with an EDX system of 20 mm² surface area. The latter (X-Max) is thermoelectrically cooled and coupled to a multichannel analyzer. For Co characterization in all plated metallic systems (CoFe, CoAgFe and AgCoFe), a low beam voltage of 10 KV has been chosen so as to analyze the outer layer of plated iron particles without getting deeper into iron core particles; otherwise, Co emission will be hindered by Fe emission peaks (K_α and L_α). However, for metallic systems exempted from Co (e.g. Fe and AgFe), characterization was successful at low and high voltages as well (10-20 KV). Mineralization of SMX was measured by a total organic carbon (TOC) analyzer (GE 5310C) equipped with an autosampler and a CO₂ conductivity detector. Samples were centrifuged (Heraeus Megafuge 1.0 R) at 4000 g and filtered prior to analysis. A minimum volume of 17 mL was required for each analysis.

CHAPTER III

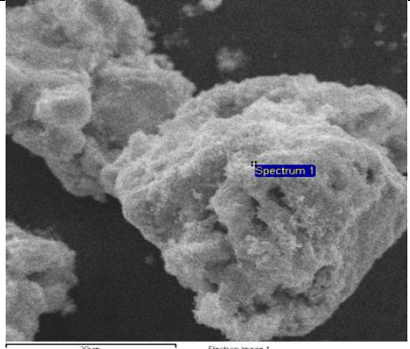
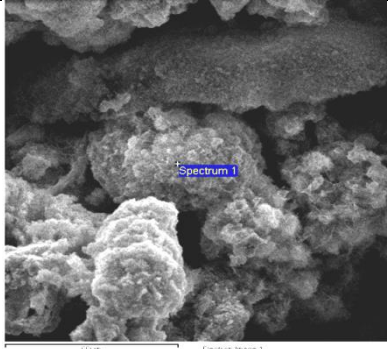
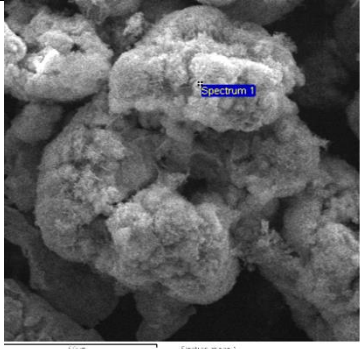
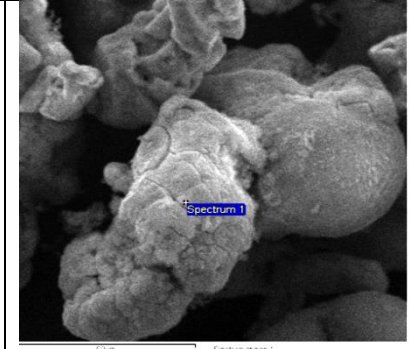
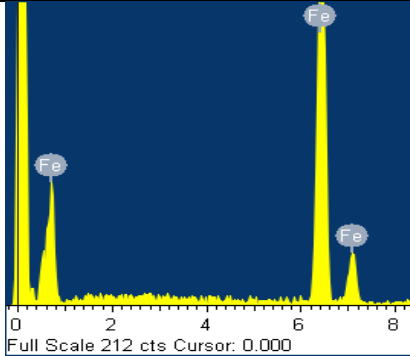
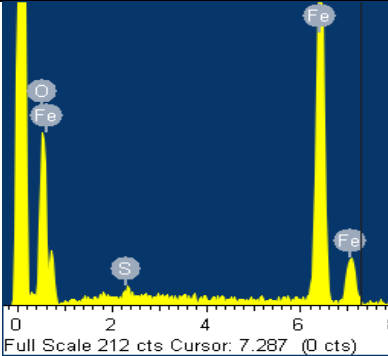
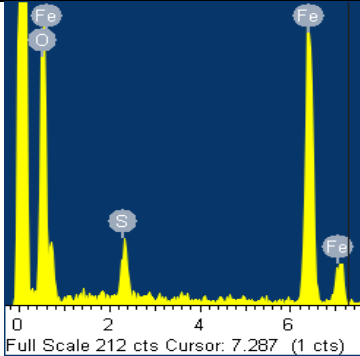
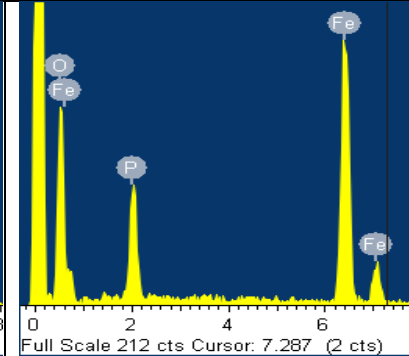
DEGRADATION OF SULFAMETHOXAZOLE BY PERSULFATE ASSISTED MICROMETRIC Fe⁰ IN AQUEOUS SOLUTION

A. Results and Discussion

1. Characterization of Fe⁰ Particles in Different Systems

Four systems were compared in order to understand the role of PS in the process of iron corrosion and to comprehend the role of PB in iron activated PS systems: system **1** (wFe/SMX), system **2** (wFe/PS), system **3** (wFe/SMX/PS) and system **4** (wFe/SMX/PS/PB). **Table 5** summarizes the results obtained after capturing SEM images and performing EDX analysis. The reaction was done after 2 h, and the concentrations of the reactants present were as follows: [Fe]₀ = 17.85 mM, [SMX] 39.5 μM, [PS] = 1.0 mM, [PB]= 1.0 mM. As it can be noticed from system **1** (**Table 5**) that after 2 h of reaction, the surface of MIPs surface in PS free solution is composed of 100% Fe⁰. Whereas, in system **2**, due to direct contact of MIPs with PS solution, EDX spectrum showed elements other than Fe (56%) which are oxygen (44.6%) and sulfur (0.87%). The same elements were present in system **3**, but with different percent composition. As it can be seen, that the iron particle surface showed less iron (36.2%) and more oxygen (60.4%) and sulfur (3.55%).

Table 5. SEM/EDX of iron particles after reaction in different Fe⁰/H₂O systems over 2h. Experimental conditions: [Fe⁰]₀ = 17.85 mM or 1 g/L, [SMX]₀ = 39.5 μM, [PS]₀ = 1.0 mM, [PB] = 1.0 mM.

System 1	System 2	System 3	System 4
Fe ⁰ /SMX	Fe ⁰ /PS	Fe ⁰ /SMX/PS	Fe ⁰ /SMX/PS/PB
			
			
Fe 100%	Fe 54.6%, O 44.6%, S 0.87%	Fe 36.2%, O 60.4%, S 3.5%	Fe 31.3%, O 59.7%, P 9.0%
pHi 5.63	5.57	5.54	7.00
pHr 6.66	5.36	5.28	6.85
[Fe ^{2+/3+}] mg L ⁻¹ 3.50	20.86	17.75	11.46

In the presence of PB (system **4**), EDX analysis didn't show the presence of any sulfur atoms on the surface of MIPs. This is due to the deposition of phosphate on iron oxides formed at the surface of MIPs [102]. Therefore, phosphate atoms rapidly cover the MIPs surface blocking the access of PS on MIPs surface area; consequently, minimal iron corrosion occur at such neutral pH conditions.

To better understand the impact of phosphate species on the reactive medium, the concentration of total dissolved iron species ($[\text{Fe}]_t = [\text{Fe}^{2+}] + [\text{Fe}^{3+}]$) was studied. Without acidification, the concentration of Fe^{2+} species was below the maximum concentration limit (MCL) set by WHO (e.g. 0.3 mg L^{-1} or $5.4 \text{ }\mu\text{M}$) (38 in SMX). Nonetheless, after acidification the color of the solution changed from rusty to colorless confirming the dissolution of ICPs and thus Fe^{2+} quantification. Results showed less iron concentration in the PS free system (system **1**) e.g. $[\text{Fe}]_t = 3.5 \text{ mg L}^{-1}$ compared to PS containing systems (Systems **2-4**) after 2 h of reaction. For instance, 20.88 and 17.75 mg L^{-1} of ICPs were found in system 2 and system 3, respectively, while only 11.46 mg L^{-1} was present in phosphate containing system (system **4**). These results confirmed that the surface of iron particles were more seriously affected by the presence of PS (systems **2-4**) than by its absence (system **1**). A pitting trend appeared on the surface of iron particles in contact with PS containing solution. Such an observation was absent for iron particle surfaces in PS free systems as well as PB containing solutions as seen in SEM results of **Table 5**. The pitting phenomena is due to the direct reaction of PS with MIPs (**Eq.10**) to yield ferrous ions Fe^{2+} .

Accordingly, excess of PS might produce excess of $\text{Fe}^{2+/3+}$ and ICPs yielding more $\text{SO}_4^- \bullet$ quenching (**Eq.9**). As a result, the concentration of PS should be rigorously optimized in order to conserve an acceptable RSE. However, phosphate species can delay or even halt the iron corrosion process after fixation on nascent iron oxides formed at the surface of MIPs. Furthermore, iron species can form different complexes with PB (e.g. $\text{Fe}(\text{H}_2\text{O})_4(\text{H}_2\text{PO}_4)^{2+}$, $\text{Fe}(\text{H}_2\text{O})_4(\text{H}_2\text{PO}_4)_2^+$, $\text{Fe}(\text{H}_2\text{O})(\text{PO}_4)_2^{3-}$, etc.) and thus hinder the release of Fe^{2+} /ICPs responsible for the activation of PS into SRs. Consequently, phosphate concentration in solution should be controlled so that iron species are not totally complexed, keeping some free Fe^{2+} and nascent iron oxides in solution, which play a crucial role in the production of SRs (**Eq. 2**). This might present a disadvantage especially for the treatment of effluents containing phosphate species.

2. Direct vs Sequential Addition of Fe^{2+} and Fe^0

Fig. 1 shows a comparative study for SMX degradation using either Fe^{2+} activator through direct and/or sequential spiking or Fe^0 feeding producing PS activation species upon water corrosion. To do so, control experiment in Fe^0 -free SMX/PS solution were undertaken showing neither SMX degradation nor PS consumption over the same period of treatment (upper curves). In contrast, the presence of either Fe^{2+} or Fe^0 contributed to SMX degradation; however, to a different extent due to PS activation into SRs known by their powerful oxidative properties. For example, 100% SMX degradation was noticed after 2 h of reaction in Fe^0 fed system where almost 83% of the degradation occurred in the first 10 min of the reaction. However,

when similar concentration of Fe^{2+} is used in direct spiking at the beginning of the experiment, only 34% of SMX degradation is noticed at 10 min of reaction followed by a steady state reaching a maximum of only 40% by the end of the experiment.

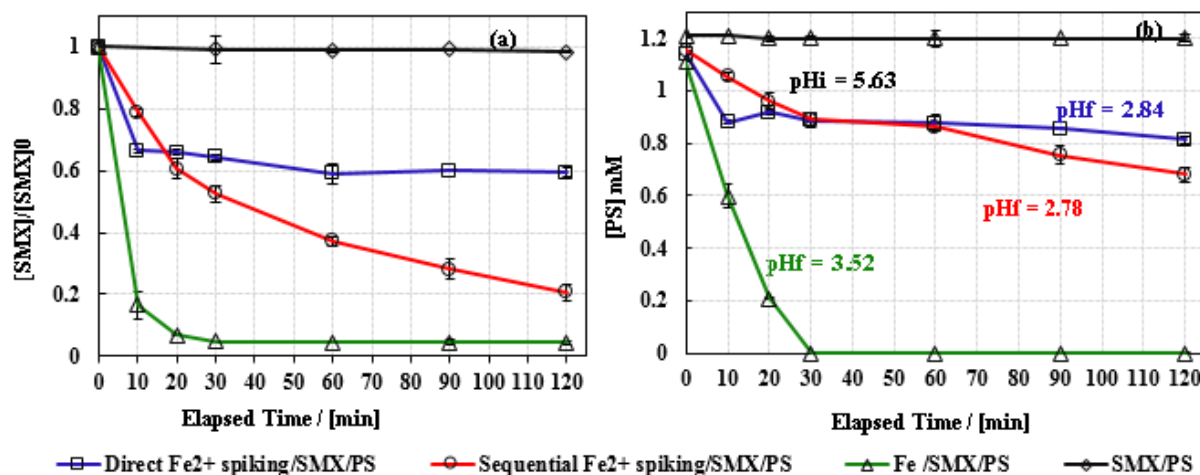


Fig. 1. SMX (a) and PS (b) degradation under the influence of direct and sequential Fe^{2+} spiking compared to Fe^0 powder additive in PS/ H_2O systems. Experimental conditions: $[\text{SMX}]_0 = 39.5 \mu\text{M}$, $[\text{PS}]_0 = 1.0 \text{ mM}$, $[\text{Fe}^{2+}] = [\text{Fe}^0] = 2.23 \text{ mM}$; $m(\text{Fe}^0) = 2.5 \text{ mg}$, Error bars represent uncertainty at 95% confidence level.

This observation can be explained by (i) the rapid activation of PS (in excess) and (ii) the quenching of most of the SRs by Fe^{2+} as previously demonstrated (Eq. 9). However, sequential addition of Fe^{2+} can overcome quenching phenomenon by only activating a minimum of PS units able to produce adequate amount of SRs for SMX oxidation. This has been confirmed after spiking stepwise ($n = 6$) the SMX/PS solution by $120 \mu\text{L}$ of Fe^{2+} solution (equivalent in reactor to 0.372 mM) corresponding to a total of 2.23 mM by the end of the reaction. As it can be clearly seen from Fig. 1a, sequential addition of Fe^{2+} degraded only 20% of SMX the first 10 min of the reaction however, the degradation process continues with an almost constant rate reaching 80% of

degradation after 2 h of reaction. The same trend has also been noticed for PS loss into the solution as it appears in **Fig. 1b**. For example, a sudden loss of 260 μmoles of PS is noticed at 10 min after direct Fe^{2+} spiking while 510 μmoles and only 100 μmoles were consumed in Fe^0 and sequential Fe^{2+} -fed systems. The production of a high number of SRs (through direct Fe^{2+} spiking) in a very short time is responsible for the decrease in the degradation rate of SMX due to SRs quenching (**Eq. 9**). However, if Fe^{2+} is added sequentially, SRs are progressively produced resulting in greater SMX degradation rates. As for Fe^0 feeding, PS consumption is greater because of dual reactions occurring simultaneously: Direct reaction of PS with Fe^0 yielding no SRs production (**Eq. 10**) and reaction of PS with generated ICPs resulting in SRs production (**Eq. 2**). Moreover, ICPs released in solution include highly reactive iron oxides which play considerable role in gradual PS activation avoiding SRs quenching [50]. Furthermore, a calculation of the % average RSE over 30 min of reaction for all studied cases showed comparable values for Fe^{2+} /SMX/PS system in direct spiking (5.55%) followed by Fe /SMX/PS (5.20%) and Fe^{2+} /SMX/PS in sequential spiking (7.79%).(**Fig. 2**). The latter showed greater % RSE because Fe^{2+} was the limiting reagent compared to PS. In contrast, the % RSE for the direct Fe^{2+} spiking was lower since SRs quenching have occurred in a medium where Fe^{2+} is available in excess compared to PS. The similar % RSE (5.20%) noticed with Fe^0 activated system is not reflecting the real number of SRs produced and interacting with SMX molecule; otherwise we should have observed a similar decreasing trend for SMX in both cases (Fe^0 and direct Fe^{2+} spiking).

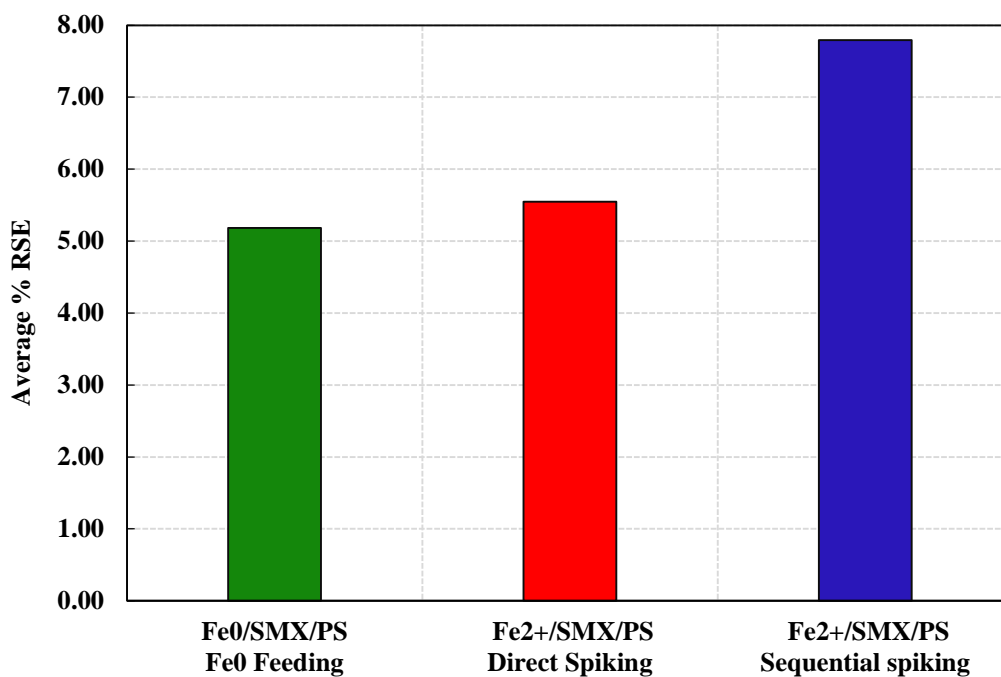


Fig. 2. Effect of direct vs sequential addition of Fe²⁺ compared to Fe⁰ in PS/SMX solution on average % RSE over 30 min of reaction. Experimental conditions: [SMX]₀ = 39.5 μM, [Fe²⁺] = [Fe⁰] = 2.23 mM, m (Fe⁰) = 2.5 mg, pHi = 5.63.

For this reason one can deduce that in Fe⁰ activated system more SRs are generated favoring thereby full SMX vanishing at early stage of the reaction compared to other systems. This might be due to synergetic effects based on the following: Oxidation reactions take place upon SRs and HRs generated (1) in homogenous medium (bulk solution) as well as in (2) heterogeneous environment at the surface of iron particles by the means of nascent iron oxides [103]. A catalytic mechanism in Fe⁰ fed system might be responsible for the total degradation of SMX and full consumption of PS after 30 and 60 min of reaction, respectively. In contrast, even though PS is not totally consumed in Fe²⁺ fed systems, SMX degradation was not complete with only 40 and 80% after 2 h of reaction. Accordingly, Fe⁰-based system is adopted for further

consideration with emphasis on the use of bimetallic and trimetallic iron-based systems as PS activators.

3. Effect of Iron Surface and Phosphate Buffer on the Degradation of SMX

Fig. 3 shows the effect of iron particle surface nature (acid washed or used as received / un-washed) on the degradation yield of SMX in the presence and in the absence of PS and PB at distinct pH values. As it is demonstrated that reactions with acid-washed MIPs (wFe/SMX) were more successful than those carried out with un-washed MIPs (nwFe/SMX). As an illustration, it was determined that 27% of SMX disappeared in wFe systems, in contrast to only 7% for nwFe systems. This may be attributed to the omnipresence of aged iron oxides on the surface of commercial MIPs making the oxide scale non-porous and consequently resistant to corrosion. There is a delay in the disappearance of SMX in nwFe/SMX/PS/PB as well as wFe/SMX/PS/PB systems compared to PB free systems. This is attributed to the different lag times taken by wFe and nwFe to corrode in the presence of phosphate species. As an illustration, only 12% of SMX was degraded after 20 min of the reaction in the nwFe/SMX/PS/PB in contrast to 72% in the wFe/SMX/PS/PB to yield finally comparable SMX removal rates at later stage. However, SMX degradation rate was less than that obtained in PS spiked PB free systems (wFe/SMX/PS and nwFe/SMX/PS). This is due to the deposition of phosphate species at the surface of MIPs hindering quick iron corrosion and sequestration/adsorption of SMX molecules into the iron oxides matrix covering the surface of iron particles. Moreover, this can also be attributed to the complexation

of iron (Fe^{2+}) species with phosphate which limits the free Fe^{2+} in solution responsible for PS activation. Actually, PB free systems such as wFe/SMX/PS and nwFe/SMX/PS were the most efficient in degrading almost 91% and 89% of SMX, respectively.

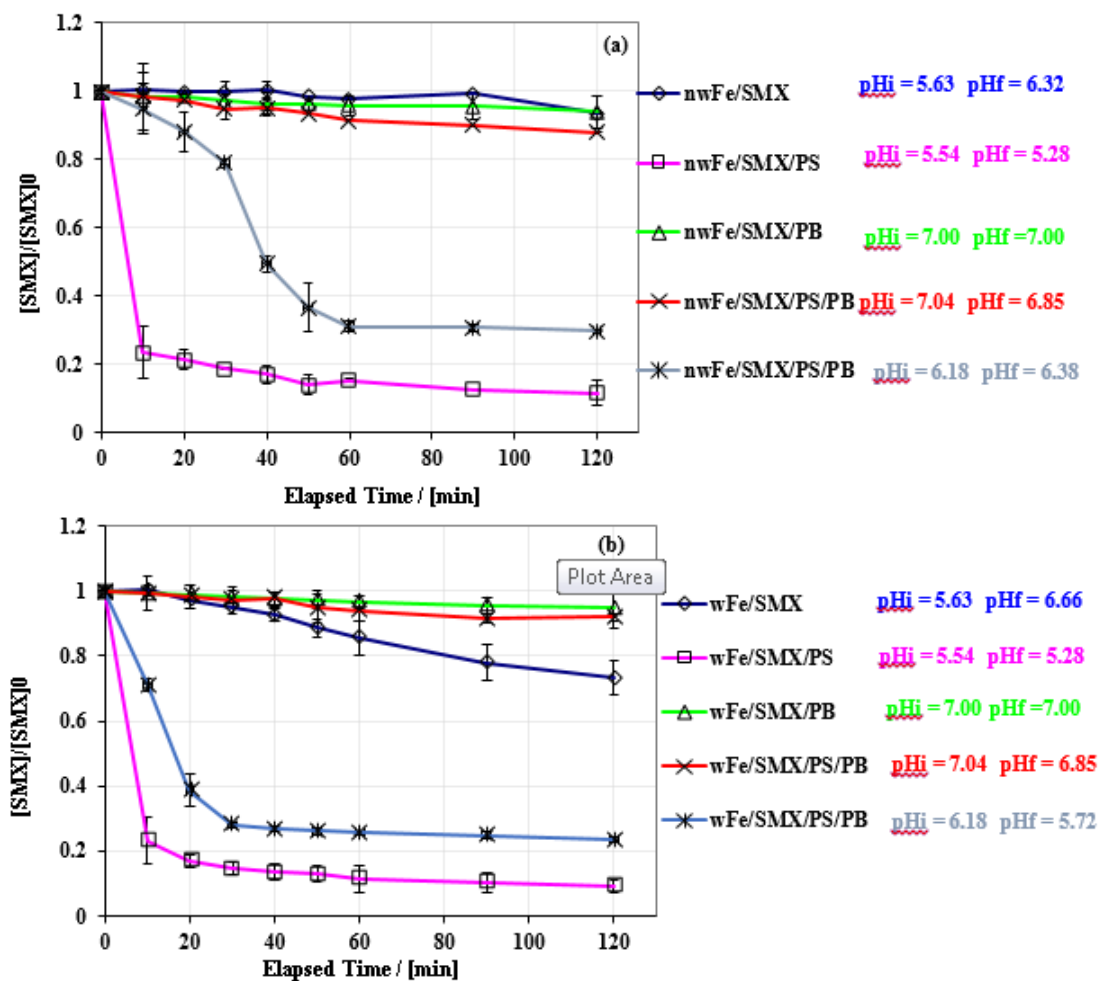


Fig. 3. Influence of MIPs surface and PB on the oxidation of SMX by PS. (a) MIPs used as received (nwFe for non-washed Fe), (b) acid-washed MIPs (wFe for acid-washed Fe). Experimental conditions: $[\text{Fe}^0] = 17.85 \text{ mM}$, $[\text{PS}]_0 = 1.0 \text{ mM}$, $[\text{SMX}]_0 = 39.5 \text{ }\mu\text{M}$, $[\text{PB}] = 1 \text{ mM}$. Solid lines are only used to connect data. Error bars represent uncertainties at a 95% confidence interval.

Such systems were accompanied by small pH change; the pH decreased from 5.54 to 5.28 assuring that using 1.0 mM PS concentration (in excess) was reasonable for SMX

degradation. On the other hand, the concentration of remaining PS showed complete consumption on PB free systems and at an early stage of the reaction (10 min) whereas, PS was partially consumed (45%) in PB systems even at the end of the reaction (e.g. 2 h). Accordingly, one can deduce that PS or derived SRs might have reacted with the iron-phosphate complexes yielding less SMX degradation, probably due to SRs quenching. PS remaining is in harmony with the steep decline in SMX curves for the first 10 min of reaction in wFe/SMX/PS and nwFe/SMX/PS systems followed by a moderate degradation rate till the end of the reaction (1 h). Such a slow rate might be due to the continuous action of nascent iron oxides formed upon MIPs corrosion after PS depletion into the solution. Nascent iron oxides are very active at the surface of MIPs and present high adsorption properties toward organic and inorganic species [9-11]. Eventually, these results imply that commercial iron can be used as received without prior conditioning in the presence or absence of phosphate species whose concentration might be significant in special effluents.

4. Iron Load Effect on SMX Degradation

A set of experiments was designed to optimize MIPs load for the degradation of SMX in nwFe/SMX/PS systems. The aim was to define a minimum amount of MIPs able to activate enough PS into SRs for SMX degradation without encountering radical quenching (**Eq. 9**) due to the presence of high concentration of iron species released into solution. Loads ranging from 0.05 to 1.0 g L⁻¹ correspond to a Fe⁰ concentration of about 0.89-17.85 mM. **Fig. 4** depicts the results obtained for a set of experiments. The

upper curve shows a control experiment carried out in the nwFe/SMX system with the highest MIPs load of about 17.85 mM in PS free system (**Fig. 4a**). The latter system didn't show any significant SMX degradation. However, a sudden decrease in the concentration of SMX happened at a different rate depending on the MIPs load in 1.0 mM PS systems. All SMX degradation curve are composed of two different parts (**Fig. 4a**). The first part shows a steep decline in SMX during the first 10 min of the reaction; whereas, the second part is distinguished by the slow decrease at different MIPs load with an asymptotic behavior. The first part can be explained by the oxidative action of SRs on SMX up to 10 min and for moderate iron loads (<4.46 mM) PS is not yet depleted (**Fig. 4b**) and produced upon Fe²⁺ release (**Fig. 4c**) a consequent number of SRs. Nonetheless, if SRs are in excess, radical-radical reactions occur (**Eq. 20**) decreasing the degradation rate.



For example, only 59% and 68% of SMX is removed after 10 min of reaction time with 17.85 and 8.92 mM of MIPs loads, respectively, while 76%, 73%, and 82% of SMX removal is noticed with lesser MIPs loads e.g. 4.46, 2.23, and 0.89 mM, respectively.

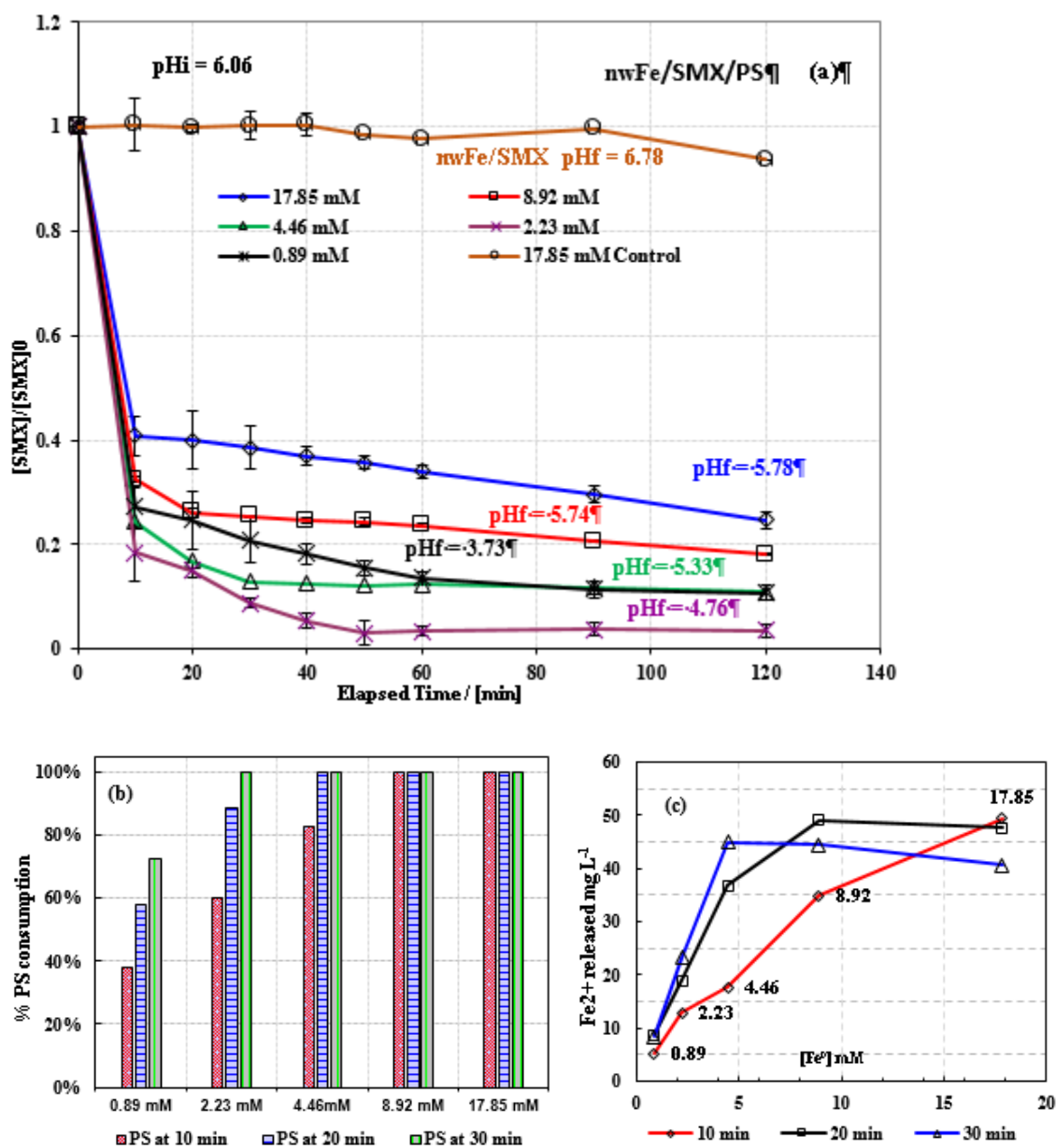


Fig. 4. (a) Influence of iron load on the oxidation yield of SMX in deionized water. (b) PS consumption at 10, 20 and 30 min of the reaction. (c) Concentration of total dissolved iron species into the reactor at 10, 20 and 30 min of the reaction. Experimental conditions: $[Fe^0] = 0.89-17.85$ mM, $[PS]_0 = 1.0$ mM and $[SMX]_0 = 39.5$ μ M. Solid lines are only used to connect data. Error bars represent uncertainties at a 95% confidence interval.

Fig. 4b depicts PS depletion particularly at high iron loads. For instance, after 20 min of the reaction, all PS was consumed for MIPs >4.46 mM. Only for MIPs load

with of 0.89 and 2.23 mM, PS consumption was partial. As an illustration, at 10 min of reaction 38%, 60%, and 83% of PS has been consumed for 0.89, 2.23, and 4.46 mM MIPs loads, respectively. Whereas, at 20 min, 58%, 89%, and 100% PS has been consumed for 0.89, 2.23, and 4.46 mM MIPs loads respectively. After half an hour of the reaction, all PS has been consumed and the system is only governed by the interaction of SMX molecules with MIPs surface, as well as generated ICPs.

Accordingly, the additional SMX removal (16.1% and 14.3%) observed for the highest MIPs loads (17.85 and 8.92 mM) from 10 min till the end of the reaction is only due to MIPs able to adsorb and sequester (at pH >5.0) SMX molecules into nascent iron oxides formed upon iron corrosion in oxic medium. However, for lesser iron loads, some of the PS remained unconsumed and contributed to additional SMX removal (e.g. 16.4%, 14.8%, and 13.4% for MIPs loads of 0.89%, 2.23, and 4.46 mM, respectively).

A survey of the concentration of the total iron species ($\text{Fe}^{2+/3+}$) produced in the reactors at early stages of the reaction e.g. 10, 20, and 30 min (**Fig. 4c**) confirmed that for higher loads, more $\text{Fe}^{2+/3+}$ is present, which may affect the performance of the PS activated systems in terms of SRs quenching (**Eq. 9**). For example, 50 mg L⁻¹ (892 μM) of $\text{Fe}^{2+/3+}$ was noted at 10 min of the reaction; whereas, 5 mg L⁻¹ (89.2 μM) were found at the lowest MIPs load (e.g. 0.89 mM). The concentration of $\text{Fe}^{2+/3+}$ reported here at 17.89 mM of MIPs load is greater than the one reported in the previous section (**Table 5**, system **3**) due to the fast shaking. This allowed more MIPs interactions, and therefore more iron oxide cracks, which increases the total iron content in solution. Accordingly, the metallic iron load in solution should be carefully chosen based on the corrosion

potential of the medium (e.g. specific surface area and particle size) as well as initial PS concentration. **Fig. 4c** also shows that linear relationship between MIPs loading and iron in solution (ICPs) is not likely to occur, especially at later stages of the reaction and for MIPs load >4.46 mM. This can be attributed to the solubility limit of iron species and to an equilibrium reached under experimental conditions. This is obvious on $\text{Fe}^{2+/3+}$ curves at 20 and 30 min where a maximum of iron concentration is reached followed by a steady state or even a slight decrease especially for iron loads greater than 4.46 mM. In the current case, the most performing system at 1.0 mM PS was the system issued with 2.23 mM of MIPs load. At this concentration, SMX degradation was the fastest until the end of the reaction (2 h) with 97% removal efficiency. However, with 0.89 mM, Fe^{2+} acted as a limiting reagent resulting in less PS activation efficiency. On the other hand, one should not ignore the direct reaction between PS and MIPs, which decreases the number of PS molecules available for the activation by Fe^{2+} and ICPs as well. A progressive release of Fe^{2+} should be maintained in solution in order to maintain PS activation with minimal radical quenching. These conditions are met under the experimental conditions of 2.23 mM MIPs load at a starting pH around 6.0. For this reason, PS activation will be tested under those conditions in order to optimize the conditions for the best % RSE.

5. Effect of PS Content on SMX Degradation.

Fig. 5a shows that SMX is more degraded at the highest PS load. For instance, 95% of SMX has disappeared after 2 h of reaction for 1.0 mM PS additive ; whereas,

only 50%, 69%, and 85% of SMX degradation was obtained with PS load of 0.4 mM, 0.6 mM, and 0.75 mM, respectively. Moreover, most of the SMX degradation have occurred at an early stage of the reaction (up to 20 min) followed by a steady state (asymptotic behavior) during which insignificant SMX degradation occurred. Such an observation can be attributed to the excessive PS activated at an early stage of the reaction (0-20 min) into SRs as revealed in **Fig. 5b** displaying the remaining PS concentration into the solution. PS was completely consumed after 20 min of reaction in all systems. This clearly explain the steady state of the SMX decline curves observed after 20, 30, 40, and 50 min of the reaction for 0.4, 0.6, 0.75, and 1.0 mM PS loads, respectively.

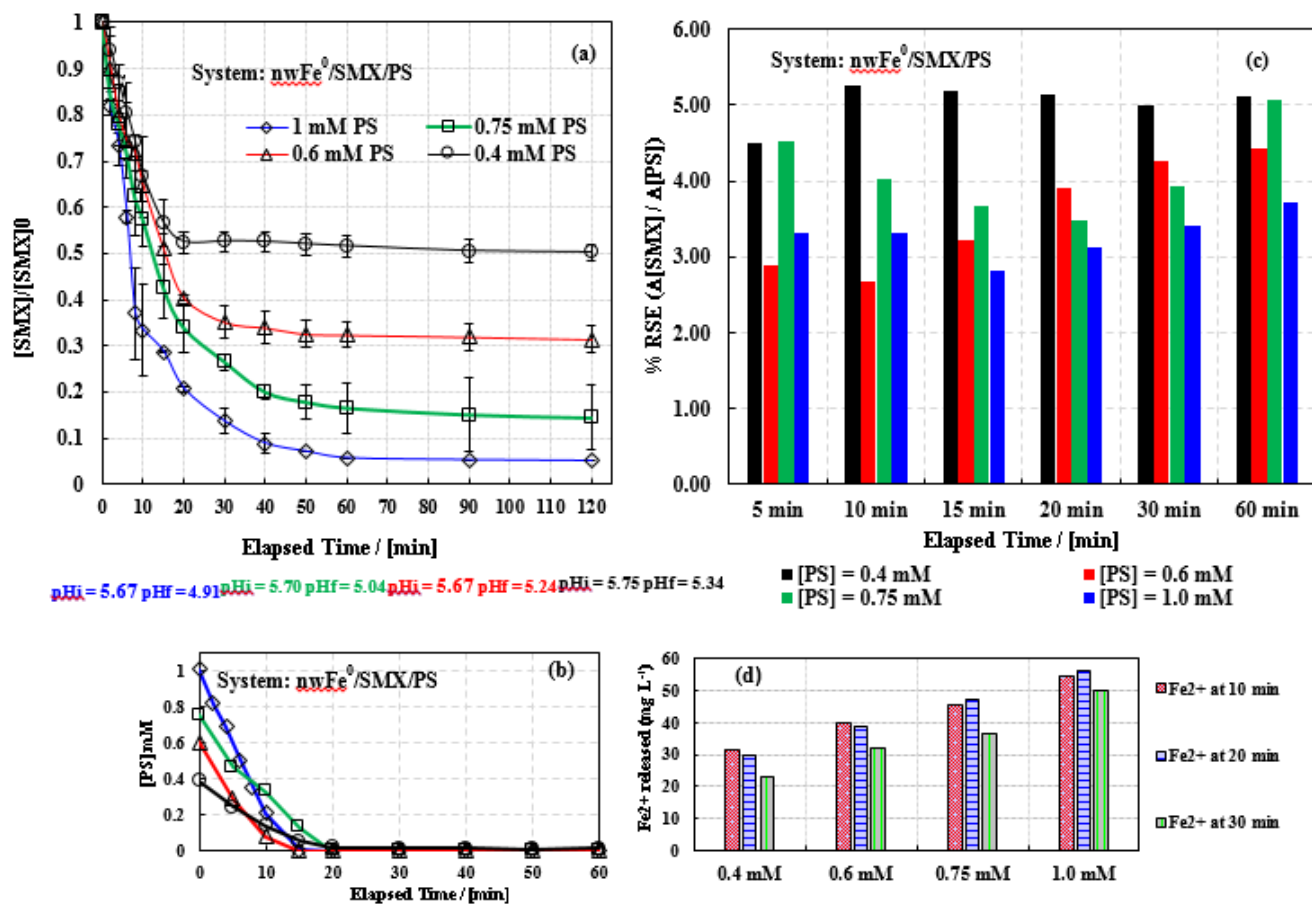


Fig. 5. (a) Influence of PS additives on the oxidative treatment of SMX in deionized water. (b) Time course of PS during the reaction. (c) The RSE relative to each PS concentration in Fig. 5a calculated at different reaction times (5-60 min). (d) Concentration of iron species (equivalent Fe²⁺) at after 10, 20 and 30 min of the reaction. Experimental conditions: [nwFe⁰] = 2.23 mM, [PS]₀ = 0.40-1.00 mM, [SMX]₀ = 39.5 μM. Solid lines are used to connect data. Error bars represent uncertainties at 95% confidence interval.

In order to better understand this observation in terms of SRs reactivity, the RSE was calculated for all PS concentrations used at different reaction times (5-60 min). **Fig. 5c** depicts the RSE averages (calculated for each PS load at all selected times 5-60 min) ranged between 3.28% and 5.03%; the highest RSE being for the lowest PS load (e.g. 0.4 mM), while the lowest RSE was noticed for the highest PS load (e.g. 1.0 mM). For the same initial MIPs content, the more ICPs were produced in systems having more PS additives upon direct reaction of PS with MIPs (**Eq. 10**). The corresponding results are presented in **Fig. 5d**. For example, the concentration of $\text{Fe}^{2+/3+}$ increased linearly from 31 to 55 mg L^{-1} after 10 min of the reaction when PS load increases from 0.4 to 1.0 mM given that the starting pH was 5.65. The same trend was also observed after 20 and 30 in of reaction time. Accordingly, more SRs was produced at higher PS loads due to the formation of Fe^{2+} activators. This favored radical- Fe^{2+} reaction (**Eq. 9**) and radical-radical reaction (**Eq. 20**) [85], and radical- H_2O reaction (**Eq. 5**) [104]. Nevertheless, for the less PS content (0.4 mM), fewer iron species are produced and thus less SRs are generated, which disfavors side reactions and increase the calculated RSE. The RSE values found in the current work are not comparable to RSE values found in thermally activated persulfate systems (e.g. Bisoprolol and ibuprofen) for the treatment of pharmaceuticals [74, 75]. For example, the minimum and the maximum RSE values reported after 1 h of 1.0 mM PS reaction with 50 mM bisoprolol were about 20% and 100% at 40 and 50° C of activation temperature, respectively. Whereas, the RSE reported in this work has a maximum of 3.7% for the same PS concentration and reaction time. The direct reaction between PS and MIPs is

in part responsible for the low RSE values obtained, but also the acidic medium ($5.67 < \text{pH} < 5.75$) which improves the iron corrosion and results in excess of ICPs that might quench SRs. As previously reported (**Eq. 9**), most of the SRs produced are quenched with an excess of Fe^{2+} species resulting for the rapid oxidation of MIPs especially under acidic conditions. This was confirmed by the final pH values (pH_f) being more acidic for the highest PS solution load (e.g. $[\text{PS}] = 1.0 \text{ mM}$). For example, the lowest and highest reported pH_f were 5.91 and 5.34 for SMX dissolutions containing initial $[\text{PS}]$ of about 1.0 and 0.4 mM, respectively. Recall that this pH decrease is due to of bisulfite formation (**Eqs. 5, 11**) and dissociation (**Eq. 12**). pH_f reported are usually greater than 2 unless an extremely high persulfate concentration is used [105, 106]. **Fig. 5c** also reveals that above a certain $[\text{PS}]$ limit (e.g. 0.4 mM), RSEs are almost comparable. Accordingly, one can conclude that MIPs content is the limiting factor and once controlled in terms of corrosion rate can contribute to longer PS lifetime and consequently sustainable SR generation into the solution. This will result in continuous SMX degradation instead of reaching a steady state where no more SMX degradation occurs. Further experiments were performed to evaluate the potential of the remaining oxidized MIPs and their corresponding ICPs activated by additional PS spiked at a later stage of the reaction. This was carried out by conducting successive experiments where different water matrices were tested.

6. Mineralization of SMX in $nwFe^0$ /SMX/PS System

A mineralization analysis was done on an SMX solution prepared in 40 mL reactor in order to have enough solution to conduct TOC measurements [107]. The reactants were set at the optimum concentrations previously determined e.g. $[SMX] = 39.5 \mu M$, $[PS] = 1.0 \text{ mM}$, $[Fe^0] = 2.23 \text{ mM}$. The theoretical TOC value of the solution was 4.74 mg L^{-1} and the experimental TOC value given by the instrument was about 4.79 mg L^{-1} . After 2 h of reaction, the solution was centrifuged and filtered giving a TOC content of 3.02 mg L^{-1} and a TOC removal of 37%. Such a value is similar and even exceeds those detailed in the literature for similar oxidation experiments at room temperature. For instance, the % TOC removal obtained by Vicente and collaborators [108] on $85.8 \mu M$ Diuron solution reached 27% and 45% at 20 and $50^\circ C$, respectively with $[PS] = 2.6 \text{ mM}$ and Fe^{2+} feeding (50 mg L^{-1}) instead of MIPs. Although, the experimental conditions are not comparable in terms of selected probes, PS concentration, temperature, ionic strength, iron content and iron feeding, thus one can deduce that SMX mineralization obtained through oxidation in $nwFe^0$ /SMX/PS system at room temperature is very encouraging.

B. Water Matrix Effect on SMX Degradation in Successive Degradation Cycles

Three different studies were conducted to study the effect of the water matrix on the performance of Fe/PS system used for the degradation of SMX using the optimized conditions previously reported. Case **1** consists of tap water ($G = 1146 \mu mhos/cm$); Case **2** corresponds to DI water ($G = 1.96 \mu mhos/cm$) and Case **3** consists

of underground water ($G = 490 \mu\text{mhos/cm}$). Each experiment consists of three cycles each of 1 h duration. Residual PS concentration was also monitored in all the cases.

1. Case 1 (Tap water)

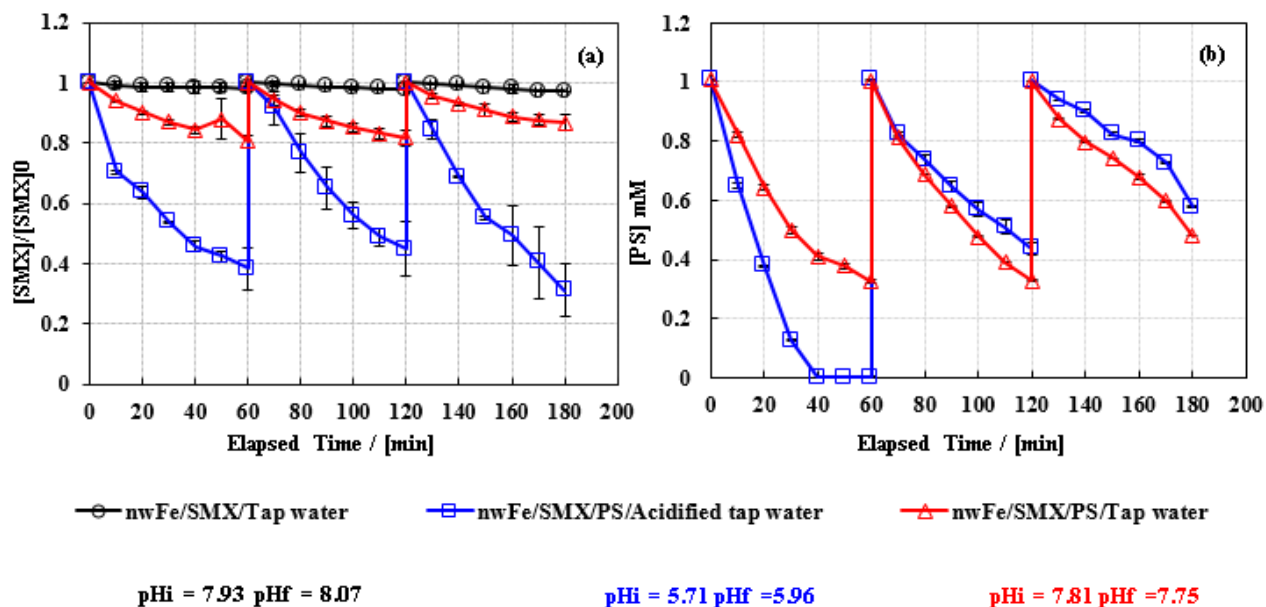


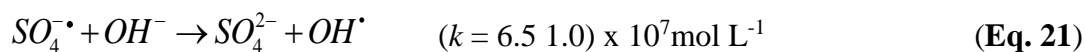
Fig. 6. (a) SMX degradation and (b) PS remaining after repetitive oxidation cycles in tap water matrix. Experimental conditions: $[\text{nwFe}^0] = 2.23 \text{ mM}$, $[\text{PS}]_0 = 1.0 \text{ mM}$, $[\text{SMX}]_0 = 39.5 \mu\text{M}$. Solid lines are not fitting functions, they are only used to connect data. Error bars represent uncertainties at 95% confidence interval.

Fig. 6a shows that nwFe/SMX/tap water is not efficient in removing SMX.

Insignificant loss in SMX concentration was reported for the three successive cycles.

This is due to (i) the absence of PS and SRs precursor and (ii) the low load of MIPs used (2.23 mM) which is not ample to impose any reduction and/ or co-precipitation of SMX. Furthermore, the basic pH of the tap water ($\text{pH}_i = 7.93$) doesn't favor MIPs oxidation as well as the formation of ICPs responsible for SMX elimination. A slight

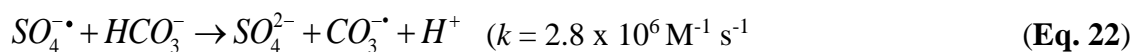
increase in the pH of the resulting solution was anticipated (pH_f = 8.07) which correlates with iron oxidation and thus the formation of hydroxide species. Whereas, in the nwFe/SMX/PS/tap water system, SMX degradation yielded 20% for the first two cycles and 16% for the third cycle. This small percent degradation of SMX is attributed to the poor release of ferrous ion species into the solution due to initial basic pH of the reactor (pH_i = 7.81). The occurrence of iron oxidation at slightly basic pH results in the release of Fe²⁺ into the solution and therefore PS activation occurs. Consequently, a drop in the pH was detected from pH_i = 7.81 to pH_f = 7.75 due to the formation of bisulfite species (*HSO₄⁻*) (**Eqs 5, 11**). **Fig. 6b** depicts PS consumption which reveals 70% consumption by the end of the second cycle and about 58% by the end of the third cycle. This incomplete consumption suggests that most of the SRs have interacted with foreign species present in the tap water including *OH⁻* resulting in lesser SMX degradation. (**Eq. 21**) [79].



In order to highlight the contribution of the basic pH of the starting solution in the small degradation yield of SMX, 5 µL of the concentrated HCl was added to the reactor to obtain a pH of 5.71. The resulting system (nwFe/SMX/PS/acidified tap water) augmented SMX degradation to about 60%, 58%, and 70% for the first, second, and third cycle, respectively. The residual PS remaining at the end of first, second, and third cycle was about 0%, 40%, and 60%, respectively resulting in faster PS

consumption in acidic pH particularly during the first cycle. (**Fig. 6b**). During the run term cycles, PS consumption have decreased due to less Fe^{2+} species available in solution after MIPs depletion. Moreover, SMX degradation yield was less than that obtained in DI water matrix under the same conditions. This can be attributed to some species present in tap water which are responsible for SRs and OH^\bullet quenching. For example, carbonate species known for their reaction with sulfate and hydroxyl radicals at considerable reaction rate constants (**Eqs 22, 23**) [70, 109].

In order to ascertain this assumption, further experiments were done in DI water, but they were saturated with bicarbonate at concentration dose close to the one encountered in drinking and underground water (e.g. $[NaHCO_3] = 160 \text{ mg L}^{-1}$).



2. Case 2 (DI water)

The same recycling experiments performed in case 1 are repeated, but this time by using DI water instead of tap water. **Fig. 7a** exhibits similar behavior for nwFe/SMX/PS/DI/Bicarbonate to those reported in Case 1 (e.g. nwFe/SMX/PS/tap water). As an illustration, 20%, 16%, and 10% of SMX was degraded during the first, second, and third cycle, respectively. The decrease in pH from 8.26 to 7.00 confirms the activation of PS into SRs after iron corrosion; although, the pH is slightly basic. PS consumption was also 80%, 60%, and 58% as well for the first, second, and third cycle,

respectively (**Fig. 7b**). Nonetheless, better SMX degradation was achieved in nwFe/SMX/PS/DI system where SMX degradation have reached 90% for the first and second cycle; whereas, 20% degradation for the third cycle. The latter behavior was most probably due to MIPs depletion at the end of the third cycle. In order to assure this hypothesis, PS remaining was monitored (**Fig. 7b**); and it has been depicted that PS was completely consumed at 20 min of the reaction time and 90% consumption at 60 min of the second cycle and 17% by the end of the third cycle. The high SMX degradation yield is attributed to the suitable starting pH (pHi = 5.66) which is responsible for the MIPs oxidation into Fe²⁺ which in its turn contribute to PS activation.

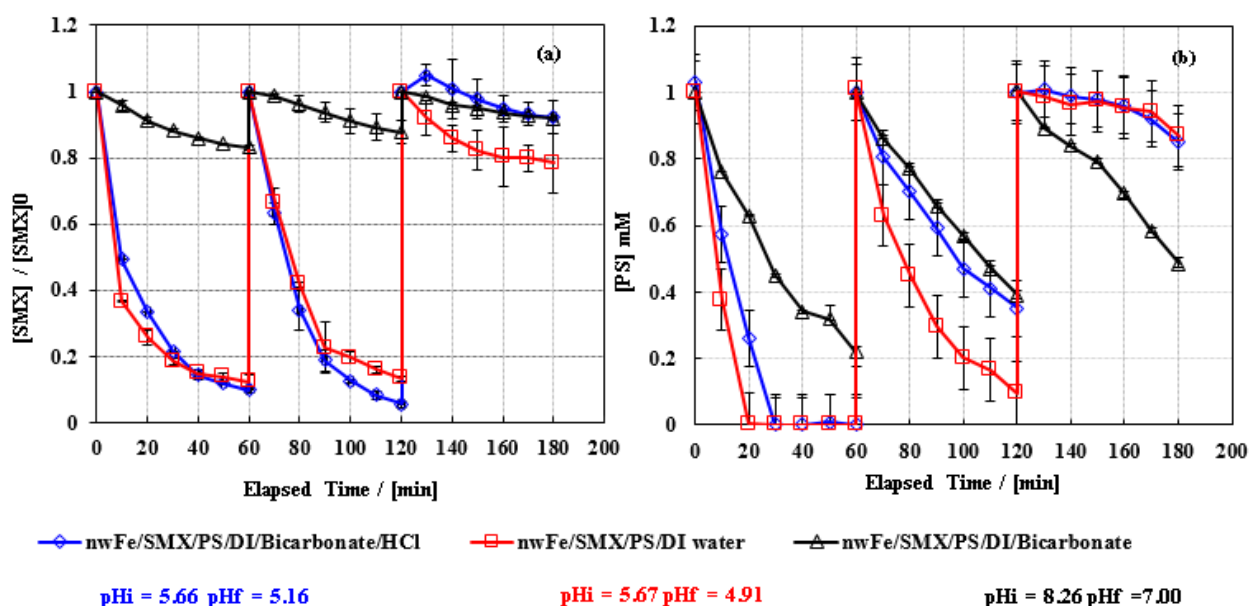


Fig. 7. (a) SMX degradation and (b) PS remaining after repetitive oxidation cycles in DI water matrix. Experimental conditions: [nwFe⁰] = 2.23 mM, [PS]₀ = 1.0 mM, [SMX]₀ = 39.5 μM. Solid lines are not fitting functions, they are only used to connect data. Error bars represent uncertainties at 95% confidence interval.

To assure that bicarbonate are the primary species responsible for SRs and HOs quenching, the nwFe/SMX/PS/DI/Bicarbonate was acidified by adding 5 μ L of concentrated HCl to obtain a starting pH of 5.66, which is the same as the pH of DI water. The results depicted in **Fig. 7b** are similar to those obtained in nwFe/SMX/PS/DI system. The value of the starting pH (5.66) being less than the pK_1 of carbonic acid ($pK_1 = 6.4$ and $pK_2 = 10.3$); therefore, most of the carbonate species were in the form of H_2CO_3 that will dissociate into H_2O and CO_2 and thus escaping from the solution. Consequently, the generated SRs and CO_2 will react with SMX without being quenched. However, the minimal SMX degradation in the third cycle (5% only) is due to the depletion of the MIPs hastily by the end of the second cycle; confirming the role of HCl in the quick MIPs dissolution.

3. Case 3 (Underground water, UGW)

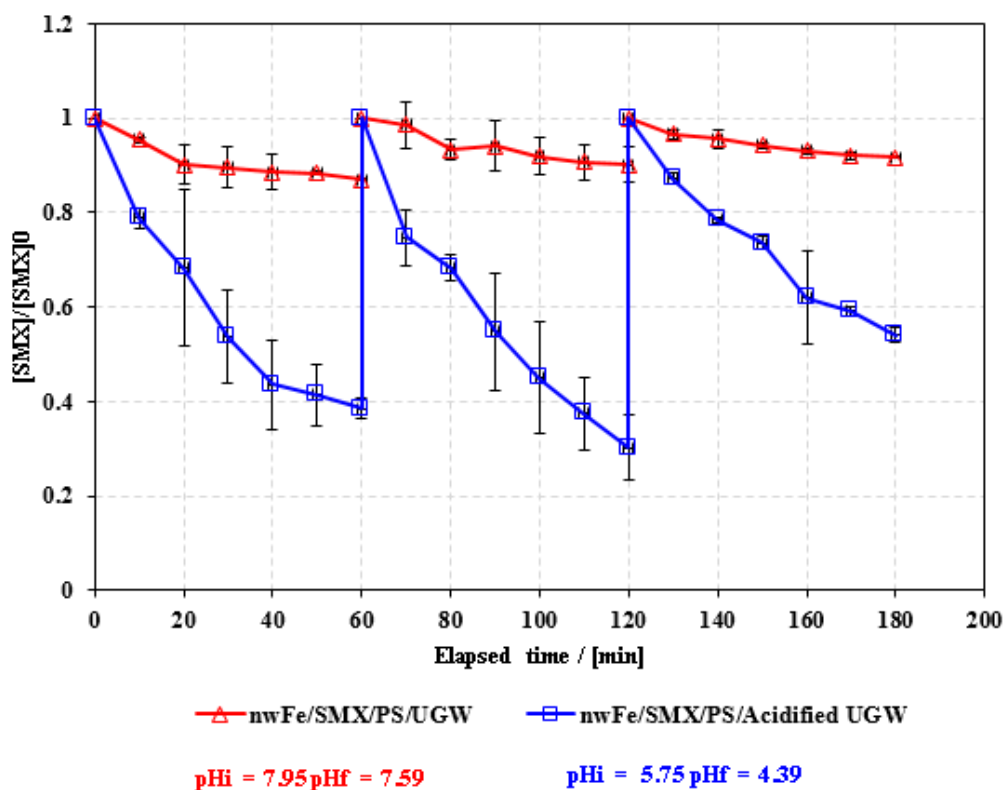


Fig. 8. SMX degradation after repetitive oxidation cycles in an UGW matrix. Experimental conditions: $[\text{nwFe}^0] = 2.23 \text{ mM}$, $[\text{PS}]_0 = 1.0 \text{ mM}$, $[\text{SMX}]_0 = 39.5 \text{ }\mu\text{M}$. Solid lines are not fitting functions, they are only used to connect data. Error bars represent uncertainties at 95% confidence interval.

Experiments similar to those conducted in Case 1 and Case 2 were undertaken, but in UGW. The latter has a pH of 8.05 and was collected from an aquifer, through a well at a depth of 300 m by means of a pump at a 313 m altitude (Position given by google earth: 34° 08' 56.58''N 35 °40'37.22''E). After dissolution of SMX, the new pH dropped slightly to 7.95. Two systems were tested in Case 3. The first (nwFe/SMX/PS/UGW) was carried out without pH adjustment; whereas, the second system (nwFe/SMX/PS/acidified UGW) with pH adjustment by adding 5 μL of

concentrated HCl to the starting solution. As seen in **Fig. 8**, the results of the nwFe/SMX/PS/UGW system showed an SMX degradation yield of about 17%, 10%, and 8% for the first, second, and third cycle, respectively. These results are close to those obtained with the nwFe/SMX/PS/DI/Bicarbonate system (Case 2). The similarity among results reveals the common content of UGW and bicarbonate enriched DI water in bicarbonate species at slightly basic pH. Nonetheless, once the system nwFe/SMX/PS/UGW is acidified, it results in greater SMX degradation yield of about 62%, 71%, and 43% at the end of first, second, and third cycle, respectively. These results are close to those obtained in the Case 1 study with the nwFe/SMX/PS/acidified tap water. Another essential phenomena in **Fig. 8** is the continuous reactivity of PS leading more SMX degradation. This can be attributed to the omnipresence of MIPs which are not totally dissolved in acidified UGW during the first two cycles. This is also the case in the nwFe/SMX/PS/ acidified tap water system (**Fig. 6**) where PS remained efficient till the third cycle; whereas, in Case 2 (nwFe/SMX/PS/DI system) the activity of PS was terminated by the end of the second cycle due to the consumption of MIPs by the end of the second cycle. This is advantageous in terms of application of nwFe/SMX/PS systems to natural effluents which have almost the same composition to the components present in tap water and UGW and far away from that DI water which is exempted from inorganic species.

C. Effect of Iron Ageing on SMX Degradation and its Transformation Product

1. SMX Case in *nwFe*/SMX/PS System

$\text{Fe}^0/\text{H}_2\text{O}$ system was inefficient in removing SMX in a reasonable time and acceptable MIPs loads. Therefore, three systems (1-3) were tested to investigate the possibility of making the $\text{Fe}^0/\text{H}_2\text{O}$ system more efficient after PS feeding. **Fig. 9** shows the SMX solutions treated with *nwFe*⁰ particles (100 mg Fe^0 /20 mL SMX solution; $[\text{Fe}^0] = 89.2 \text{ mM}$) for 2 h (Zone A). Henceforth, the solutions were treated in three different ways (Zone B in **Fig. 9**) prior being fed by an appropriate volume of PS ($[\text{PS}] = 1.0 \text{ mM}$) as follows:

For system **1**: the resulting solution was immediately spiked with PS without prior magnetic filtration. For system **2**: the 20 mL vial was placed on magnet so that MIPs settle down at the bottom of the reactor. Thereafter, the solution was transferred via a 1.0 mL syringe to a new reactor. For system **2**, the resulting magnetically filtered solution was spiked with 1.0 mM PS solution simultaneously spiked with 2.5 mg *nwFe*⁰ particles corresponding to 2.23 mM. For system **3**, the magnetically filtered solution was only spiked with PS (1.0 mM). The aims of the former experiments were to: (i) used/oxidized MIPs (*uFe*⁰) in the original solution are able to activate PS even at high load (system **1**); (ii) less fresh *nwFe*⁰ (in our case 2.5 mg compared to 100 mg) can rapidly activate the PS under the same conditions (system **2**) and (iii) dissolved ICPs are capable of sustaining PS activation into SRs (system **3**). Results depicted in **Fig. 9** show that SMX degradation have reached only 18% after 2 h of reaction for an iron load of 89.2 mM (Zone A).

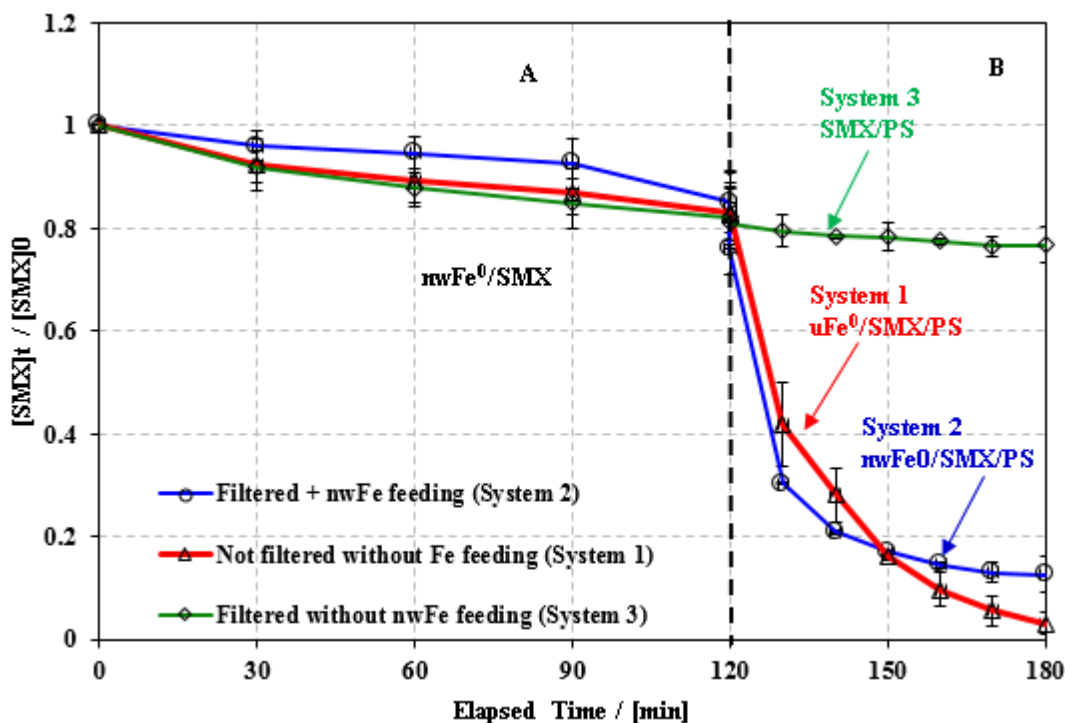


Fig. 9. Time course of SMX in Fe^0 and Fe^0/PS systems. Zone A is a PS free system. Zone B corresponds to PS-spiked systems. System 1 is made of the resulting solution at 120 min of reaction time to which 170 μL of PS is added with $[\text{PS}]_0 = 1 \text{ mM}$. System 2 is similar however after magnetic filtration of the resulting solution at 120 min of reaction time and addition of 1.6 mg of nwFe^0 so as to obtain $[\text{Fe}^0] = 2.23 \text{ mM}$. System 3 is similar to system 2 however without any Fe^0 addition.

System 1 showed complete SMX degradation 97% after PS spiking; most of which have occurred during the first 10 min (60%) of spiking. System 2 which was spiked by PS after the magnetic filtration followed nwFe^0 supply has also revealed significant SMX degradation (88%) by the end of the treatment (180 min). On the other hand, system 3 was less reactive toward SMX degradation which showed only 24% removal at the end of the reaction. This can be explained by the non-activation of PS into SRs due to the absence of Fe^{2+} species and other ICPs. In both systems 1 and 2, it is expected that SRs are produced and most of them are involved in SMX degradation; however, self-quenching reactions are likely to occur especially if excess of dissolved

Fe (II) species are present into the solution (system 1). This was accompanied by the appearance of transformation product at 5.7 min, which can be seen in the chromatograms presented in **Fig. 11**. The difference between systems 1 and 2 in terms of SMX removal is not significant; nonetheless, the chromatograms revealed the following: In system 1, one can notice the appearance of transformation product whose concentration increased as long as the treatment duration continued (up to 180 min, **Fig. 11b**). However, system 2 is not accompanied by the appearance of any transformation product along with SMX degradation. This can be explained as follows: in system 1, PS additive reacted with a large excess of Fe⁰ particles after activation into SRs. During the first 2 h of Fe⁰ treatment, the surface of iron particles is mostly oxidized and covered by an imperious layer (non-diffusive). However, after reaction with PS, MIPs become clean with lesser oxide layer. This makes the oxide scale diffusive thereby allowing SMX adsorption and transformation into SMX derivative compound before being released again into the solution. This observation is obvious in **Fig. 11b** in which all SMX has disappeared with the elution of the transformation product at 5.7 min. In contrast, for system 2, MIPs load was much less (2.5 mg). Accordingly, SRs are not quenched by an excess of Fe²⁺ in solution but directly reacted with SMX molecules. The outcome of the latter reaction is non-stable intermediate that also undergo oxidative reaction by SRs as well. Moreover, the intermediate was also undetectable (in system 2) while in system1, its presence was obvious with maximum concentration. As for system 3, the presence of SMX transformation product at 5.7 min was insignificant.

2. SMX Transformation Product Case in nwFe⁰/SMX/PS System

To determine whether PS additive destroyed SMX transformation product or if Fe⁰ alone was involved, two experiments (systems **4** and **5**) were performed in parallel with an extended reaction time up to 240 min. At the early stages, the experimental procedure was similar to that of system **1** described in previous section. However, in system **4** and at 180 min of reaction time (end of zone **B**) the resulting solution was magnetically filtered, spiked with PS, and supplied with nwFe⁰ particles (2.23 mM). In system **5**, the resulting solution was filtered and spiked with PS without the addition of nwFe⁰ particles at 180 min.

Fig. 10 shows that SMX transformation product, stable in Fe⁰ solution, was completely degraded after PS addition. This have occurred in an early stage of spiking between 180 and 200 min of reaction time and on **Fig. 11c** where a rapid vanishing of the corresponding chromatographic peak at Rt = 5.7 min occurred. As for system **5**, SMX transformation products exhibited partial disappearance to an extent of 58% of its maximum at 180 min. This can be explained by the action of some SRs produced after activation of PS by some residual Fe²⁺ remaining in solution. The final chromatogram reveals the appearance of two peaks between 4.2 and 5.6 min. Those peaks are almost stable in terms of chromatographic areas and not clearly resolved. In addition, their UV/Vis and MS spectra was not clear for further investigation. Accordingly, efforts were done in order to understand the mechanism behind SMX degradation. This was performed by studying the MS spectra of the main transformation product.

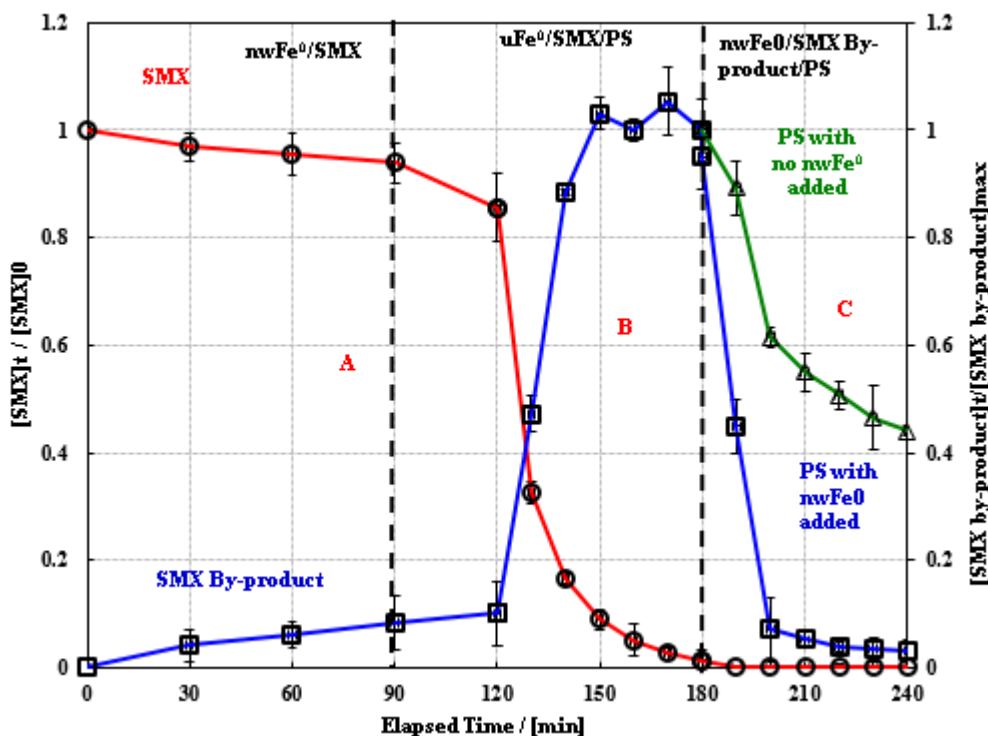


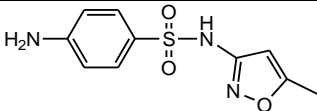
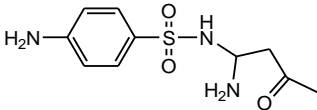
Fig. 10. Time course of SMX and its transformation product during treatment in $\text{Fe}^0/\text{SMX}/\text{PS}$ system. Zone A corresponds to wFe^0/SMX system. Zone B corresponds to $\text{uFe}^0/\text{SMX}/\text{PS}$ (u: used) system in which PS was added to the resulting solution of Zone A; Zone C corresponds to SMX by-product/PS system in which the resulting solution of Zone B was magnetically filtered, spiked with PS and supplied or not with nwFe^0 . Experimental conditions: Zone A $[\text{nwFe}^0] = 5 \text{ g L}^{-1}$, $[\text{SMX}]_0 = 39.5 \text{ }\mu\text{M}$; Zone B: $[\text{PS}]_0 = 1.0 \text{ mM}$; Zone C: $[\text{nwFe}^0] = 0.1 \text{ g L}^{-1}$ for the upper curve, $[\text{nwFe}^0] = 0 \text{ g L}^{-1}$ for the lower curve, $[\text{PS}]_0 = 1.0 \text{ mM}$.

D. Identification of Transformation Product, Structure Elucidation and Proposed Reaction Pathway

LC-MS and LC-MSⁿ analysis done on SMX and its transformation product. As seen in **Fig. 11** and **Table 7**, the MS spectrum of SMX presented a molecular ion $[\text{M}+\text{H}]^+$ at 254 m/z in positive ionization and a molecular ion $[\text{M}-\text{H}]^-$ at 251.8 m/z in negative ionization mode. Whatever mode was used, a 155.9 m/z fragment has appeared that corresponds to the loss of the $\text{C}_4\text{H}_6\text{N}_2\text{O}^+$ moiety. These results corroborated those obtained in previous investigations on the removal of SMX via

microbially mediated abiotic transformation under iron-reducing soil conditions [110]. Different fragments were also identified after MS² and MS³ analysis as reported in **Table 7**. The transformation product eluted at 5.7 min was determined to be b-aminoenone SMX derivative after studying its MS spectrum. This transformation product showed a molecular ion [M+H]⁺ at 256 m/z in positive ionization and a molecular ion [M-H]⁻ at 251.8 m/z in negative ionization mode. The increase by 2 amu in the mass of an organic compound upon chemical reaction in an aqueous acidic environment is an indicator of hydrogenation. However, in oxidative medium (PS/H₂O system) hydrogenation is not plausible; whereas, in reductive medium (Fe⁰/H₂O system) hydrogenation is feasible [92].

Table 6. MS and chromatographic characteristics of SMX and its transformation product after reaction in Fe0/SMX/PS system.

Product	λ_{\max} (nm)	[M+H] ⁺ (m/z) ^a	[M-H] ⁻ (m/z) ^b	+MS/MS (m/z)	-MS/MS (m/z)	+MS ³	-MS ³	Proposed Structure ^d
SMX	200, 262	254	251.8	188 155.9 ^c 147 108 92.2	155.6 ^c 91.9	254→155.8	251.8→155.9	
SMX transformation product	200, 270	256	253.8	214 ^c 173 155.9 101.2 83.8	170.8 ^c , 82.1	256→214	253.8→170.8	
						108, 92.1, 80.3	107.8, 91.9, 64.2	
						196.9, 155.9 ^c , 140, 121, 106, 75.4	106.8, 79.9 ^c , 64.3	

^aMass for pseudo molecular ion formed by protonation of the neutral molecule shown in the structure.

^bMass for pseudo molecular ion formed by deprotonation of the neutral molecule shown in the structure.

^cIndicate most abundant fragment ion in MS² and/or MS³ spectrum.

^dStructural interpretations of MS² and MS³ fragments provided in Table 8.

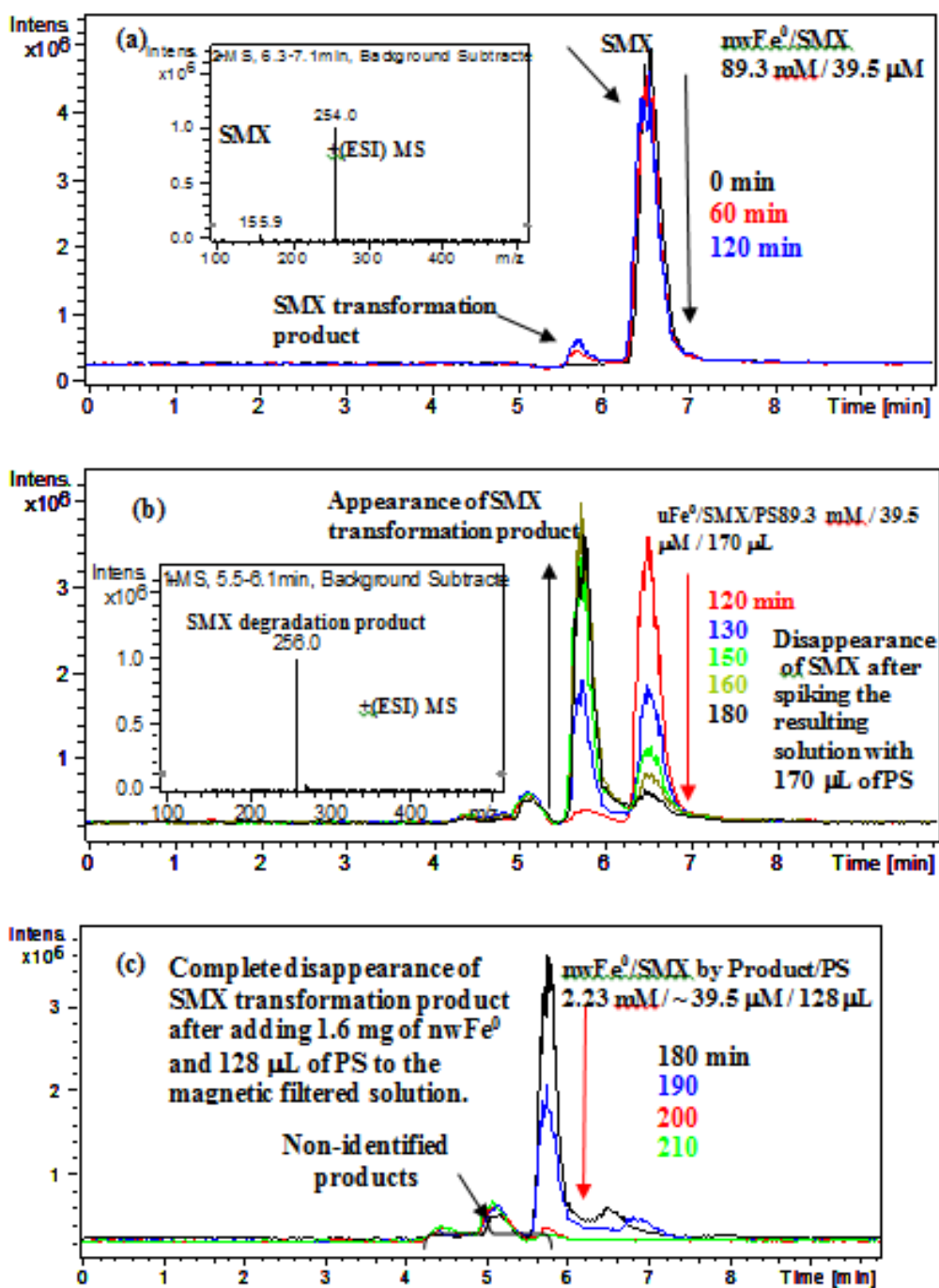
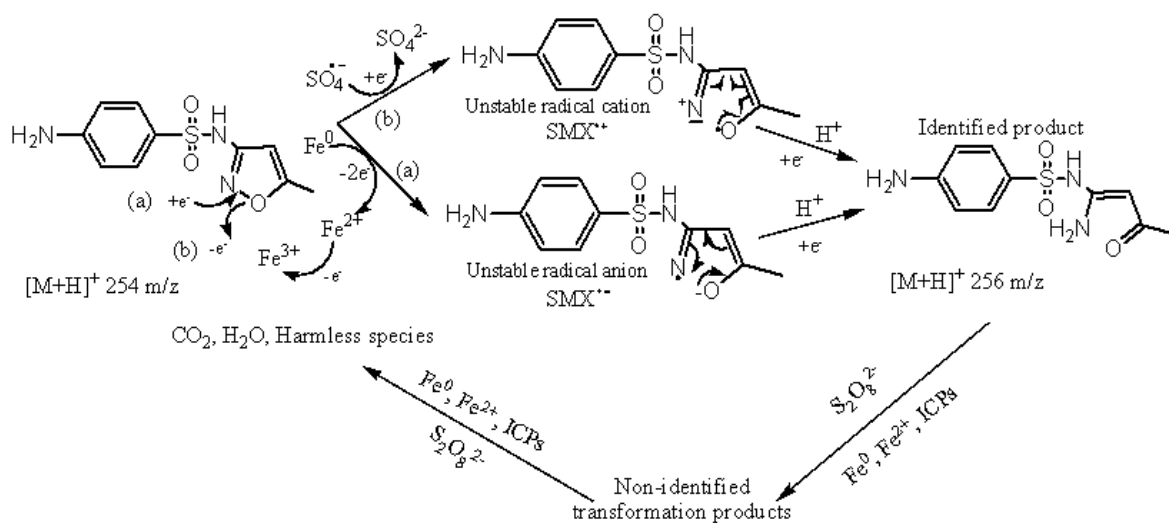


Fig. 11. LC-MS total ion chromatograms of SMX solution (20 mL) treated with nwFe⁰ and PS. (a) nwFe⁰/SMX system, [Fe⁰] = 89.2 mM, [SMX]₀ = 39.5 μM. The inset is the MS spectrum of SMX obtained in (+) ESI. (b) uFe⁰/SMX/PS system: the resulting solution was spiked with 170 μL PS at 120 min. The inset is the MS spectrum of SMX transformation product obtained in (+) ESI and eluted at 5.8 min. (c) nwFe⁰/SMX/PS system: the resulting solution (17 mL) was magnetically filtered, spiked with 128 μL PS and supplied with 1.6 mg of nwFe⁰ (2.23 mM).

Accordingly, one might expect isoxazole ring opening yielding 4-amino-N-(1-amino-3-oxobut-1-enyl) benzene sulfonamide through two different routes: (1) by electron abstraction upon SRs attack [57] and thus the formation of unstable radical cation ($\text{SMX}^{+\bullet}$) followed by electron acceptance from MIPs in acidic medium; (2) by electron addition originated from Fe^0 surface yielding the formation of an unstable radical anion ($\text{SMX}^{\bullet-}$) that will be converted into the same transformation product upon protonation as shown in the mechanism of **scheme 2**.



Scheme 2. Proposed degradation mechanism of SMX in (a) $\text{Fe}^0/\text{H}_2\text{O}$ and (b) $\text{Fe}^0/\text{PS}/\text{H}_2\text{O}$ systems at room temperature.

MS^2 and MS^3 analysis in (-) and (+) ionization mode confirmed the loss of respective moieties yielding fragments for which significant abundances were present (**Fig. 12, 13**).

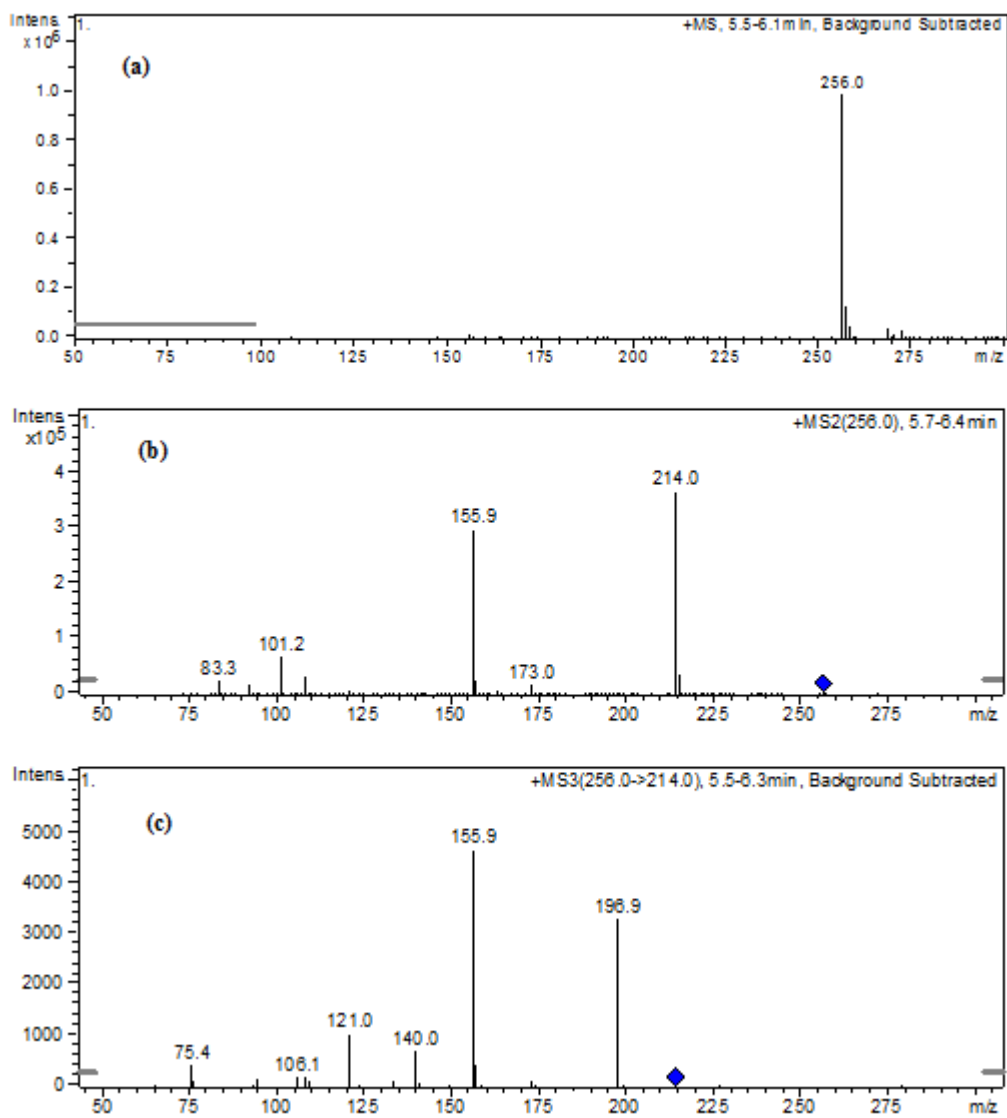


Fig. 12. (a) MS, (b) MS/MS and (c) MS³ spectra of SMX transformation product (positive ionization).

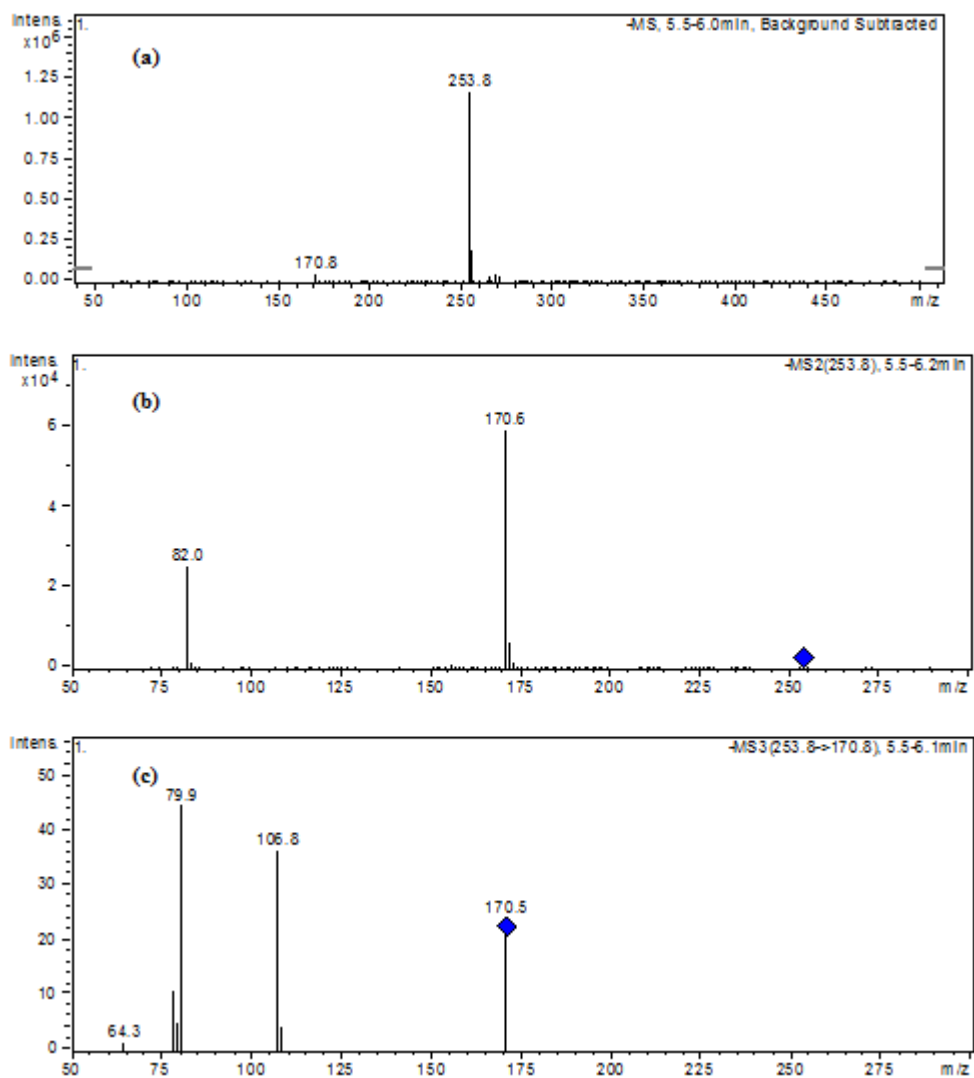


Fig. 13. (a) MS, (b) MS/MS and (c) MS³ spectra of SMX transformation product (negative ionization).

Our findings were also confirmed by UV/Vis absorbance of SMX transformation product as demonstrated in **Fig. 14**. The latter showed a bathochromic shift from 262 to 270 nm corresponding to lesser transition energy of the transformation product that might be due to the formation of carbonyl and primary ammonium groups [107].

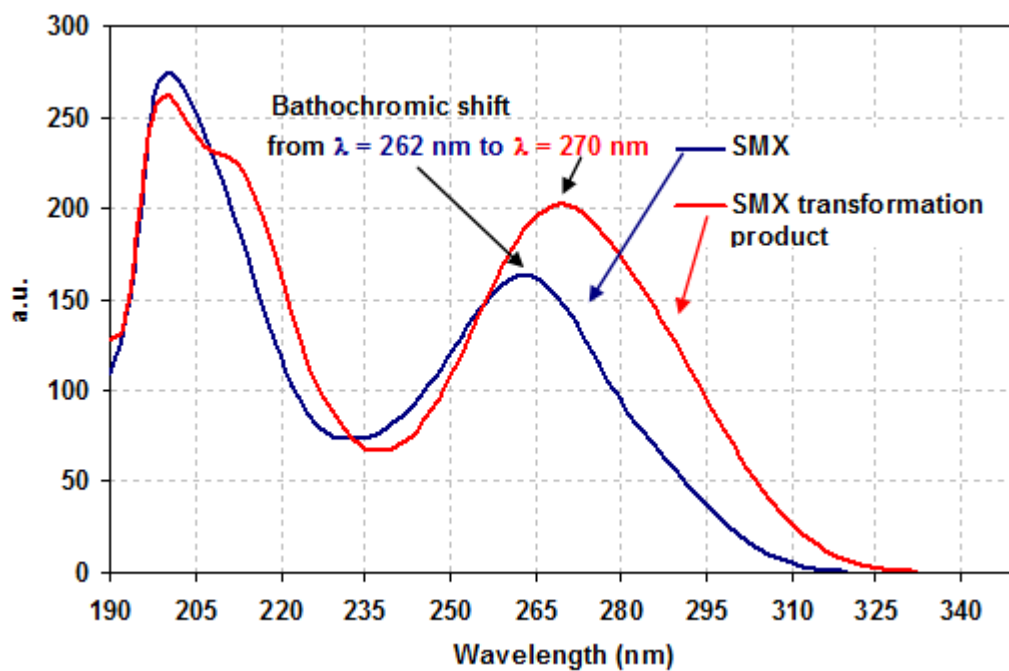
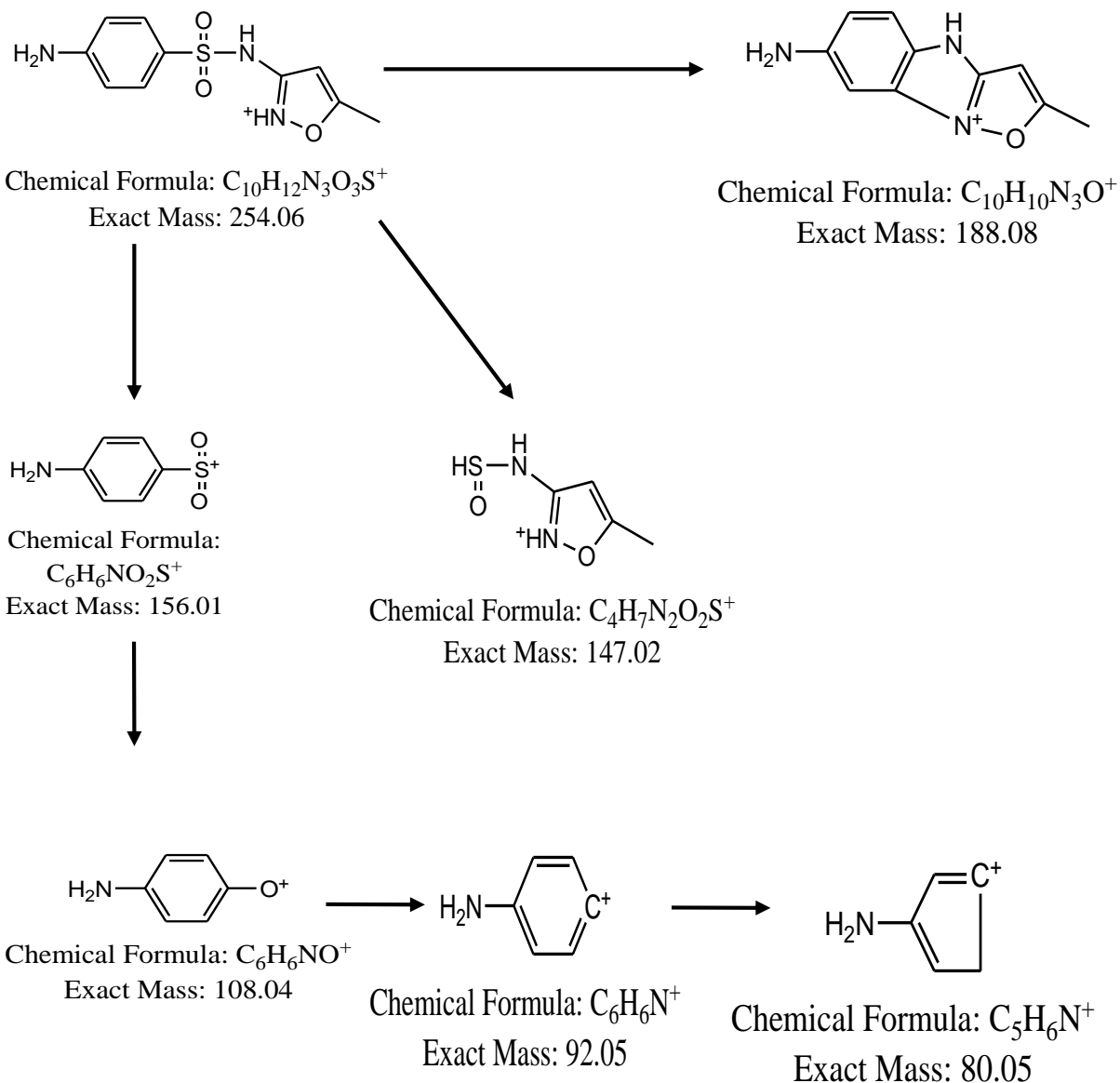


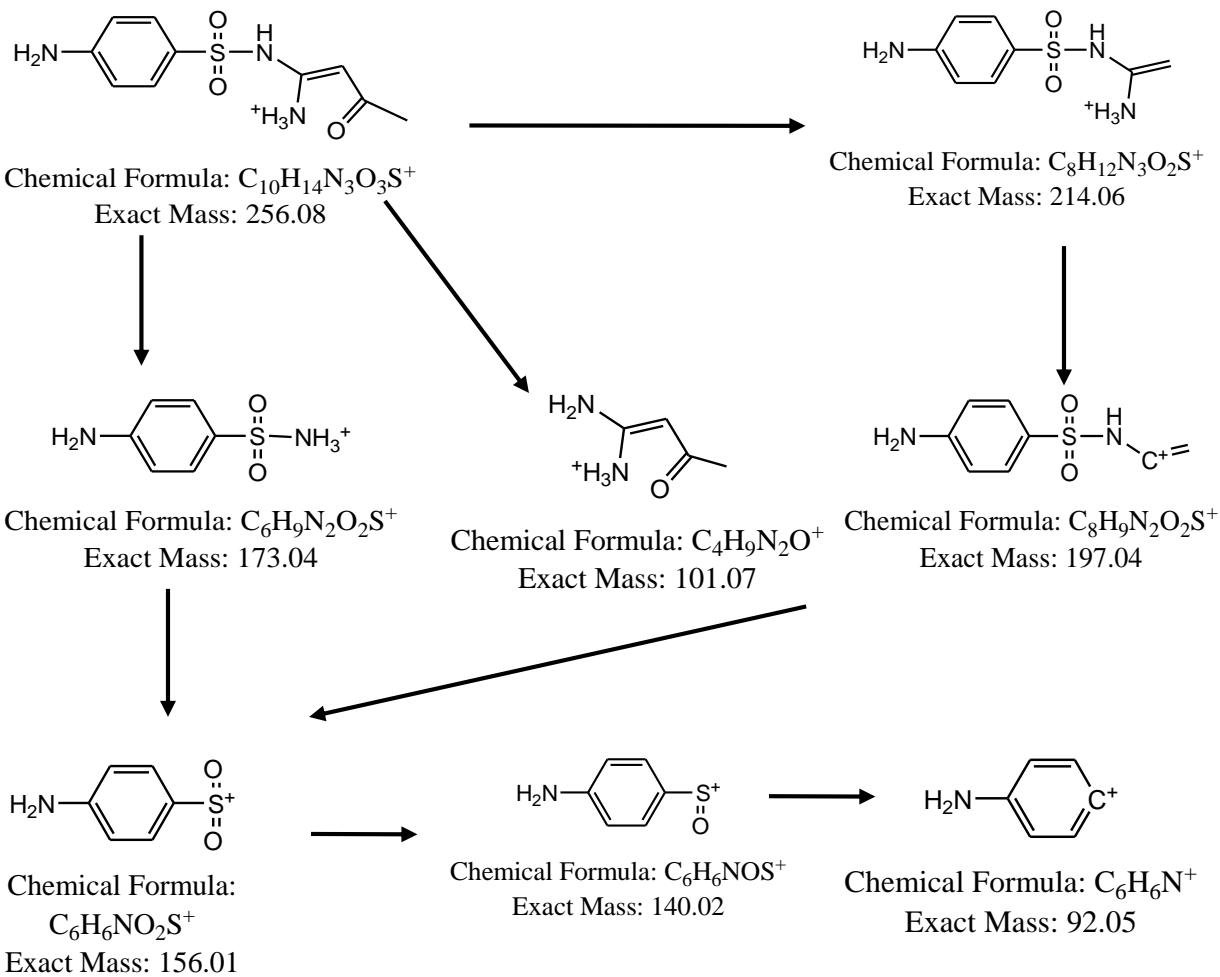
Fig. 14. UV/Vis absorbance spectra of SMX and its transformation product showing bathochromic shift from 262 nm to 270 nm.

Table 7. Structural interpretation of LC-MS/MS and LC-MS3 fragmentation data obtained for SMX and its transformation product in Fe0/SMX/PS system.

SMX



SMX transformation product



CHAPTER IV

ASSESSMENT OF BIMETALLIC AND TRIMETALLIC IRON-BASED SYSTEMS FOR PERSULFATE ACTIVATION: APPLICATION TO SULFAMETHOXAZOLE DEGRADATION

A. Results and Discussion

1. Characterization of Fe⁰ Plated Particles in Different Systems

a. Bimetallic systems (CoFe and AgFe)

Fig. 15 depicts the SEM images and EDX analysis of acid washed bimetallic (CoFe and AgFe) systems before reaction in PS/SMX solution. Two systems were compared: CoFe (System 1) and AgFe (System 2); both systems were plated with molecularity of more than 5:100. This helped in getting better images and more resolved peaks on the EDX analyzer in terms of clarity and emission intensities as well.

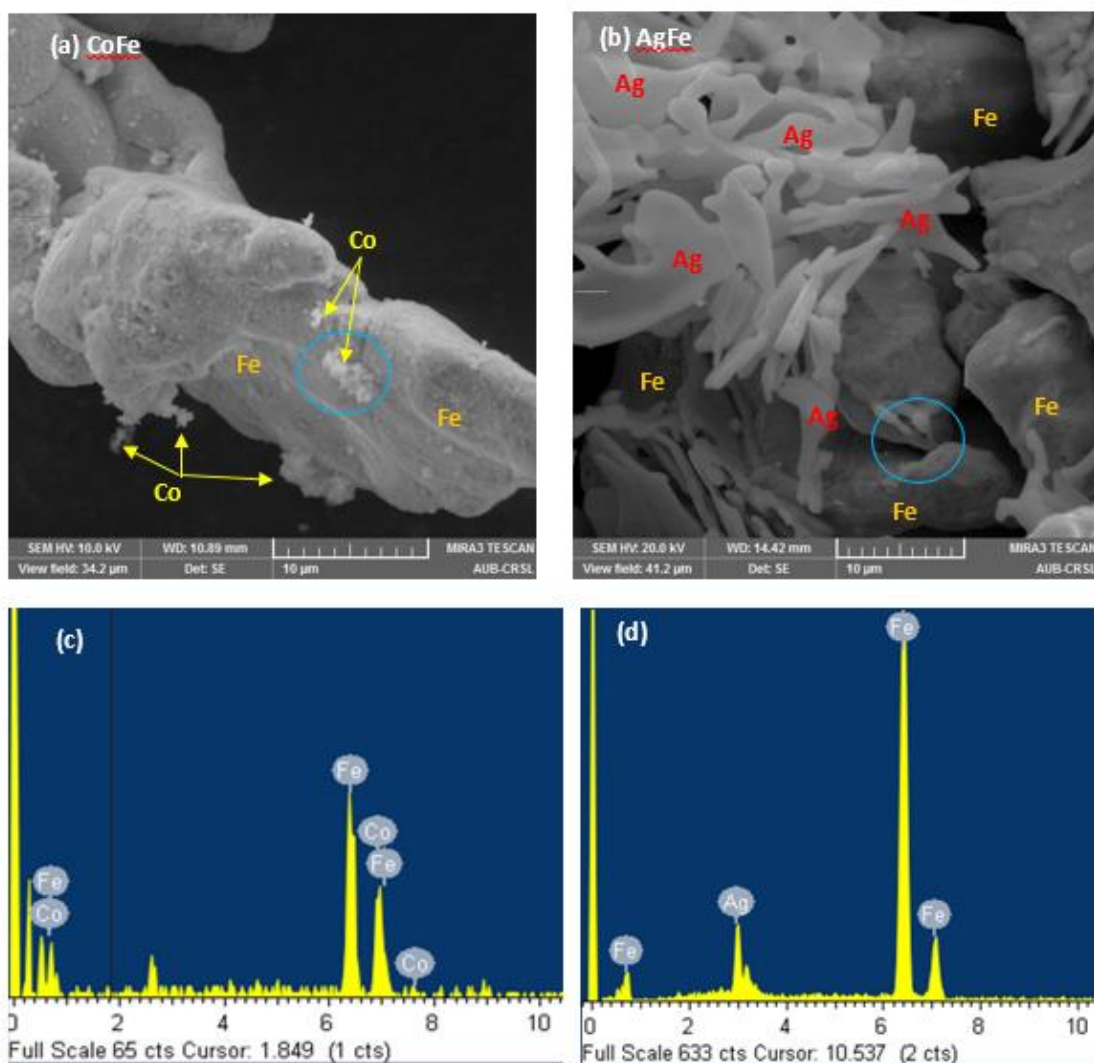


Fig. 15. Secondary electron images of (a) CoFe and (b) AgFe in addition to their corresponding X-ray spectra (c) and (d) collected within the circled area. Iron particles are plated with 1.3 μmole of Ag and 3.60 μmoles of Co.

It is worth noting that emission energies of Co ($k_{\alpha} = 6.9254$ Kev and $L_{\alpha} = 0.7763$ Kev) are very close to that of Fe ($k_{\alpha} = 6.3996$ Kev and $L_{\alpha} = 0.7048$ Kev) atoms which might cause Co and Fe emission peaks overlapping especially at low plating molecularly (1:100).

In terms of morphology, Fe^0 particles after acid-wash and plating showed a smooth surface embedded by cobalt and silver atoms. System **1** (CoFe) is characterized by small cryptocrystalline clusters of $\text{Co}_{(s)}$ which were detected at 10 KV beam voltage. These clusters are not homogeneously distributed; for instance, their X-ray spectra showed that some regions are totally exempted from Co whereas, other regions exhibited an average elemental atomic composition of 41.5% Co and 58.5% Fe. Based on that, one can easily deduce that the plating process is heterogeneous and experiments should be done, at least, in triplicate in order to overcome the heterogeneous metal distribution which might affect the expected results.

As it can be noticed from **Fig. 15b**, system **2** (AgFe) is formed of tiny shiny silver clusters deposited at the surface of Fe particles. The morphology of deposited silver cluster is characterized by the acicular aggregate formation with needle shape rods. EDX analysis done on defined surface area shows similar observation as for system **1** in terms of heterogeneous atomic distribution. In fact, within the same spot, there are regions completely exempted from Ag while others showed partial Ag coverage with a confirmed range of 20-80%. Further analysis was also done on the plated systems (CoFe and AgFe); however, using the mapping optional analysis provided by TESCAN MIRA software. The scanned surface area of about $500\ \mu\text{m} \times 500\ \mu\text{m}$ showed some specific dots corresponding to the plated metals (Ag and Co) with a heterogeneous distribution on Fe^0 matrix (**Fig. 16**).

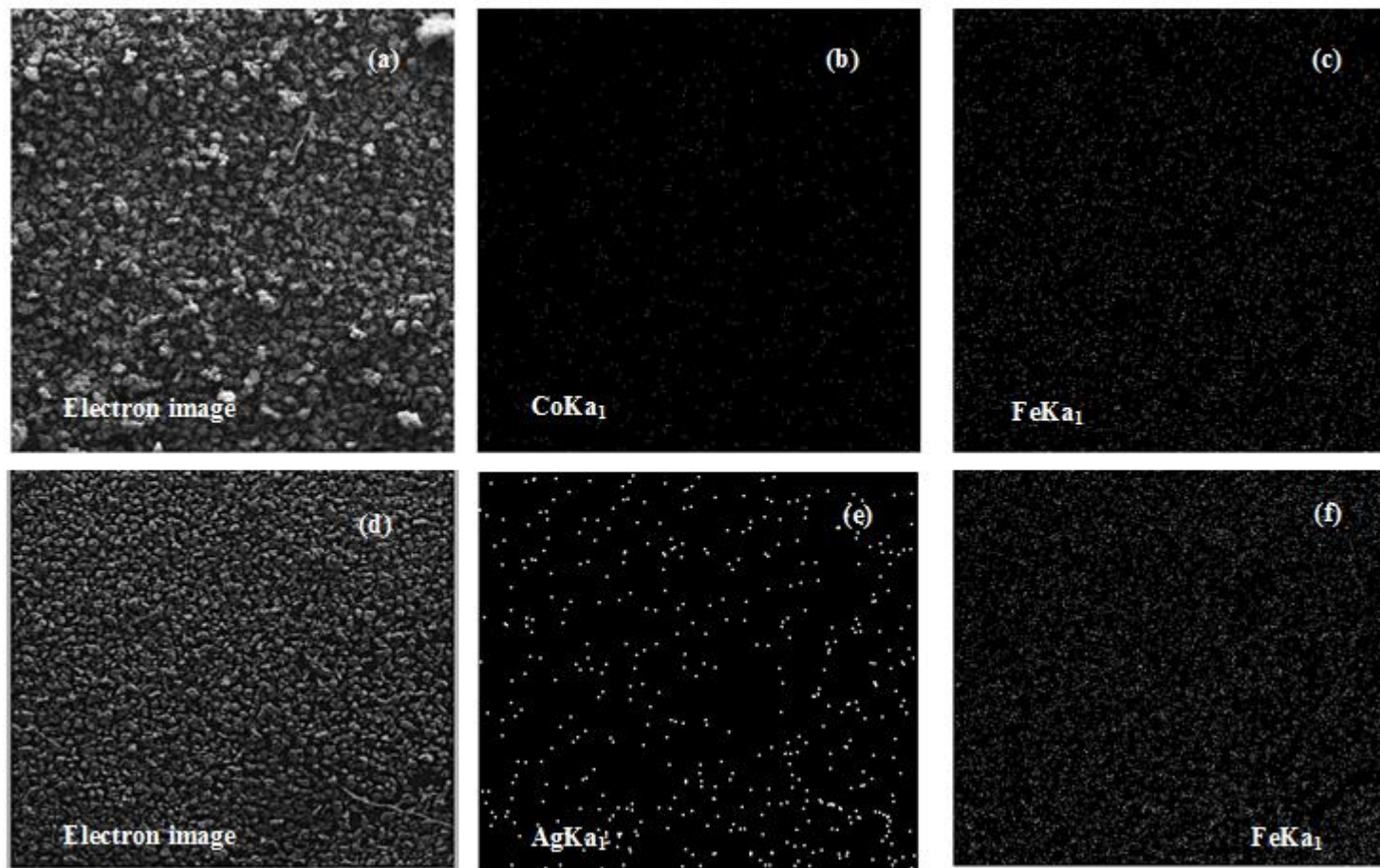


Fig. 16. SEM images of CoFe (a) and AgFe (d) bimetallic systems as presented in Fig. 15. The corresponding X-ray maps of (b) Co ($K\alpha_1$), (c) Fe ($K\alpha_1$) and (e) Ag ($K\alpha_1$) obtained from the two bimetallic systems CoFe and AgFe over the entire shown surface area (a, d). Areas of relatively high Fe concentrations are shown as bright regions in (c) and (f). In (b) less bright spots indicate areas of Co deposition whereas in (e) brighter spots indicate deposition of Ag at the surface of iron particles.

b. Trimetallic systems (AgCoFe and CoAgFe)

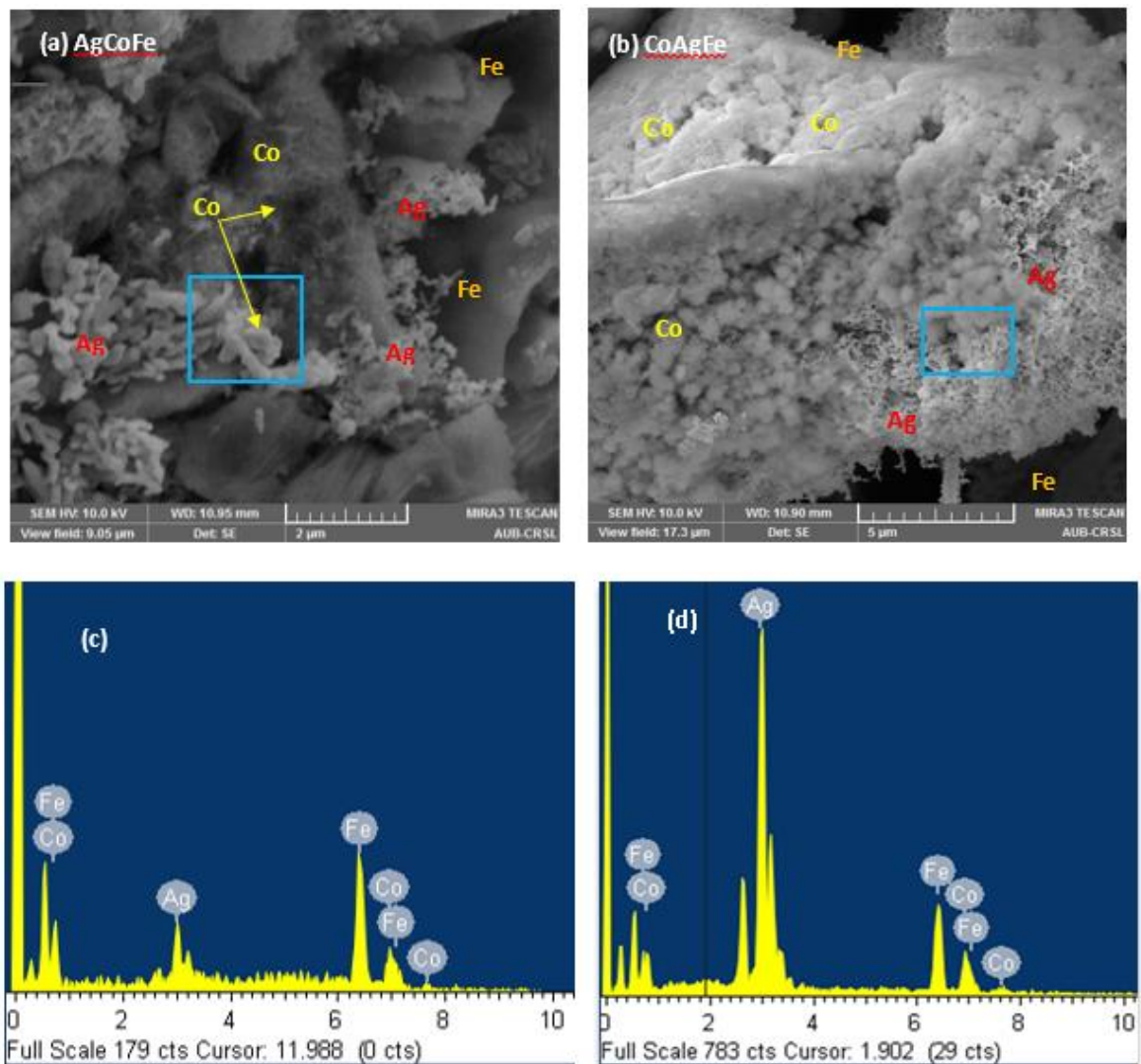


Fig. 17. Secondary electron images of (a) AgCoFe and (b) CoAgFe in addition to their corresponding X-ray spectra (c) and (d) collected within the squared area. Iron particles are plated with 1.3 μmol of Ag and 3.60 μmol of Co.

Fig. 17 shows two plated trimetallic systems that differ by their plating order.

System **3** corresponds to AgCoFe (**Fig. 17a**) obtained after plating CoFe bimetallic system

by Ag. System **4** corresponds to CoAgFe (**Fig. 17b**) obtained after depositing Co on

previously prepared AgFe bimetallic system. In the first case (System **3**), successive plating processes are thermodynamically favored based on the redox potential of the corresponding metals (**Table 2**). For example, once Co^{2+} ions are deposited heterogeneously as Co atoms on Fe particles ($\Delta E = 0.158 \text{ V}$) to form CoFe, Ag^+ ions can be further deposited either on Fe^0 atoms exempted from Co ($\Delta E = 1.239 \text{ V}$) or on CoFe bimetallic particles ($\Delta E = 1.081 \text{ V}$). As it can be seen on the SEM image of the trimetallic system AgCoFe (**Fig. 17a**), Ag and Co are well distinguished based on their morphologies which are similar to those reported for bimetallic systems (AgFe and CoFe). Furthermore, the assumption of having superimposed atoms of Fe, Co and Ag is very plausible. This observation is confirmed by the squared area where Ag clusters possessing acicular aggregate morphology and Co clusters having minute cryptocrystalline shape are not well distinguished in contrast to bimetallic systems. In the second case (System **4**) successive plating processes are not both thermodynamically favored (**Table 2**). For example once Ag^+ ions are deposited heterogeneously as Ag atoms on Fe particles ($\Delta E = 1.239 \text{ V}$) to form AgFe, Co^{2+} ions cannot be further deposited on Ag (negative $\Delta E = -1.081 \text{ V}$) however, they can make it on Fe^0 forming CoFe bimetallic particles ($\Delta E = 0.158 \text{ V}$). In such case, this trimetallic system (CoAgFe) is effectively composed of two adjacent bimetallic systems (CoFe and AgFe) without the possibility of being superimposed in contrast to the previous one (AgCoFe). This is illustrated by the SEM image (**Fig. 17b**) showing separate deposited metallic atoms (Ag and Co) as seen for bimetallic systems (**Fig. 15**). Mapping has also been done on the trimetallic systems (AgCoFe and CoAgFe).

The scanned surface area of about 500 μm x 500 μm confirmed the presence of some specific dots corresponding to the transition metals Co and Ag (**Fig. 18**).

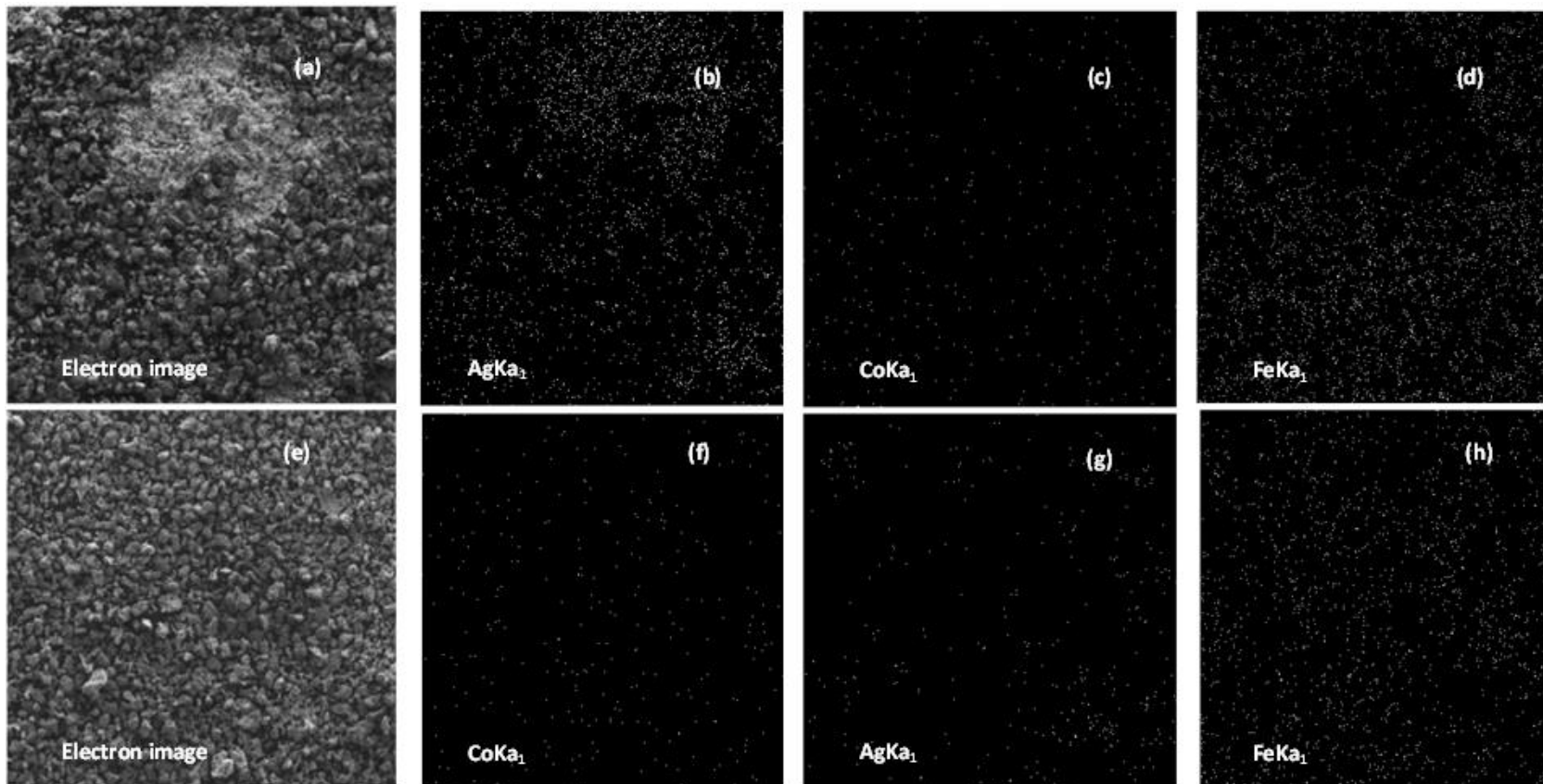


Fig. 18. SEM images of AgCoFe (a) and CoAgFe (d) trimetallic systems as presented in Fig. 17. The corresponding X-ray maps of (b) Ag ($K\alpha_1$), (c) Co ($K\alpha_1$) and (d) Fe ($K\alpha_1$) obtained from the two trimetallic systems AgCoFe and CoAgFe over the entire shown surface area (a, e). Areas of relatively high Fe concentrations are shown as bright regions in (d) and (h). In (c), (f) and (g) less bright spots indicate areas of Co and primary Ag deposition whereas in (b) brighter spots indicate deposition of Ag at the surface of iron particles as second deposited metal after Co.

B. Effect of Plated Systems on SMX Degradation

1. Bimetallic Systems

a. CoFe and AgFe vs Fe⁰

It has been demonstrated that an increase in solution of PS activators e.g. Fe²⁺, Co²⁺, Ag⁺ led to greater SRs production [50, 64]. Accordingly, one might expect greater contaminant destruction. Nonetheless, previous studies reported that further increases of Fe²⁺ concentration actually result in no proportional increases of contaminant destruction due to quenching phenomena (**Eq. 9**). Based on this premise, we conducted experiments using 2.5 mg as iron load (Fe⁰ and bimetallic systems) which previously showed better efficiency for SMX degradation [50].

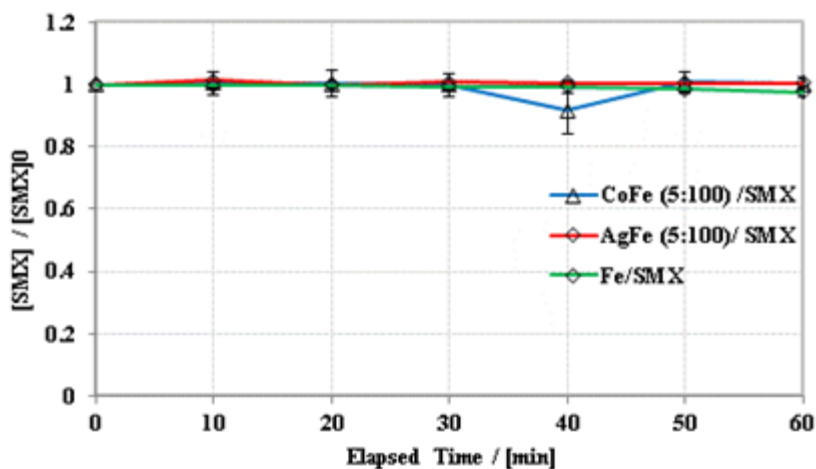


Fig. 19. Effect of bimetallic systems (CoFe and AgFe) and Fe⁰ on SMX degradation in PS-free solutions. Experimental conditions: [SMX]₀ = 39.5 μM, m (Fe⁰) = m (AgFe) = m (CoFe) = 2.5 mg (2.23 mM), pH_i = 5.63. Error bars represent uncertainty at 95% confidence level.

To do so, control experiments were carried out in PS-free solutions for all considered systems. The results did not show any significant decrease in the concentration of SMX as illustrated in **Fig. 19**. However, in the presence of PS, SMX degradation is noticed.

Fig. 20 illustrates the effect of metal plating on SMX degradation in PS/SMX systems compared to non-plated systems ($\text{Fe}^0/\text{SMX}/\text{PS}$). As it can be noticed, AgFe and CoFe bimetallic systems retard the reactivity of Fe^0 according to the redox potential of those metals compared to that of $\text{Fe}^{2+}/\text{Fe}^0$ and $\text{O}_2/\text{H}_2\text{O}$ couples (**Table 2**) in terms of corrosion products e.g. iron species released into the solution. AgFe and CoFe degraded only 30% and 63%, respectively of SMX during the first 10 min of the reaction. However in non-plated systems, SMX degradation reached 80% for the same period. The concentration of total dissolved iron species, monitored throughout the reaction, corroborates these findings (Inset **Fig. 20**). In fact, the smallest amount of iron species released into the solution corresponds to AgFe system (1.0 mg L^{-1}) resulting in less PS consumption (**Fig. 21**); consequently, less SRs are present in solution; thus, less SMX degradation occurs. Whereas, greater amount of total dissolved iron is found for CoFe bimetallic system (2.6 mg L^{-1}) at early stages of the reaction with an increasing trend up to 60 min of reaction time (e.g. 37.3 mg L^{-1}). Moreover, the highest concentration of iron dissolved species is present in Fe^0 system reaching a maximum value of 71.9 mg L^{-1} . It is worth noting that SRs generated by Ag^+ have comparable chances to react with organic compounds as well as Ag^+ [61] which can explain less SMX degradation when AgFe is used as PS activator (**Fig. 21**).

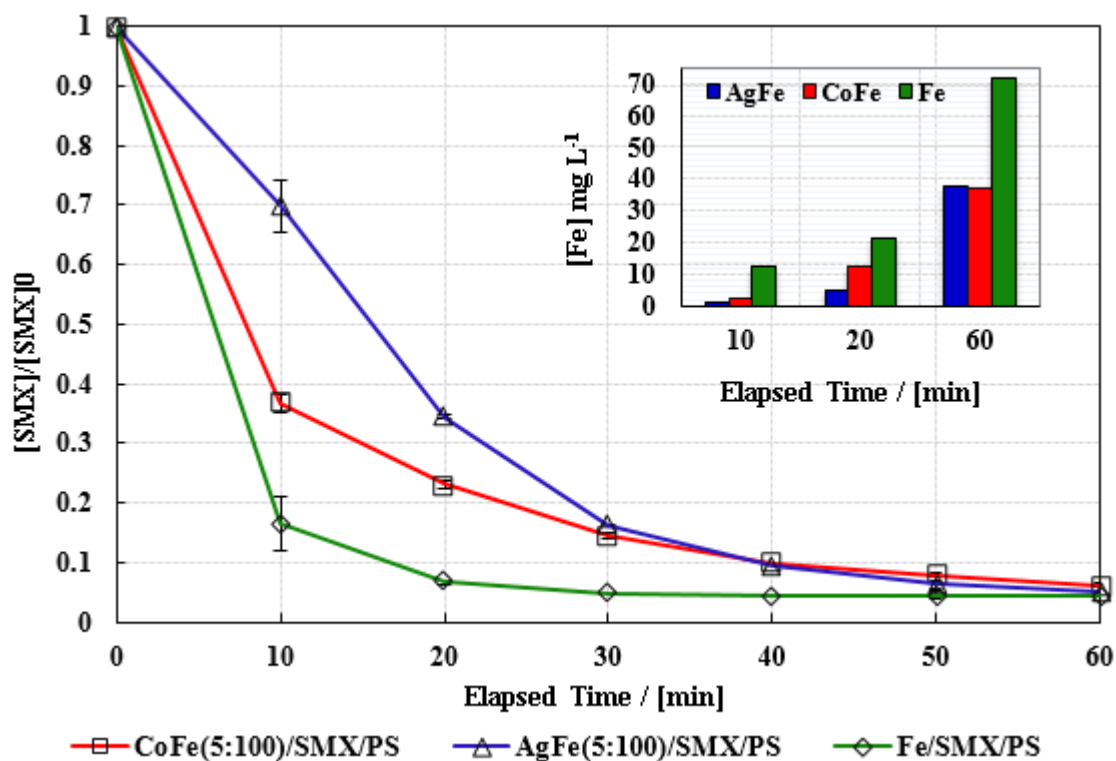
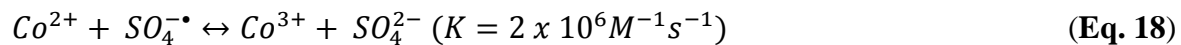
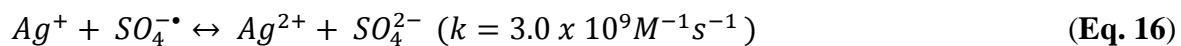


Fig. 20. Effect of bimetallic systems (CoFe and AgFe) and non-plated Fe^0 on SMX degradation in PS / H_2O systems. Inset: Concentration of total dissolved iron species in bimetallics (AgFe and CoFe) and mono-metallic Fe^0 at 10, 20, and 60 min. Experimental conditions: $[\text{SMX}]_0 = 39.5 \mu\text{M}$, $[\text{PS}]_0 = 1 \text{ mM}$, $m(\text{Fe}^0) = m(\text{AgFe}) = m(\text{CoFe}) = 2.5 \text{ mg}$ (2.23 mM). Error bars represent uncertainty at 95% confidence level.

This has been confirmed after conducting SMX degradation experiment in PS-free solutions as it can be seen in **Fig. 19** but also by monitoring the remaining PS in solution. In fact, no PS consumption has been noticed in the first 10 min of the reaction in AgFe system (**Fig. 21**), upper curve). Accordingly, Ag^+ is, at least, responsible of SMX degradation at early stage of the reaction until further bimetallic corrosion happens where SRs can take over after Fe^{2+} appearance in solution. Moreover, it has been reported that Ag^+ and Fe^{2+} are more efficient scavengers of SRs than Co^{2+} (their relative k values are 1,000 times greater than that of Co^{2+}); however, this condition is met only if these ions are present excessively into the solution (**Eqs. 9, 16-18**).



In contrast to AgFe system, CoFe shows 28% of PS consumption at 10 min until vanishing by the end of the reaction. This was confirmed by the presence of high amount of dissolved iron species (PS activators) in solution equivalent to 12.5 mg L⁻¹ (inset **Fig. 20**) (**Eq. 2**). Such an observation can be attributed to the excessive PS activated at the beginning of the reaction into SRs without reaching the critical threshold above which SRs quenching can take place [66]. PS was consumed completely after 30 min of the reaction in Fe/SMX/PS system (**Fig. 21**); whereas, it was maintained for almost the end of the reaction (e.g. 50 min) in the case of plated systems (CoFe and AgFe).

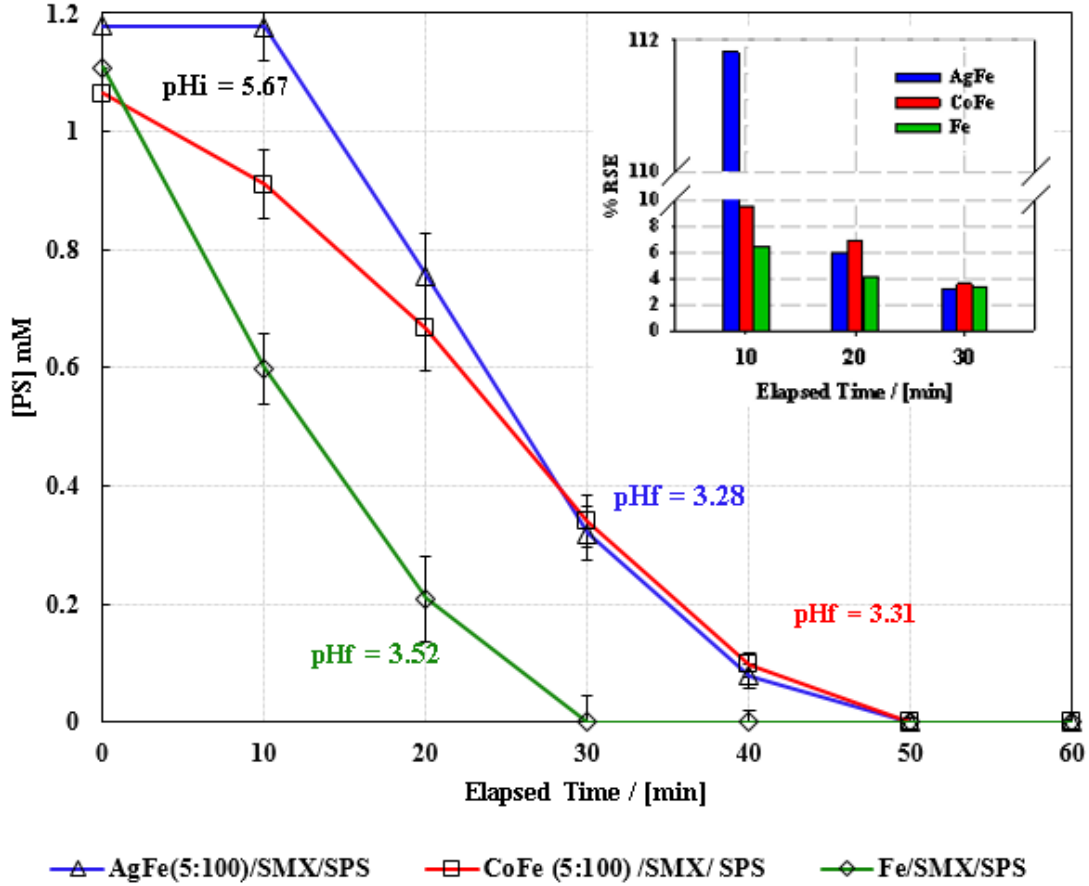


Fig. 21. Effect of plated (AgFe and CoFe 5:100) and non-plated Fe⁰ on PS activation. Inset: Influence of bimetallics (AgFe and CoFe) systems on the % RSE calculated at different reaction times (10, 20, and 60 min) Experimental conditions: [SPS]₀ = 1 mM, [SMX]₀ = 39.5 μM, m(Fe⁰) = m(AgFe) = m(CoFe) = 2.5 mg (2.23 mM). Error bars represent uncertainty at 95% confidence level.

This was accompanied by a pH decrease from 5.41 to 3.41 after 60 min (Eqs. 19-21). This low pH value is sustained by the presence of bisulfate (HSO₄⁻) in solution and supported by the hydration of ferric iron generating protons to the medium (Eqs. 21-24) [91].





For a better comparison among metallic systems activators, the % RSE values for plated (AgFe and CoFe) and non-plated Fe⁰ systems were compared. As it can be noticed from **Fig. 21**, the % RSE was the highest in the case of AgFe during the first 10 min of the reaction which is attributed to the role of Ag⁺/H₂O system in degrading SMX (**Fig. 22**) instead of generated SRs. However, CoFe system showed 9.5% RSE (t = 10 min), lower than that calculated for AgFe system (> 100%) mainly due to direct reaction between silver ions and SMX (**Fig. 22**) without PS consumption. As for Fe⁰/PS system, the calculated % RSE was the lowest (**Eqs. 2, 5, 7**) probably due to (i) the high reactivity of PS with Fe⁰ (ΔE = 2.45 V) compared to that of Ag⁰ (ΔE = 1.21 V) and Co⁰ (ΔE = 2.29 V) (**Table 2**) and (ii) the quenching of SRs by Fe²⁺ more present in Fe⁰/H₂O system than in AgFe and CoFe systems (inset **Fig. 20**). However, for all systems, one can notice that the % RSE decreased over time due to (i) PS consumption with a rate greater to that of SMX degradation and (ii) to metallic systems exhausted at the end of the reaction.

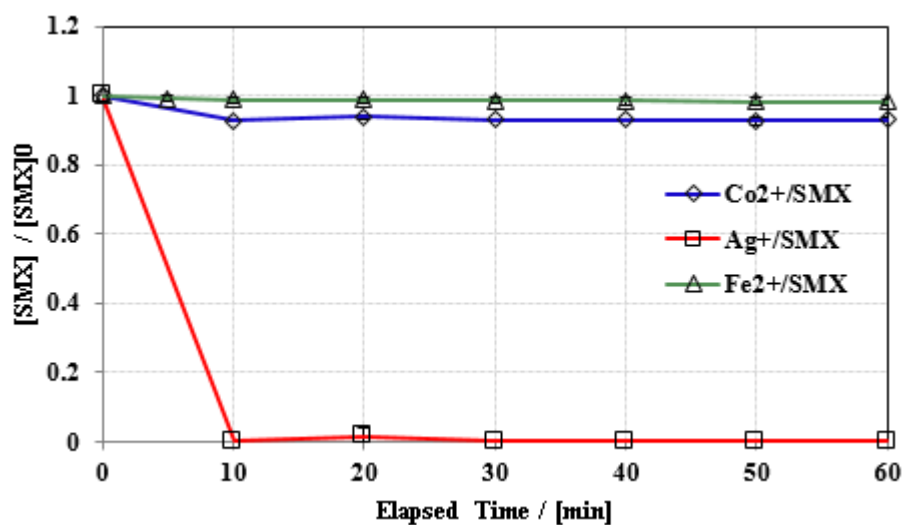


Fig. 22. Effect of transition metal ions Co^{2+} , Fe^{2+} , and Ag^{+} on SMX degradation in PS / H_2O free systems. Experimental conditions: $[\text{SMX}]_0 = 39.5 \mu\text{M}$, $[\text{Fe}^{2+}]$, $[\text{Co}^{2+}] = [\text{Ag}^{+}] = 2.23 \text{ mM}$, $\text{pHi} = 5.63$. Error bars represent uncertainty at 95% confidence level.

Finally, SMX degradation follows a pseudo-first order reaction pattern with all metallic systems used. All relative kinetics parameters are summarized in **Table 6**. As it can be noticed, there is no significant difference between AgFe and CoFe in their calculated k_{obs} ratios taking $k_{\text{obs (Fe)}}$ as reference. Also, their calculated half-lives did not vary significantly (11.0 min and 11.4 min for CoFe and AgFe, respectively). However, a reduced $t_{1/2}$ was obtained with non-plated Fe^0 ($t_{1/2} = 6.9 \text{ min}$) (**Table 6**). Finally, **Table 6** can also reveal that changing the molecularity of the plated systems used for PS activation from 5:100 to 1:100 did not affect significantly k_{obs} . For instance, slight increase of about 0.003 and 0.005 min^{-1} (ΔK_{obs}) has been noticed for CoFe and AgFe, respectively. This can be explained by the non-sustainability of plated systems in aqueous solutions where bimetallic systems behave as monometallic systems once the reaction proceeds toward more corrosion [92].

Table 8. Observed first order (K_{obs}) kinetics rate constants of SMX degradation in PS solutions activated by different iron-based systems.

Iron-based systems in SPS/SMX solution	Fe		CoFe		AgFe		AgCoFe		CoAgFe	
Molecularity	100	5:100	1:100	5:100	1:100	5:5:100	1:1:100	5:5:100	1:1:100	
$K_{obs} \times 10^{-2}$ (min⁻¹)	9.9	6.3	6.6	6.1	6.6	6.5	5.9	9.2	4.8	
$t_{1/2}$ (min)	6.95	11.0	10.5	11.4	10.5	10.7	11.8	7.5	14.4	
$\frac{K (obs amended Fe)}{K obs (Fe)}$	1.0	0.63	0.66	0.61	0.66	0.65	0.59	0.92	0.48	

2. Trimetallic Systems

a. AgCoFe and CoAgFe vs Fe⁰

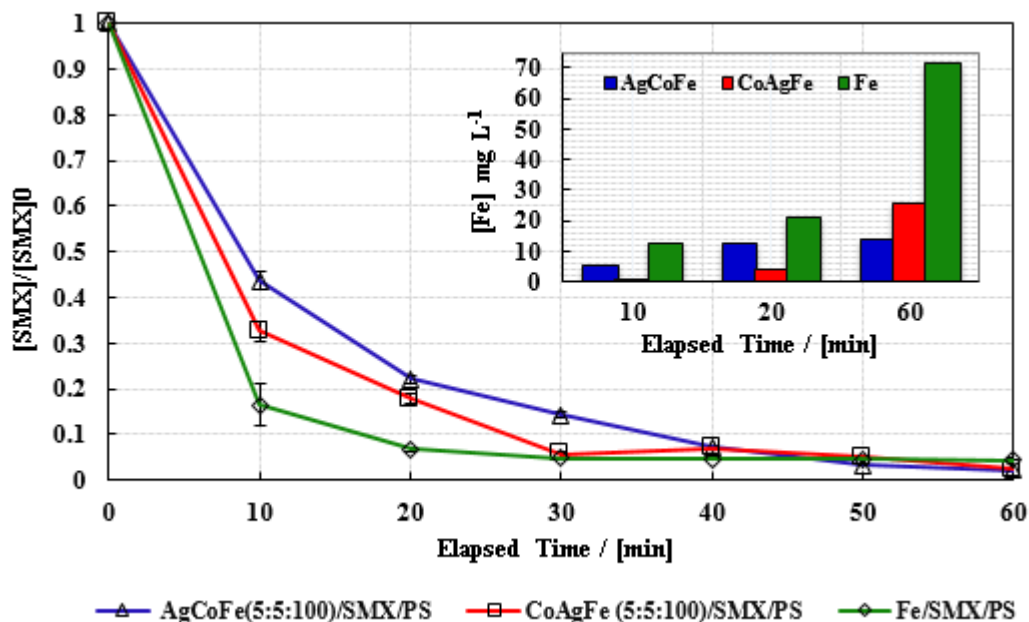


Fig. 23. Effect of trimetallic systems (AgCoFe and CoAgFe) and non-plated Fe⁰ on SMX degradation in PS / H₂O systems. Inset: Concentration of total dissolved iron species in trimetallic systems (AgCoFe and CoAgFe) and mono-metallic Fe⁰ systems at 10, 20, and 60 min. Experimental conditions: [SMX]₀ = 39.5 μM, [PS]₀ = 1.0 mM, m(Fe⁰) = m (AgCoFe) = m (CoAgFe) = 2.5 mg (2.23 mM). Error bars represent uncertainty at 95% confidence level.

The effect of trimetallic systems on PS activation and its consequence on SMX degradation rate is presented in **Fig. 23**. The three different systems Fe⁰/SMX/PS, AgCoFe/SMX/PS, and CoAgFe were compared in order to study the effect of plating and plating order on the activation of PS as well as on the degradation extent of SMX. As it can be noticed, CoAgFe showed better degradation of SMX (67%) compared to AgCoFe reaching only 56% at 10 min of the reaction; however, both systems were less reactive than Fe⁰ for the same period of treatment (80% over 10 min). Eventually, complete degradation of

SMX was achieved in the three studied systems by the end of the reaction (e.g. 60 min). And this is due to trimetallic systems being exhausted as it has been the case for bimetallic systems (previous section) whose PS activation rate becomes close to the one obtained with non-plated Fe^0 . Accordingly, full PS consumption took place by the end of the reaction. The different SMX degradation rates observed are related to (i) PS consumption and (ii) PS activators generated into the solution. The former depends mostly on direct PS reaction with zero valent metals (e.g. Fe, Co and Ag) and their relative ions (Fe^{2+} , Co^{2+} and Ag^+) available in solution; the latter depends on the ability of those metals to corrode in solution while producing corresponding ions. However, due to the heterogeneity of the plating process (**Fig. 18**) and the compatibility of ions (**Table 2**) to be deposited at the surface of solid particles, one might expect some irregularities in terms of concentration of dissolved iron species released into the solution (Inset **Fig. 23**). For example, AgCoFe system released more Fe dissolved species than CoAgFe until 20 min of reaction. This is attributed to the presence of three metallic systems (CoFe, AgFe and AgCoFe) formed at the surface of iron particles during the successive plating processes so as to obtain AgCoFe. In fact, this plating is thermodynamically favored taking into account redox potentials of relative couples (**Table 2**). In contrast, CoAgFe system showed less release of dissolved iron species in solution and this up to 20 min of reaction. Actually, while successively plating Fe^0 with Ag followed by Co, two separate bimetallic systems (AgFe and CoFe) are formed at the surface of iron particles because depositing Co on Ag is thermodynamically not favored (**Table 2**).

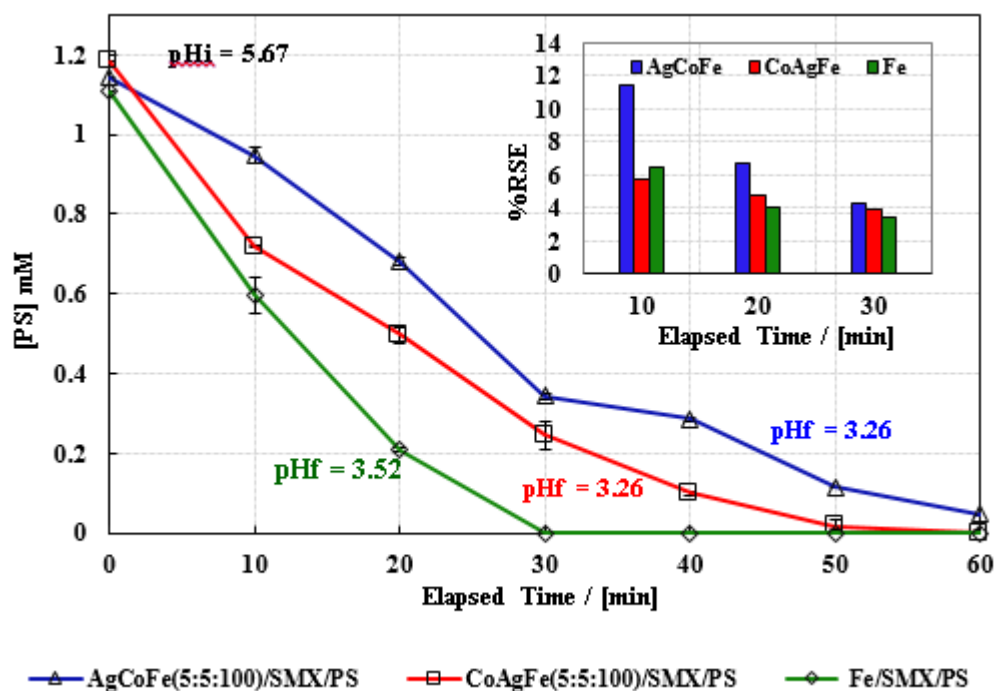


Fig. 24. Effect of plated (AgCoFe and CoAgFe) and non-plated Fe^0 on PS activation. Inset: Influence of trimetallics (AgCoFe and CoAgFe) systems on the %RSE calculated at different reaction times (10, 20, and 30 min) Experimental conditions: $[\text{PS}]_0 = 1.0 \text{ mM}$, $[\text{SMX}]_0 = 39.5 \text{ }\mu\text{M}$, $m(\text{Fe}^0) = m(\text{AgCoFe}) = m(\text{CoAgFe}) = 2.5 \text{ mg}$ (2.23 mM). Error bars represent uncertainty at 95% confidence level.

Accordingly, PS consumption is less in the case of AgCoFe (17.5% at 10 min) since Fe^0 surface is more hindered with three metallic systems compared to PS consumed (40%) in CoAgFe system where only two bimetallic systems partially cover iron surface particles. The calculated k_{obs} of CoAgFe system is 1.41 times greater than the one obtained with AgCoFe (Table 6). Also, it is worth noting that decreasing molecularity of trimetallics from 5:5:100 to 1:1:100 leads to a decrease in the calculated k_{obs} of about 0.006 min^{-1} and 0.044 min^{-1} for AgCoFe and CoAgFe, respectively. This is contrary to what has been obtained with bimetallic systems where an increase in k_{obs} has been obtained. Such observation can be explained by the complexity of metallic systems formed as well as their new electrochemical

and intrinsic properties. However, in most cases, all plated metallic systems lose their new properties progressively during the corrosion process as previously reported. In fact, Ghauch and co-workers [97, 111] showed that bimetallic (CoFe, PdFe, CuFe, NiFe, IrFe, SnFe) and trimetallic (CuPdFe, NiPdFe, PdCuFe, PdNiFe) systems lose most of their catalytic activities over time in aqueous solution while removing diclofenac pharmaceutical at early stages on the reaction. However, in the actual case, because of the use of PS in solution, different behavior of those metallic systems has to be considered. This is concretized by total consumption of PS yielding thereby full SMX degradation toward potential mineralization by the end of the reaction (60 min).

Finally, it is important to note that plated systems in the absence of PS are more iron corrosion products (ICPs) generators due to the formation of a galvanic couple driving the reaction toward more iron corrosion [112]. However, in the presence of PS, more release of ICPs takes place because of the most thermodynamically favored reaction between PS and Fe^0 ($\Delta E = 2.45$ V) rather than between PS and Ag^0 ($\Delta E = 1.21$ V) or PS and Co^0 ($\Delta E = 2.29$ V). That is why the highest concentration of total dissolved iron species was found in non-plated Fe^0 systems while a lower concentration in all other plated systems.

C. Effect of Agitation on SMX Degradation: Non-Disturbed Systems

1. Fe^0 vs CoFe and AgFe

Fig. 25a depicts the results of SMX degradation in PS activated solutions; however, under non-disturbed conditions for $t = 4$ h contrary to previous experiments where degradation experiments occurred in disturbed systems under vortex mixing and for a period

of 1 h. As it can be seen, the bimetallic systems (CoFe and AgFe) showed almost the same behavior in terms of SMX degradation where only 20% removal occurs by the end of the reaction.

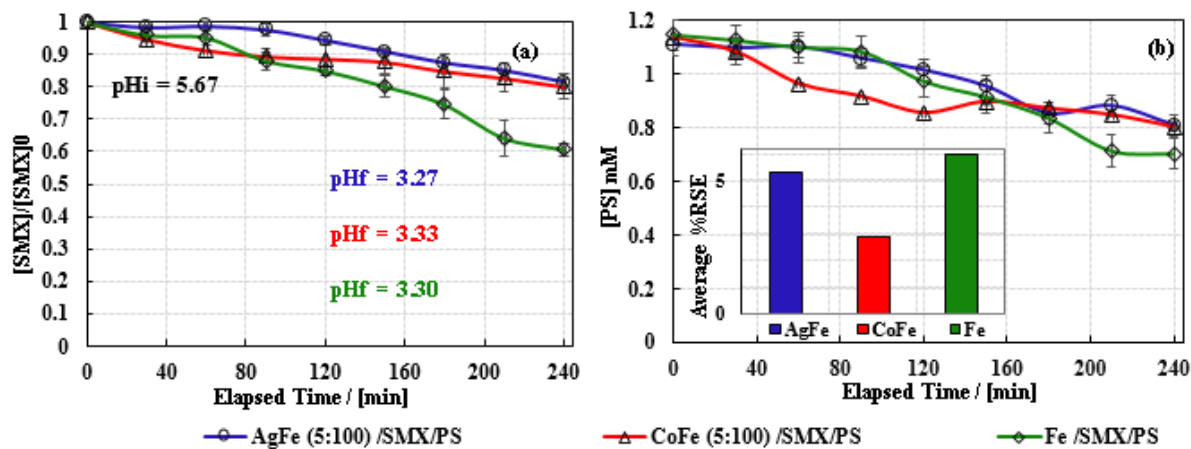


Fig. 25. Effect of bimetallic systems (CoFe and AgFe) and non-plated Fe^0 on (a) SMX degradation and (b) PS consumption in PS / H_2O systems under non-disturbed conditions. The inset shows the calculated average % RSE at 60 min reaction time. Experimental conditions: $[SMX]_0 = 39.5 \mu M$, $[PS]_0 = 1 \text{ mM}$, $m(Fe^0) = m(AgFe) = m(CoFe) = 2.5 \text{ mg}$ (2.23 mM). Error bars represent uncertainty at 95% confidence level.

On the other hand, Fe^0/PS system was more powerful contributing to 40% of SMX degradation over the same period (4 h). Compared to disturbed systems, SMX was completely degraded in even less time ($t = 1 \text{ h}$) (**Fig. 20**). This is attributed to the effective hydrodynamic phenomena occurring at constant shaking intensity favoring mass transfer improving thereby collision between reactants for quicker kinetics. Mass transfer includes the release of ICPs in the bulk solution and the production of SRs at proximity to iron particles surface. In fact, agitation yields friction between iron particles which can favor a kind of pitting corrosion in acidic medium. Such a phenomenon is much appreciated for enhancing the corrosion process [113, 114]. SMX degradation accompanied with iron corrosion is in harmony with PS consumption (**Fig. 25b**). For instance, only 28% and 30% of PS was

degraded in bimetallic (AgFe and CoFe) and Fe⁰ systems, respectively over 4 h of reaction. Degradation curves are both following the same trend where PS consumption happened smoothly in contrast to disturbed systems where similar concentration of PS lasted only 60 min. In order to better understand the reactivity of SRs in non-disturbed systems in terms of applicability for long term remediation processes, the average % RSE was calculated for the first 60 min of the reaction so that comparison is possible with disturbed systems (conducted for 1 h). In fact, the results showed that in all non-disturbed systems, the average % RSE is greater when Fe⁰ is used as standalone activator (% RSE = 5.99) compared to that of all other plated systems. Bimetallic systems showed average % RSE of about 5.31% and 2.88% for AgFe and CoFe, respectively (Inset **Fig. 25**). Accordingly, no noticeable advantage is found for amended Fe⁰ systems compared to non-plated systems except of minimal PS consumption. However, greater average % RSE is noticed for AgFe system (5.31%) compared to CoFe system (2.88%). This is attributed to the direct reaction of Ag and its corrosion products with SMX as previously reported (**Fig. 22**). Nonetheless, this highest RSE (e.g. 5.31) decreases with time (up to 4 h) and matches those reported for all other plated systems (2.28-3.00%). Such an observation corroborates the wear of plated systems over time in an acidic and corroded medium where plated systems becomes exhausted and behaves as non-plated systems [36]. Also, as much as the reaction time is moving forward, more ICPs are formed and might contribute to the activation of PS with potential SRs quenching decreasing thereby the average % RSE of the reaction [50].

2. Fe^0 vs AgCoFe and CoAgFe

Fig. 26 shows the time course of (a) SMX degradation and (b) PS consumption over 4 h of reaction when trimetallic systems AgCoFe and CoAgFe are used for PS activation under non-disturbed conditions.

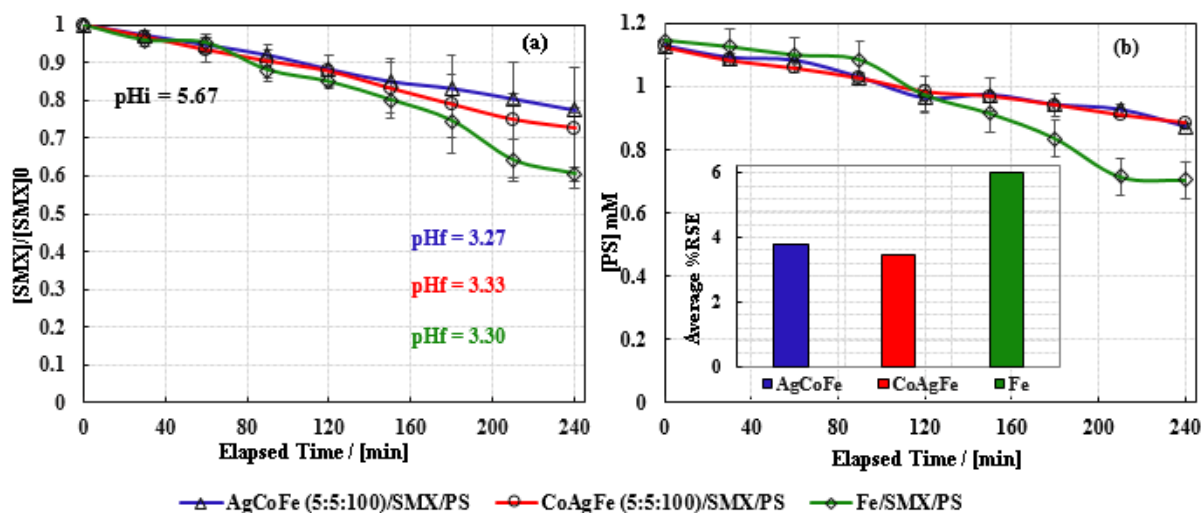


Fig. 26. Effect of trimetallic systems (AgCoFe and CoAgFe) and non-plated Fe^0 on (a) SMX degradation and (b) PS consumption in PS / H_2O systems under non-disturbed conditions. The inset shows the calculated average %RSE at 60 min reaction time. Experimental conditions: $[SMX]_0 = 39.5 \mu M$, $[PS]_0 = 1.0 mM$, $m(Fe^0) = m(AgCoFe) = m(CoAgFe) = 2.5 mg$ (2.23 mM). Error bars represent uncertainty at 95% confidence level.

The amended Fe^0 activators tested showed average % RSE of about 3.78% and 3.44% for AgCoFe and CoAgFe, respectively over 60 min of reaction (Inset **Fig. 26**). These values are less than that obtained with Fe^0 alone (e.g. 5.99%) under similar conditions. The same behavior as for bimetallic systems is noticed for longer reaction time (e.g. 4 h). For instance trimetallic systems lose their properties with corrosion moving forward in acidic medium to behave like standalone Fe^0 systems. The average % RSE calculated over 4 h of reaction time is found to be 3.54% and 3.98%, very close to average % RSE values calculated over 60 min. Accordingly, one can deduce that plated systems cannot maintain

their properties as supporting matrix of different galvanic couples responsible of more corrosion over time. Although trimetallic systems got exhausted under non-disturbed conditions; however, they can be considered more reliable in terms of PS consumption over longer periods. For example, only 22% of PS is consumed in trimetallic systems after 4 h of reaction compared to 28% consumption for bimetallic systems and this under similar conditions. However, the greatest PS consumption is noticed with Fe⁰ system (38.5%) which is due to the standard potential of the relative redox couples that favors more PS reaction with Fe⁰ rather than with Co and Ag (**Table 2**). The increasing order of PS consumption versus metallic systems activators is as follows: Trimetallic < Bimetallic < Fe⁰ meaning that plating is an advantage that can be used to sustain PS in solution without being rapidly consumed. Another feature of using trimetallic systems is found in the plating order of iron particles. For example, in CoAgFe system, 27.3% of SMX was degraded whereas only 22.6% in the case of AgCoFe over 4 h of reaction (**Fig. 26a**). Furthermore, CoAgFe systems showed similar calculated average % RSE under non-disturbed conditions and in agitated systems (3.98 and 4.05 %, respectively). Besides, in AgCoFe systems, the average % RSE values were bit different (3.54% for non-disturbed systems against 5.65% under agitation). This can be attributed to the presence of Ag at the surface of iron particles and their role in degrading SMX molecules after the latter being more exposed through mass transfer (collision) to Ag and Co atoms deposited at the surface of iron particles. This condition is not met with CoAgFe systems where only two bimetallic systems (AgFe and CoFe) are present at the surface of iron particles without the possibility of forming superposed trimetallic systems CoAgFe as it is the case for AgCoFe and this for thermodynamic reasons (**Table 2**).

All the above mentioned non-disturbed systems showed pseudo-first order kinetics behavior with calculated k_{obs} much less than those obtained under disturbed systems for mass transfer reason as stated above. Also, a similar decreasing trend of k_{obs} is observed in the case of amended Fe^0 systems compared to Fe^0 standalone systems. All calculated ratios are summarized in **Fig. 27**.

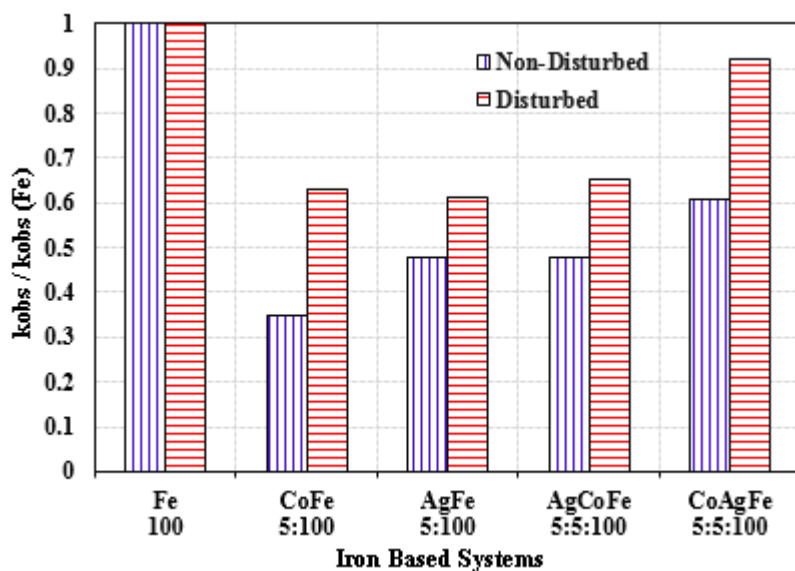


Fig. 27. Reactivity of plated and non-plated iron-based systems: vertical bars display the ratio of k_{obs} measured for each of the amended Fe^0 systems to the k_{obs} values measured for the standalone Fe^0 system $\left(\frac{k_{obs}(amended\ Fe)}{k_{obs}(Fe)}\right)$.

D. Transformation Products

Based on our previous work [50], the main transformation product obtained upon SMX oxidation by activated PS is eluted at 5.7 min and was assumed to be the b-aminoenone SMX derivative (**Fig. 28**). However, this transformation product having a maximum absorbance at $\lambda = 262$ nm (Inset **Fig.28**) might persist in solution especially if high loads of iron particles are used for the activation of PS (**Fig. 28**).

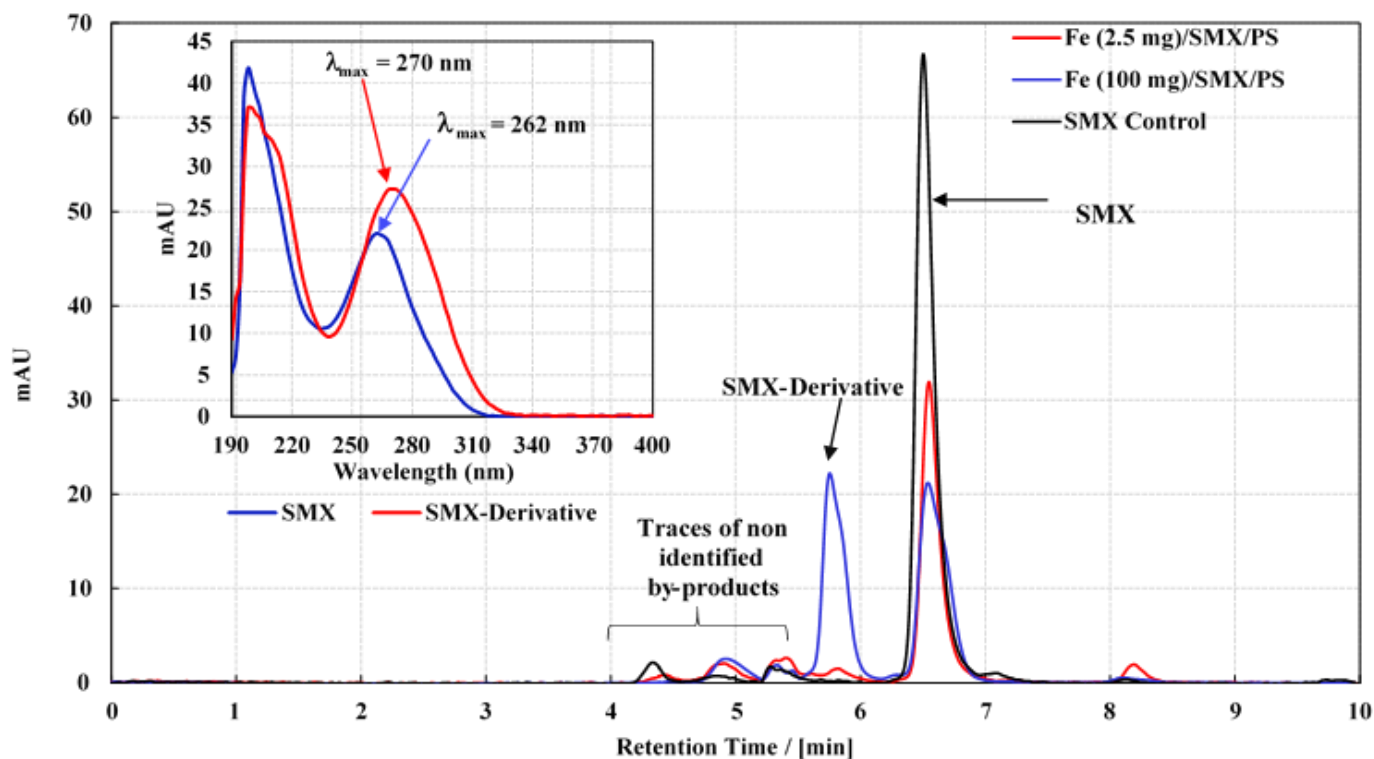


Fig. 28. Trace chromatograms of SMX treated in Fe^0/PS systems with different Fe^0 loads. Inset is the UV-Vis absorption spectra of SMX and its derivative in Fe^0/PS systems during the first 10 min of the reaction. Experimental conditions: $[\text{SMX}]_0 = 39.5 \mu\text{M}$, $[\text{PS}]_0 = 1.0 \text{ mM}$, $m(\text{Fe}^0) = 2.5$ and 100 mg .

For instance, in PS-free solution, the more iron particles are present in solution, the more transformation products can adsorb at the surface of oxidized iron particles, enmesh into the iron oxide spider-like network, and co-precipitate within the mixture of ICPs formed into the reactive medium [115]. In contrast, if PS is used in $\text{Fe}^0/\text{H}_2\text{O}$ systems, adsorbed and co-precipitated transformation products can be easily desorbed and expelled from the iron oxide matrix by the mean of the reaction between PS and Fe^0 , the latter being partially covered with oxide scales of different nature (Fe_2O_3 , Fe_3O_4 , FeOOH , etc.). Accordingly, the quantity of iron particles in solution should be well optimized so as to avoid the adsorption of transformation products subjected to further oxidation if kept in solution. All tested metallic

systems showed at low iron particles loads (e.g. 2.5 mg / 20 mL) non-significant appearance of SMX derivative in contrast to higher load of Fe⁰ (100 mg / 20 mL) where SMX-derivative showed strong appearance and this after only 10 min of reaction as noticed in **Fig. 28**. SMX-derivative persisted in solution unless if additional PS is spiked into the reactive medium as previously demonstrated [50]. Chromatograms of all tested systems e.g. Fe⁰, AgFe, CoFe, AgCoFe and CoAgFe are presented in **Fig. 29**.

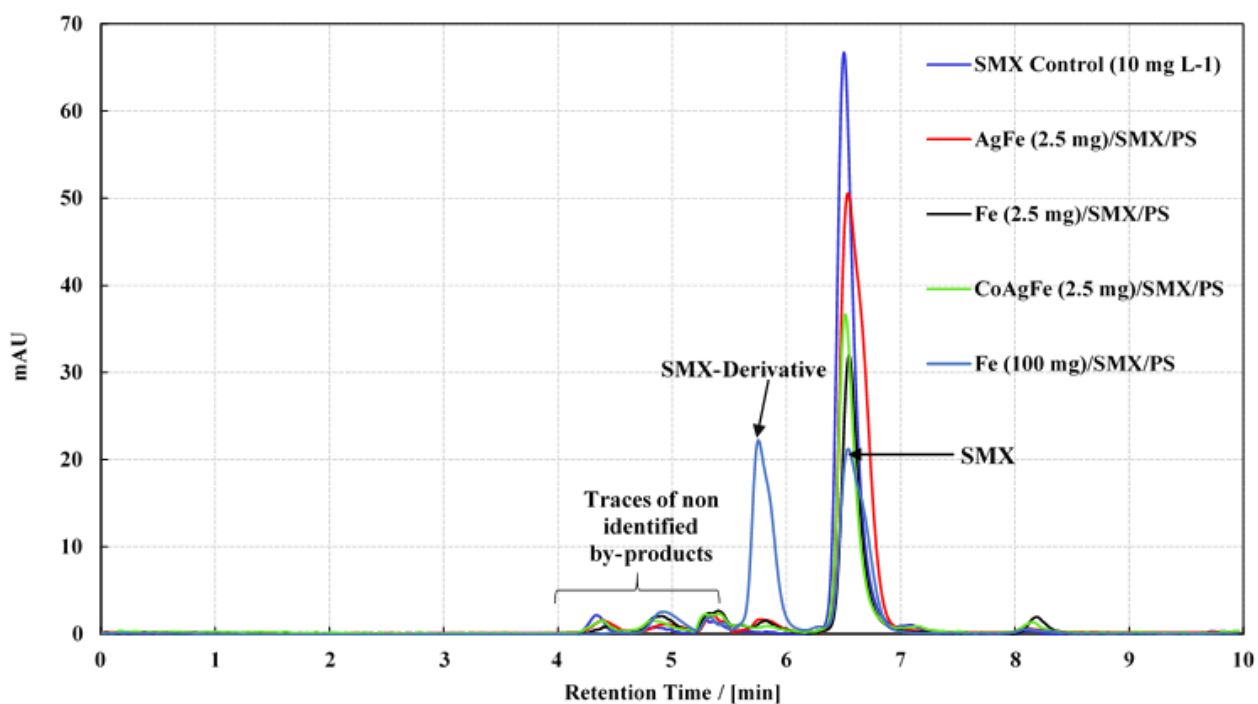


Fig. 29. Trace chromatograms of SMX treated in different metallic systems (Fe⁰, AgFe, and CoAgFe). Chromatograms with CoFe and AgCoFe are similar to those presented; however, they are not shown for clarity reasons during the first 10 min of the reaction. Experimental conditions: [SMX]₀ = 39.5 μM, [PS]₀ = 1.0 mM, m (Fe⁰/AgFe / CoAgFe) = 2.5 and m (Fe⁰) = 100 mg.

CHAPTER V

CONCLUSION

AOPs has proved its successful application for water remediation technology after the injection of PS among a group of other oxidants. The latter is characterized by its high oxidative potential and unique characteristics after its activation. PS activators chosen in this work were Fe^0 and modified Fe^0 . Those metallic systems presented offered a great potential to catalytically activate PS and convert it into SRs having excellent oxidative properties. The main advantage found in those systems is their efficacy, even at a very low load (e.g. 0.125 g L^{-1}) after PS injection to degrade recalcitrant pharmaceutical molecules e.g. SMX in PS/ H_2O systems. While high loads of iron particles (40 g L^{-1}) are needed to remove pharmaceutical compounds from water through reduction, adsorption and co-precipitation, only 0.125 g L^{-1} of Fe^0 , bimetallic (CoFe, AgFe) and trimetallic (CoAgFe, AgCoFe) systems were able to degrade not only SMX molecules but also their transformation products until complete mineralization. Upon remediation, one should consider the overall perspective of the cleaning process. As an illustration, the ultimate aim is to eliminate such hazardous contaminants from water and at the same time with the minimal sludge production. This was achieved by utilizing small iron load which generates less sludge in treated solutions; and the concentration of dissolved iron species in effluents remained within a considerable level and below the maximum concentration limit as per WHO guidelines ($< 0.3 \text{ mg L}^{-1}$). The initial pH of the solution is also a significant parameter to consider especially in the context of initiating iron corrosion responsible for the release of Fe^{2+} species for PS activation. For

instance, reactions carried in DI, tap, and UG water revealed similar results between tap and UG water due to the presence of bicarbonate species. In contrast, after its elimination through acidification, all solutions showed almost similar behavior to DI water toward SMX degradation over 3 cycles of 1 h until complete MIPs depletion. SMX degradation in Fe⁰/PS systems showed the presence of a stable transformation product which was eliminated after spiking the solution again with PS. In modified Fe⁰/PS systems and upon utilizing the minimal iron load (2.23 mM), SMX was completely degraded; however, with the absence of its transformation product in the chromatograms. This can be due to their conversion to smaller fragments which were difficult to identify and detect on the MS.

The presence of Ag and Co atoms at the surface of iron particles at trace level (moleularity 1:100 and 5:100) provided iron systems with new intrinsic properties yielding an optimized PS activation process for which full SMX degradation occurred in less than 1 h. Furthermore, activated PS systems using metallic iron-based particles showed a more powerful oxidation process compared to that of Fe²⁺ fed systems in both direct and sequential addition in terms of complete SMX destruction. In fact, heterogeneous PS activation seems to be more efficient than homogeneous activation due to the presence of specific sites at the surface of iron particles embedded with oxides of nascent catalytic properties. However, results showed that plated systems cannot last longer time in solution due to advanced corrosion in aqueous media of acidic properties. As long as the oxidation reaction progresses, amended iron becomes similar to non-amended iron in solution confirming the excellent properties of such systems only at early stage of the reaction especially under disturbed conditions. The results showed also that in non-agitated systems, SMX degradation occurred

smoothly by following a best fitted pseudo-first order reaction. Under these conditions, plated systems are not rapidly depleted in an aqueous medium and PS lasted more in solution for long term applications. Transition metals plated at the surface of iron particles showed also the advantage of slowing down the direct reaction between PS and iron surface increasing thereby the reaction stoichiometric efficiency compared to non-plated iron particles. Although PS systems showed their reliability in degrading contaminants after being chemically activated, photolysis using solar energy can however add more credits to such AOPs especially for field application in open environments. Research in this direction is in progress in our laboratory.

BIBLIOGRAPHY

- [1] S. Esplugas, D.M. Bila, L.G.T. Krause, M. Dezotti, Ozonation and advanced oxidation technologies to remove endocrine disrupting chemicals (EDCs) and pharmaceuticals and personal care products (PPCPs) in water effluents, *J. Hazard. Mater.* 149 (2007) 631-642.
- [2] T.A. Ternes, N. Herrmann, M. Bonerz, T. Knacker, H. Siegrist, A. Joss, A rapid method to measure the solid–water distribution coefficient (K_d) for pharmaceuticals and musk fragrances in sewage sludge, *Water Res.* 38 (2004) 4075-4084.
- [3] L.J. Puckett, Identifying the Major Sources of Nutrient Water Pollution, *Environ. Sci. Technol.* 29 (1995) 408A-414A.
- [4] P.E. Stackelberg, E.T. Furlong, M.T. Meyer, S.D. Zaugg, A.K. Henderson, D.B. Reissman, Persistence of pharmaceutical compounds and other organic wastewater contaminants in a conventional drinking-water-treatment plant, *Sci. Total Environ.* 329 (2004) 99-113.
- [5] D. Avisar, Y. Lester, D. Ronen, Sulfamethoxazole contamination of a deep phreatic aquifer, *Sci. Total Environ.* 407 (2009) 4278-4282.
- [6] K.-M. Yao, M.T. Habibian, C.R. O'Melia, Water and waste water filtration. Concepts and applications, *Environ. Sci. Technol.* 5 (1971) 1105-1112.
- [7] T. Heberer, Occurrence, fate, and removal of pharmaceutical residues in the aquatic environment: a review of recent research data, *Toxicol. Lett.* 131 (2002) 5-17.
- [8] T.A. Ternes, Occurrence of drugs in German sewage treatment plants and rivers, *Water Res.* 32 (1998) 3245-3260.
- [9] D.W. Blowes, C.J. Ptacek, S.G. Benner, C.W.T. McRae, T.A. Bennett, R.W. Puls, Treatment of inorganic contaminants using permeable reactive barriers, *J. Contam. Hydrol.* 45 (2000) 123-137.
- [10] K.J. Cantrell, D.I. Kaplan, T.W. Wietsma, Zero-valent iron for the in situ remediation of selected metals in groundwater, *J. Hazard. Mater.* 42 (1995) 201-212.

- [11] J.L. Ginner, P.J. Alvarez, S.L. Smith, M.M. Scherer, Nitrate and nitrite reduction by Fe⁰: influence of mass transport, temperature, and denitrifying microbes, *Environ. Eng. Sci.* 21 (2004) 219-229.
- [12] O.K. Dalrymple, D.H. Yeh, M.A. Trotz, Removing pharmaceuticals and endocrine-disrupting compounds from wastewater by photocatalysis, *J. Chem. Technol. Biotechnol.* 82 (2007) 121-134.
- [13] C.G. Daughton, T.A. Ternes, Pharmaceuticals and personal care products in the environment: agents of subtle change?, *Environ. Health Perspect.* 107 (1999) 907.
- [14] A. Chatzitakis, C. Berberidou, I. Paspaltsis, G. Kyriakou, T. Sklaviadis, I. Poullos, Photocatalytic degradation and drug activity reduction of chloramphenicol, *Water Res.* 42 (2008) 386-394.
- [15] F. Méndez-Arriaga, S. Esplugas, J. Giménez, Photocatalytic degradation of non-steroidal anti-inflammatory drugs with TiO₂ and simulated solar irradiation, *Water Res.* 42 (2008) 585-594.
- [16] J.P. Bound, K. Kitsou, N. Voulvoulis, Household disposal of pharmaceuticals and perception of risk to the environment, *Environ. Toxicol. Pharmacol.* 21 (2006) 301-307.
- [17] M. Cleuvers, Mixture toxicity of the anti-inflammatory drugs diclofenac, ibuprofen, naproxen, and acetylsalicylic acid, *Ecotoxicol. Environ. Saf.* 59 (2004) 309-315.
- [18] E.R. Cooper, T.C. Siewicki, K. Phillips, Preliminary risk assessment database and risk ranking of pharmaceuticals in the environment, *Sci. Total Environ.* 398 (2008) 26-33.
- [19] V.L. Cunningham, S.P. Binks, M.J. Olson, Human health risk assessment from the presence of human pharmaceuticals in the aquatic environment, *Regul. Toxicol. Pharm.* 53 (2009) 39-45.
- [20] O.V. Enick, M.M. Moore, Assessing the assessments: pharmaceuticals in the environment, *Environ. Impact Assess. Rev.* 27 (2007) 707-729.
- [21] J.L. Flippin, D. Huggett, C.M. Foran, Changes in the timing of reproduction following chronic exposure to ibuprofen in Japanese medaka, *Oryzias latipes*, *Aquat. Toxicol.* 81 (2007) 73-78.
- [22] *The Use of Drugs in Food Animals: Benefits and Risks*, The National Academies Press, 1999.

- [23] A. Białk-Bielińska, J. Maszkowska, W. Mroziak, A. Bielawska, M. Kołodziejaska, R. Palavinskas, P. Stepnowski, J. Kumirska, Sulfadimethoxine and sulfaguanidine: their sorption potential on natural soils, *Chemosphere* 86 (2012) 1059-1065.
- [24] C.W. Knapp, C.A. Engemann, M.L. Hanson, P.L. Keen, K.J. Hall, D.W. Graham, Indirect evidence of transposon-mediated selection of antibiotic resistance genes in aquatic systems at low-level oxytetracycline exposures, *Environ. Sci. Technol.* 42 (2008) 5348-5353.
- [25] J.C. Underwood, R.W. Harvey, D.W. Metge, D.A. Repert, L.K. Baumgartner, R.L. Smith, T.M. Roane, L.B. Barber, Effects of the antimicrobial sulfamethoxazole on groundwater bacterial enrichment, *Environ. Sci. Technol.* 45 (2011) 3096-3101.
- [26] B.A. Wilson, V.H. Smith, F. deNoyelles, C.K. Larive, Effects of three pharmaceutical and personal care products on natural freshwater algal assemblages, *Environ. Sci. Technol.* 37 (2003) 1713-1719.
- [27] A.J. Feitz, S.H. Joo, J. Guan, Q. Sun, D.L. Sedlak, T. David Waite, Oxidative transformation of contaminants using colloidal zero-valent iron, *Colloids Surf. Physicochem. Eng. Aspects* 265 (2005) 88-94.
- [28] A. Ghauch, Degradation of benomyl, picloram, and dicamba in a conical apparatus by zero-valent iron powder, *Chemosphere* 43 (2001) 1109-1117.
- [29] S. Nešić, Key issues related to modelling of internal corrosion of oil and gas pipelines—A review, *Corros. Sci.* 49 (2007) 4308-4338.
- [30] Y. Jia, P. Aagaard, G.D. Breedveld, Sorption of triazoles to soil and iron minerals, *Chemosphere* 67 (2007) 250-258.
- [31] W. Kamolpornwijit, L. Liang, Investigation of gas production and entrapment in granular iron medium, *J. Contam. Hydrol.* 82 (2006) 338-356.
- [32] A. Khan, S. Rasul, A. Munir, M. Habibuddowla, M. Alauddin, S. Newaz, A. Hussam, Appraisal of a simple arsenic removal method for ground water of Bangladesh, *J. Environ. Sci. Health. Part A* 35 (2000) 1021-1041.
- [33] C. Noubactep, Characterizing the discoloration of methylene blue in Fe⁰/H₂O systems, *J. Hazard. Mater.* 166 (2009) 79-87.
- [34] C. Noubactep, G. Meinrath, P. Dietrich, M. Sauter, B.J. Merkel, Testing the suitability of zerovalent iron materials for reactive walls, *Envir. Chem.* 2 (2005) 71-76.

- [35] R. Rangsviek, M. Jekel, Removal of dissolved metals by zero-valent iron (ZVI): Kinetics, equilibria, processes and implications for stormwater runoff treatment, *Water Res.* 39 (2005) 4153-4163.
- [36] C. Noubactep, Characterizing the discoloration of methylene blue in Fe⁰/H₂O systems, *J. Hazard. Mater.* 166 (2009) 79-87.
- [37] A.L. Bojic, D. Bojic, T. Andjelkovic, Removal of Cu²⁺ and Zn²⁺ from model wastewaters by spontaneous reduction-coagulation process in flow conditions, *J. Hazard. Mater.* 168 (2009) 813-819.
- [38] P. Schmuki, From Bacon to barriers: a review on the passivity of metals and alloys, *J. Solid State Electrochem.* 6 (2002) 145-164.
- [39] G.A. Loraine, D.R. Burris, L. Li, J. Schoolfield, Mass transfer effects on kinetics of dibromoethane reduction by zero-valent iron in packed-bed reactors, *J. Environ. Eng.* 128 (2002) 85-93.
- [40] P. Rao, M.S. Mak, T. Liu, K.C. Lai, I. Lo, Effects of humic acid on arsenic (V) removal by zero-valent iron from groundwater with special references to corrosion products analyses, *Chemosphere* 75 (2009) 156-162.
- [41] W. Wilopo, K. Sasaki, T. Hirajima, T. Yamanaka, Immobilization of arsenic and manganese in contaminated groundwater by permeable reactive barriers using zero valent iron and sheep manure, *Mater. Trans* 49 (2008) 2265-2274.
- [42] J.A. Lackovic, N.P. Nikolaidis, G.M. Dobbs, Inorganic arsenic removal by zero-valent iron, *Environ. Eng. Sci.* 17 (2000) 29-39.
- [43] C. Noubactep, G. Meinrath, P. Dietrich, B. Merkel, Mitigating uranium in groundwater: prospects and limitations, *Environ. Sci. Technol.* 37 (2003) 4304-4308.
- [44] C. Noubactep, J. Sonnefeld, D. Merten, T. Heinrichs, M. Sauter, Effects of the presence of pyrite and carbonate minerals on the kinetics of the uranium release from a natural rock, *J. Radioanal. Nucl. Chem.* 270 (2006) 325-333.
- [45] S.H. Joo, A.J. Feitz, T.D. Waite, Oxidative degradation of the carbothioate herbicide, molinate, using nanoscale zero-valent iron, *Environ. Sci. Technol.* 38 (2004) 2242-2247.
- [46] C. Lee, D.L. Sedlak, Enhanced formation of oxidants from bimetallic nickel-iron nanoparticles in the presence of oxygen, *Environ. Sci. Technol.* 42 (2008) 8528-8533.

- [47] Y. Jiao, C. Qiu, L. Huang, K. Wu, H. Ma, S. Chen, L. Ma, D. Wu, Reductive dechlorination of carbon tetrachloride by zero-valent iron and related iron corrosion, *Appl. Catal. B* 91 (2009) 434-440.
- [48] H. Song, E.R. Carraway, Catalytic hydrodechlorination of chlorinated ethenes by nanoscale zero-valent iron, *Appl. Catal. B* 78 (2008) 53-60.
- [49] A. Ghauch, H. Abou Assi, A. Tuqan, Investigating the mechanism of clofibric acid removal in Fe⁰/H₂O systems, *J. Hazard. Mater.* 176 (2010) 48-55.
- [50] A. Ghauch, G. Ayoub, S. Naim, Degradation of sulfamethoxazole by persulfate assisted micrometric Fe⁰ in aqueous solution, *Chem. Eng. J.* 228 (2013) 1168-1181.
- [51] C. Liang, Y.-y. Guo, Mass Transfer and Chemical Oxidation of Naphthalene Particles with Zerovalent Iron Activated Persulfate, *Environ. Sci. Technol.* 44 (2010) 8203-8208.
- [52] R.F. Dantas, S. Contreras, C. Sans, S. Esplugas, Sulfamethoxazole abatement by means of ozonation, *J. Hazard. Mater.* 150 (2008) 790-794.
- [53] M. Schnarr, C. Truax, G. Farquhar, E. Hood, T. Gonullu, B. Stickney, Laboratory and controlled field experiments using potassium permanganate to remediate trichloroethylene and perchloroethylene DNAPLs in porous media, *J. Contam. Hydrol.* 29 (1998) 205-224.
- [54] S.-Y. Oh, S.-G. Kang, P.C. Chiu, Degradation of 2,4-dinitrotoluene by persulfate activated with zero-valent iron, *Sci. Total Environ.* 408 (2010) 3464-3468.
- [55] S.-Y. Oh, H.-W. Kim, J.-M. Park, H.-S. Park, C. Yoon, Oxidation of polyvinyl alcohol by persulfate activated with heat, Fe²⁺, and zero-valent iron, *J. Hazard. Mater.* 168 (2009) 346-351.
- [56] R. Watts, A. Teel, Chemistry of Modified Fenton's Reagent (Catalyzed Propagations-CHP) for In Situ Soil and Groundwater Remediation, *J. Environ. Eng.* 131 (2005) 612-622.
- [57] G.P. Anipsitakis, D.D. Dionysiou, Radical Generation by the Interaction of Transition Metals with Common Oxidants, *Environ. Sci. Technol.* 38 (2004) 3705-3712.
- [58] J.T. Schmidt, M. Ahmad, A.L. Teel, R.J. Watts, Hydrogen peroxide stabilization in one-dimensional flow columns, *J. Contam. Hydrol.* 126 (2011) 1-7.
- [59] Y. Ku, Y.-H. Tu, C.-M. Ma, Effect of hydrogen peroxide on the decomposition of monochlorophenols by sonolysis in aqueous solution, *Water Res.* 39 (2005) 1093-1098.

- [60] J.E. Bennett, B.C. Gilbert, J.K. Stell, Mechanisms of peroxide decomposition. EPR studies of the one-electron oxidation of the peroxymonosulphate anion (HOOSO₃⁻) and the reactions of SO₅[radical dot], *J. Chem. Soc., Perkin Trans. 2* (1991) 1105-1110.
- [61] M.G. Antoniou, A.A. de la Cruz, D.D. Dionysiou, Degradation of microcystin-LR using sulfate radicals generated through photolysis, thermolysis and e⁻ transfer mechanisms, *Appl. Catal. B* 96 (2010) 290-298.
- [62] C. Liang, C.J. Bruell, Thermally Activated Persulfate Oxidation of Trichloroethylene: Experimental Investigation of Reaction Orders, *Ind. Eng. Chem. Res.* 47 (2008) 2912-2918.
- [63] S.-X. Li, D. Wei, N.-K. Mak, Z. Cai, X.-R. Xu, H.-B. Li, Y. Jiang, Degradation of diphenylamine by persulfate: Performance optimization, kinetics and mechanism, *J. Hazard. Mater.* 164 (2009) 26-31.
- [64] C. Liang, C.J. Bruell, M.C. Marley, K.L. Sperry, Persulfate oxidation for in situ remediation of TCE. I. Activated by ferrous ion with and without a persulfate–thiosulfate redox couple, *Chemosphere* 55 (2004) 1213-1223.
- [65] X.-R. Xu, X.-Z. Li, Degradation of azo dye Orange G in aqueous solutions by persulfate with ferrous ion, *Sep. Purif. Technol.* 72 (2010) 105-111.
- [66] Y.-q. Gao, N.-y. Gao, Y. Deng, Y.-q. Yang, Y. Ma, Ultraviolet (UV) light-activated persulfate oxidation of sulfamethazine in water, *Chem. Eng. J.* 195–196 (2012) 248-253.
- [67] R.J. Watts, A.L. Teel, Treatment of contaminated soils and groundwater using ISCO, *Pract. Periodical Hazard., Toxic, Radioact. Waste Manage.* 10 (2006) 2-9.
- [68] S.P. Forsey, In situ chemical oxidation of creosote/coal tar residuals: Experimental and numerical investigation, in: University of Waterloo, 2004.
- [69] P. Neta, V. Madhavan, H. Zemel, R.W. Fessenden, Rate constants and mechanism of reaction of sulfate radical anion with aromatic compounds, *J. Am. Chem. Soc.* 99 (1977) 163-164.
- [70] R.E. Huie, C.L. Clifton, Temperature dependence of the rate constants for reactions of the sulfate radical, SO₄⁻, with anions, *J. Phys. Chem.* 94 (1990) 8561-8567.
- [71] R.E. Huie, C.L. Clifton, S.A. Kafafi, Rate constants for hydrogen abstraction reactions of the sulfate radical, SO₄⁻: experimental and theoretical results for cyclic ethers, *J. Phys. Chem.* 95 (1991) 9336-9340.

- [72] G.R. Peyton, The free-radical chemistry of persulfate-based total organic carbon analyzers, *Mar. Chem.* 41 (1993) 91-103.
- [73] R.H. Waldemer, P.G. Tratnyek, R.L. Johnson, J.T. Nurmi, Oxidation of chlorinated ethenes by heat-activated persulfate: kinetics and products, *Environ. Sci. Technol.* 41 (2007) 1010-1015.
- [74] A. Ghauch, A.M. Tuqan, Oxidation of bisoprolol in heated persulfate/H₂O systems: Kinetics and products, *Chem. Eng. J.* 183 (2012) 162-171.
- [75] A. Ghauch, A.M. Tuqan, N. Kibbi, Ibuprofen removal by heated persulfate in aqueous solution: A kinetics study, *Chem. Eng. J.* 197 (2012) 483-492.
- [76] K.-C. Huang, R.A. Couttenye, G.E. Hoag, Kinetics of heat-assisted persulfate oxidation of methyl tert-butyl ether (MTBE), *Chemosphere* 49 (2002) 413-420.
- [77] K.-C. Huang, G.E. Hoag, P. Chheda, B.A. Woody, G.M. Dobbs, Kinetics and mechanism of oxidation of tetrachloroethylene with permanganate, *Chemosphere* 46 (2002) 815-825.
- [78] K.-C. Huang, Z. Zhao, G.E. Hoag, A. Dahmani, P.A. Block, Degradation of volatile organic compounds with thermally activated persulfate oxidation, *Chemosphere* 61 (2005) 551-560.
- [79] C. Liang, Z.-S. Wang, C.J. Bruell, Influence of pH on persulfate oxidation of TCE at ambient temperatures, *Chemosphere* 66 (2007) 106-113.
- [80] C.J. Liang, C.J. Bruell, M.C. Marley, K.L. Sperry, Thermally activated persulfate oxidation of trichloroethylene (TCE) and 1, 1, 1-trichloroethane (TCA) in aqueous systems and soil slurries, *Soil and Sediment Contamination: An International Journal* 12 (2003) 207-228.
- [81] M.R. Hoffmann, S.T. Martin, W. Choi, D.W. Bahnemann, Environmental Applications of Semiconductor Photocatalysis, *Chem. Rev.* 95 (1995) 69-96.
- [82] G.V. Buxton, C.L. Greenstock, W.P. Helman, A.B. Ross, Critical Review of rate constants for reactions of hydrated electrons, hydrogen atoms and hydroxyl radicals ($\cdot\text{OH}/\cdot\text{O}^-$ in Aqueous Solution, *J. Phys. Chem. Ref. Data* 17 (1988) 513-886.
- [83] Y.-T. Lin, C. Liang, J.-H. Chen, Feasibility study of ultraviolet activated persulfate oxidation of phenol, *Chemosphere* 82 (2011) 1168-1172.

- [84] S. Yang, P. Wang, X. Yang, G. Wei, W. Zhang, L. Shan, A novel advanced oxidation process to degrade organic pollutants in wastewater: Microwave-activated persulfate oxidation, *J. Environ. Sci.* 21 (2009) 1175-1180.
- [85] R.H. Waldemer, P.G. Tratnyek, R.L. Johnson, J.T. Nurmi, Oxidation of Chlorinated Ethenes by Heat-Activated Persulfate: Kinetics and Products, *Environ. Sci. Technol.* 41 (2006) 1010-1015.
- [86] J. Criquet, N. Karpel Vel Leitner, Electron beam irradiation of aqueous solution of persulfate ions, *Chem. Eng. J.* 169 (2011) 258-262.
- [87] P. Gayathri, R. Praveena Juliya Dorathi, K. Palanivelu, Sonochemical degradation of textile dyes in aqueous solution using sulphate radicals activated by immobilized cobalt ions, *Ultrason. Sonochem.* 17 (2010) 566-571.
- [88] H. Kusic, I. Peternel, S. Ukic, N. Koprivanac, T. Bolanca, S. Papic, A.L. Bozic, Modeling of iron activated persulfate oxidation treating reactive azo dye in water matrix, *Chem. Eng. J.* 172 (2011) 109-121.
- [89] C. Liang, M.-C. Lai, Trichloroethylene degradation by zero valent iron activated persulfate oxidation, *Environ. Eng. Sci.* 25 (2008) 1071-1078.
- [90] O. Travina, Y.N. Kozlov, A. Purmal, I. ROD'KO, Synergism of the action of the sulfite oxidation initiators, iron and peroxydisulfate ions, *Russ. J. phys. chem.* 73 (1999) 1215-1219.
- [91] A. Ghauch, A. Tuqan, Catalytic degradation of chlorothalonil in water using bimetallic iron-based systems, *Chemosphere* 73 (2008) 751-759.
- [92] A. Ghauch, A. Tuqan, Reductive destruction and decontamination of aqueous solutions of chlorinated antimicrobial agent using bimetallic systems, *J. Hazard. Mater.* 164 (2009) 665-674.
- [93] C.-Y. Hu, S.-L. Lo, Y.-H. Liou, Y.-W. Hsu, K. Shih, C.-J. Lin, Hexavalent chromium removal from near natural water by copper-iron bimetallic particles, *Water Res.* 44 (2010) 3101-3108.
- [94] Y. Liu, F. Yang, P.L. Yue, G. Chen, Catalytic dechlorination of chlorophenols in water by palladium/iron, *Water Res.* 35 (2001) 1887-1890.
- [95] R. Muftikian, Q. Fernando, N. Korte, A method for the rapid dechlorination of low molecular weight chlorinated hydrocarbons in water, *Water Res.* 29 (1995) 2434-2439.

- [96] Y. Ukisu, S. Kameoka, T. Miyadera, Catalytic dechlorination of aromatic chlorides with noble-metal catalysts under mild conditions: approach to practical use, *Appl. Catal. B* 27 (2000) 97-104.
- [97] A. Ghauch, H.A. Assi, H. Baydoun, A.M. Tuqan, A. Bejjani, Fe⁰-based trimetallic systems for the removal of aqueous diclofenac: Mechanism and kinetics, *Chem. Eng. J.* 172 (2011) 1033-1044.
- [98] X. Xu, H. Zhou, D. Wang, Structure relationship for catalytic dechlorination rate of dichlorobenzenes in water, *Chemosphere* 58 (2005) 1497-1502.
- [99] H. Lucida, J. Parkin, V. Sunderland, Kinetic study of the reaction of sulfamethoxazole and glucose under acidic conditions: I. Effect of pH and temperature, *Int. J. Pharm.* 202 (2000) 47-62.
- [100] A. Ghauch, H. Baydoun, P. Dermesropian, Degradation of aqueous carbamazepine in ultrasonic/Fe⁰/H₂O₂ systems, *Chem. Eng. J.* 172 (2011) 18-27.
- [101] C. Liang, C.-F. Huang, N. Mohanty, R.M. Kurakalva, A rapid spectrophotometric determination of persulfate anion in ISCO, *Chemosphere* 73 (2008) 1540-1543.
- [102] G. Lente, M.E.A. Magalhães, I. Fábíán, Kinetics and Mechanism of Complex Formation Reactions in the Iron(III)–Phosphate Ion System at Large Iron(III) Excess. Formation of a Tetranuclear Complex, *Inorg. Chem.* 39 (2000) 1950-1954.
- [103] L. Zhu, Z. Ai, W. Ho, L. Zhang, Core–shell Fe–Fe₂O₃ nanostructures as effective persulfate activator for degradation of methyl orange, *Sep. Purif. Technol.* 108 (2013) 159-165.
- [104] D.E. Pennington, A. Haim, Stoichiometry and mechanism of the chromium(II)-peroxydisulfate reaction, *J. Am. Chem. Soc.* 90 (1968) 3700-3704.
- [105] C. Liang, C.J. Bruell, M.F. Albert, P.E. Cross, D.K. Ryan, Evaluation of reverse osmosis and nanofiltration for in situ persulfate remediated groundwater, *Desalination* 208 (2007) 238-259.
- [106] R. Van Eldik, G.M. Harris, Kinetics and mechanism of the formation, acid-catalyzed decomposition, and intramolecular redox reaction of oxygen-bonded (sulfito)pentaamminecobalt(III) ions in aqueous solution, *Inorg. Chem.* 19 (1980) 880-886.

- [107] J.K. Steehler, *Chemical Analysis: Modern Instrumentation Methods and Techniques*, 2nd Edition (Francis Rouessac and Annick Rouessac), *J. Chem. Educ.* 85 (2008) 373.
- [108] F. Vicente, A. Santos, A. Romero, S. Rodriguez, Kinetic study of diuron oxidation and mineralization by persulphate: Effects of temperature, oxidant concentration and iron dosage method, *Chem. Eng. J.* 170 (2011) 127-135.
- [109] G.V. Buxton, T.N. Malone, G.A. Salmon, Pulse radiolysis study of the reaction of SO₅[radical dot]- with HO₂[radical dot], *J. Chem. Soc., Faraday Trans.* 92 (1996) 1287-1289.
- [110] J.L. Mohatt, L. Hu, K.T. Finneran, T.J. Strathmann, Microbially mediated abiotic transformation of the antimicrobial agent sulfamethoxazole under iron-reducing soil conditions, *Environ. Sci. Technol.* 45 (2011) 4793-4801.
- [111] A. Ghauch, H. Abou Assi, S. Bdeir, Aqueous removal of diclofenac by plated elemental iron: bimetallic systems, *J. Hazard. Mater.* 182 (2010) 64-74.
- [112] Y. Xie, D.M. Cwiertny, Chlorinated solvent transformation by palladized zerovalent iron: Mechanistic insights from reductant loading studies and solvent kinetic isotope effects, *Environ. Sci. Technol.* 47 (2013) 7940-7948.
- [113] A. Ghauch, A. Tuqan, H.A. Assi, Antibiotic removal from water: elimination of amoxicillin and ampicillin by microscale and nanoscale iron particles, *Environ. Pollut.* 157 (2009) 1626-1635.
- [114] P. Gostin, S. Oswald, L. Schultz, A. Gebert, Acid corrosion process of Fe-based bulk metallic glass, *Corros. Sci.* 62 (2012) 112-121.
- [115] S. Caré, R. Crane, P.S. Calabrò, A. Ghauch, E. Temgoua, C. Noubactep, Modeling the Permeability Loss of Metallic Iron Water Filtration Systems, *CLEAN – Soil, Air, Water* 41 (2013) 275-282.

APPENDIX

RESEARCH CONTRIBUTIONS

Ghauch, A., Ayoub, G. “Investigation into bimetallic and trimetallic iron-based systems for the activation of sodium persulfate toward water treatment and sustainability: Application to sulfamethoxazole antibiotic” PAPER ID: 17075. 245th ACS National Meeting & Exposition - April 7-11, 2013, New Orleans, LA.

Ghauch, A.Naim, S., Ayoub, G. and Tuqan, A (2012) Thermally activated persulfate for the removal of pharmaceuticals from water. Gordon Research Conference, Environmental Sciences: Water, 06/24/2012 - 06/29/2012, Location: Holderness School in Holderness NH United States.

Malaeb, L., Ayoub, G., Al Hindi, M., Ghauch, A. (2011) Assessment of water quality from different sources in a novel solar still, IDA World Congress on Desalination and Water Reuse, Desalination: Sustainable Solutions for a thirsty Planet, September 4-9, 2011, Perth Convention Exhibition Center Western Australia IDAWC: REF :(PER11-058).

Ghauch, A., Baydoun, H., Ayoub, G. and Naim, S. (2011). Submicrometric iron particles for the removal of pharmaceuticals in water: Application to b-lactam antibiotics. 15-17 March 2011, Beirut, Lebanon (Talk).

Ghauch, A., Ayoub, G. “Investigation into sulfamethoxazole degradation by persulfate assisted micrometric Fe⁰ in aqueous solution”. Central Research Science Laboratory 3rd Conference- June-4-2012, American University of Beirut- Lebanon.

G. Ayoub, T. Bruton, A. Tuqan, D. Sedlak, A. Ghauch. “ Investigation into persulfate oxidation of benzene in different aqueous matrices: effect of chloride and bromide ions. 5th EuCheMS Chemistry Congress, August 31 – September 4, 2014, Istanbul / Turkey.

REFERRED PUBLICATION I: DEGRADATION OF
SULFAMETHOXAZOLE BY PERSULFATE ASSISTED
MICROMETRIC Fe⁰ IN AQUEOUS SOLUTION



Degradation of sulfamethoxazole by persulfate assisted micrometric Fe⁰ in aqueous solution

Antoine Ghauch*, Ghada Ayoub, Sahar Naim

American University of Beirut, Faculty of Arts and Sciences, Department of Chemistry, P.O. Box 11-0236 Riad El Solh, 1107-2020 Beirut, Lebanon

HIGHLIGHTS

- Sulfamethoxazole is fully degraded in Fe⁰/PS systems at room temperature.
- Very low un-washed iron load can sustain PS activation over 3 cycles of 1 h each.
- The reaction stoichiometric efficiency reaches 5.2% under controlled conditions.
- Sulfate radicals are quenched by an excess of iron particles.
- Bicarbonate delays iron corrosion and limits Fe²⁺ release into the solution.

ARTICLE INFO

Article history:

Available online 21 May 2013

Keywords:

Sulfamethoxazole
Fe⁰
Persulfate
Redox
Emergent contaminants
Water

ABSTRACT

Persulfate (PS) chemical activation using micrometric Fe⁰ particles (MIPs) was tested on sulfamethoxazole (SMX) solution (39.5 μM). MIPs load (0.89–17.85 mM), PS content (0.4–1.0 mM), pH (5.50–8.30) and alkalinity (bicarbonate) were investigated for the improvement of SMX degradation. Optimum conditions for the enhancement of the reaction stoichiometric efficiency (RSE = 5.2%) were developed. HPLC–MS results confirmed that SMX was converted into its reduced form through cleavage of the isoxazole N–O bond by two routes: (i) electron abstraction upon sulfate radicals (SRs) attack yielding non stable radical cation SMX^{•+} or (ii) electron addition through Fe⁰ oxidation yielding unstable radical anion SMX^{•-}. In both cases, the final transformation product was identified as b-aminoenone after acceptance of electrons originated from the MIPs surface and protons present in the acidic medium. This suggested that PS activated into SRs was responsible of the rapid degradation of SMX and its transformation product as well in contrast to Fe⁰ alone. Different water matrices were evaluated in order to understand the role that dissolved ions play on the reaction degradation rate. Successive experiments (*n* = 3) of 1 h each conducted on remaining Fe⁰ showed complete SMX degradation. The extent of SMX mineralization under the experimental conditions reached 37% making from Fe⁰/PS system an excellent source of SRs able to sustain oxidation reactions in aqueous media of slightly acidic pH.

© 2013 Elsevier B.V. All rights reserved.

1. Introduction

Antimicrobial agents such as sulfamethoxazole (SMX) are commonly used to treat and prevent diseases in animals, as well as promote growth and weight gain in livestock [1]. As a result of overuse, these active pharmaceutical molecules (APMs) may reach the water system through industrial activities (pharmaceutical effluents) or domestic discard (excretes, urine, toilet flushing), posing serious health and environmental risks. In addition, recent studies have highlighted the role that livestock manure may play in contaminating surface and underground water after application, even at the ng and μg levels [2]. This finding has been confirmed by several studies at many sites around the world [3,4]. Such low con-

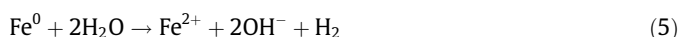
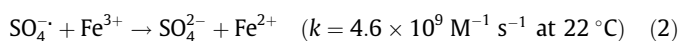
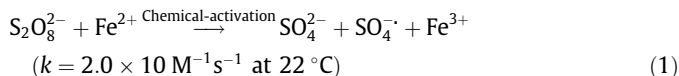
centration levels might allow antimicrobial agents altering microbial community structure yielding antibiotic resistance in environmental microbial communities [5–7]. Because APMs are generally difficult to destroy through conventional biological means in wastewater treatment plants, removal methods have been developed with the aim of restoring water quality. This is essential to avoid further pollution of the environment and enable safe reuse of such water, thereby decreasing fresh water consumption. SMX contaminated water has been treated through chlorination [8], photo-Fenton and solar photo-Fenton [9,10], ozonation [11] and photocatalysis [12–14]. Most of these treatment options are expensive (energy demanding, catalyst consuming), and may yield unstable and/or stable metabolites. Those can be reconverted into more toxic compounds or into original SMX under natural conditions. Accordingly, existing treatment methods have not shown significant advantages for field or full scale applications in

* Corresponding author. Tel.: +961 1350 000; fax: +961 1 365 217.

E-mail address: antoine.ghauch@aub.edu.lb (A. Ghauch).

terms of SMX mineralization extent and bacteria resistance developed by transformation products [15,16].

Consequently, research has been undertaken in the present work using persulfate chemical activation as an advanced oxidation process (AOP) that may be applied to SMX contaminated water using MIPs. PS chemical activation occurs through reduction upon reaction of an adequate amount of a transition metal like Fe^{2+} , Co^{2+} [17,18]. This will result in the production of sulfate radicals (SRs) which are very reactive toward organic molecules (Eq. (1)). However, excess of Fe^{2+} feeding might result in SRs quenching yielding a decrease in the reaction stoichiometric efficiency (RSE) after the formation of sulfate anion and Fe^{3+} [19,20] (Eq. (2)). RSE is the number of SMX moles degraded/the number of PS moles consumed. Therefore, a smooth Fe^{2+} releasing method can overcome such a disadvantage. This can be optimized by taking advantage of iron corrosion through MIPs dissolution in $\text{Fe}^0/\text{H}_2\text{O}$ systems. In this case, Fe^{2+} can be progressively released into the solution under natural experimental conditions where dissolved oxygen as well as the pH and species like bicarbonate could not significantly disturb mild iron corrosion [17,21–23] (Eqs. (3)–(5)).



It has also been recently demonstrated that in $\text{Fe}^0/\text{H}_2\text{O}$ systems, iron corrosion products (ICPs) including nascent iron oxides are formed in addition to Fe^{2+} , which might also contribute to the activation of PS [24,25]. However, iron load and iron characteristics are of great importance in promoting ICPs formation. This contribution is one of the first to report on the use of micrometric iron particles (MIPs) assisted PS for the degradation of a recalcitrant APM like SMX. Specific objectives were to (i) study the PS load effect on SMX removal in $\text{Fe}^0/\text{H}_2\text{O}$ systems, (ii) evaluate MIPs content on SMX degradation, (iii) elucidate SMX oxidation mechanism, (iv) optimize SMX degradation process toward mineralization and (v) assess the application of such process to many SMX water matrices with used MIPs.

2. Materials and methods

2.1. Chemicals

SMX was obtained from Sigma Aldrich (USA). Sodium Persulfate (SPS) ($\text{Na}_2\text{S}_2\text{O}_8$, 99%) was purchased from Chem-Lab (Belgium); Potassium iodide (KI) (puriss, 99–100.5%) and iron particles (puriss 99.5%, fine powder, <150 μm) were purchased from Riedel-de-Haen (Germany). Sodium dihydrogen phosphate dihydrate ($\text{NaH}_2\text{PO}_4 \cdot 2\text{H}_2\text{O}$, >99%), hydrated tri-sodium phosphate $\text{Na}_3\text{PO}_4 \cdot 12\text{H}_2\text{O}$, phosphoric acid (H_3PO_4), ammonium acetate ($\text{C}_2\text{H}_7\text{NO}_2$, >98%) (puriss ACS reagent), sodium hydrogen carbonate (NaHCO_3) and hydrochloric acid (HCl) were from Fluka (Netherlands). Di-Sodium hydrogen phosphate anhydrous (Na_2HPO_4) was purchased from Merck (Germany). Reagents for iron complexation to form “ferroin” complex (o-phenantroline, hydroxylamine and tri-sodium citrate) were acquired from Prolabo (France). HPLC solvents (methanol and acetonitrile) were of HPLC grade and purchased from Sigma.

2.2. Experimental setup

The SMX solution was prepared by adding 20 (± 0.1) mg of SMX at room temperature ($\text{C}_{10}\text{H}_{11}\text{N}_3\text{O}_3\text{S}$; M.W. 253.05 g mol^{-1} ; $\text{p}K_{\text{a}1} = 1.7$ and $\text{p}K_{\text{a}2} = 5.6$) to deionized water (DI) (capped 1 L volumetric flask) to make a 79 μM stock solution [26]. For some experiments, DI water was replaced by tap, underground, and hydrogen carbonate enriched DI water. The resulting solution was stirred overnight at room temperature until complete SMX dissolution, then filtered through a 0.45 μm filter to remove any non-dissolved particles. 200 mM stock solution of phosphate buffer (PB) was prepared by mixing 6.6860 g Na_2HPO_4 with 6.3396 g NaH_2PO_4 in 200 mL DI water in order to conduct experiments at pH 7.00. MIPs were acid washed with 15 mL of 1.0 M HCl solution for 10 min, rinsed with deoxygenated DI water, then freeze dried (Labconco) for 2 h before use. Adequate volumes of prepared stock solutions were mixed to a predefined volume of deionized water to get the desired concentration of each reactant e.g. $[\text{SMX}]_0 = 39.5 \mu\text{M}$ (10 mg L^{-1}), $[\text{SPS}]_0 = 0.4\text{--}1.0 \text{ mM}$ and $[\text{PB}] = 1.0 \text{ mM}$. Thereafter, adequate amounts (1–20 mg) of dry MIPs (acid washed or not) were introduced into several 20 mL Pyrex vials at room temperature. Reactors (in duplicate) were then positioned on a vortex shaker of variable mixing intensities. High vortex speeds will result in greater friction between MIPs, yielding more cracks in iron oxides at the MIPs surface. The vortex used had a sample holder, which could accommodate up to 8 vials. In order to minimize MIPs mass loss during sampling, each reactor was set on a magnet so that the iron particles were immobilized. Aliquots (0.5 mL) were sampled directly with a 1 mL BD syringe and filtered into a 2 mL HPLC vial using a 0.22 μm PTFE acrodisk filter (Jaytee Biosciences Ltd., UK). To stop any radical reactions after sampling, all vials were chilled at 4 $^\circ\text{C}$ in an ice bath for about 10 min before storage on the thermostated HPLC autosampler prior to HPLC analysis. This method has been used previously instead of using radical quenchers such as NaNO_2 or MeOH [27–30]. For experiments conducted with used MIPs (μFe) in PS/Fe systems, after a first cycle of 1 h, the treated solution was completely withdrawn from the reactor using a syringe. MIPs were kept immobilized at the bottom of the reactor using a magnet. A subsequent cycle was undertaken by adding 20 mL of fresh SMX solution (39.5 μM). pH was measured at the beginning and end of each experiment using a pH/Ion meter (Thermo Orion, USA) equipped with an ultra-combination pH electrode (Ross). Controls were conducted in the absence of PS and SMX for each experiment. Data presented are averaged value of four replicate samples (duplicate experiments and duplicate analyses). Final results are given as mean ($\pm ts/\sqrt{n}$) where t is the student value at 95% confidence interval, s the standard deviation and n the number of replicates.

2.3. Chemical analysis

For monitoring purposes, SMX analysis was performed on an Agilent 1100 Series LC/MS system consisting of a quaternary pump, a vacuum degasser, an autosampler, a thermostated column compartment and a diode array detector (DAD) coupled with an ion trap mass spectrometer detector (MSD). The liquid chromatography column was a C_{18} reversed phase column (5 μm ; 4.6 i.d. \times 250 mm long) coupled to a security guard column HS C_{18} (5 μm ; 4.0 i.d. \times 20 mm long) (Discovery, Supelco, USA), which was maintained at 30 $^\circ\text{C}$ during analysis. Additional details on this equipment have been previously described [29–33]. The mobile phase consisted of 50:50 (v/v) 10 mM ammonium acetate and acetonitrile under isocratic mode. The flow rate and injection volume were about 0.5 mL min^{-1} and 25 μL , respectively. The system was controlled by the LC/MSD ChemStation software version A.09.03. Under the given conditions, SMX was eluted at 6.5 min with a max-

imum absorbance at 265 nm. The persulfate anions were spectrophotometrically determined at 352 nm using a Nanodrop 2000c UV–VIS Spectrophotometer (Thermo Scientific) in accordance with the procedure developed by Liang and collaborators [34]. Total iron and ferrous ions were quantified using o-phenantroline at a wavelength of 510 nm for “ferroin” maximum absorbance [35]. MIPs characteristics were determined by Scanning Electron Microscopy (SEM). Surface morphology and elemental composition were studied by the mean of a Tescan Vega 3 LMU (Czech Republic) SEM, equipped with an EDX system with a 20 mm² X-Max thermoelectrically cooled detector coupled to a multichannel analyzer. Additional details on the SEM are given elsewhere [36]. Mineralization of SMX was measured by a total organic carbon (TOC) analyzer (GE 5310C) equipped with an autosampler and a CO₂ conductivity detector. Samples were centrifuged at 4000g and filtered prior to analysis. A minimum volume of 17 mL was required for each analysis.

3. Results and discussion

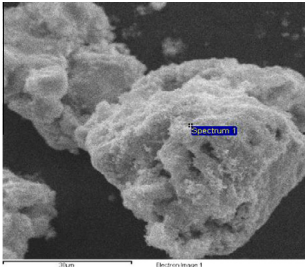
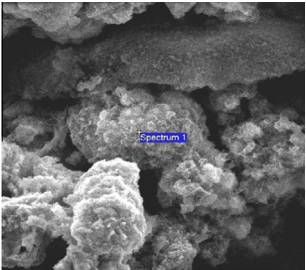
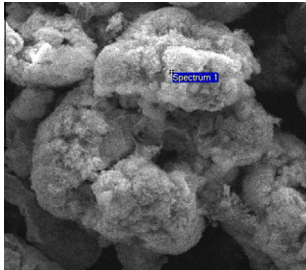
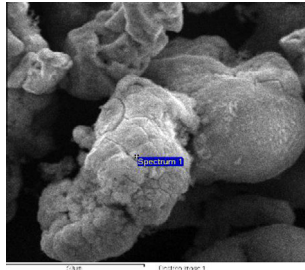
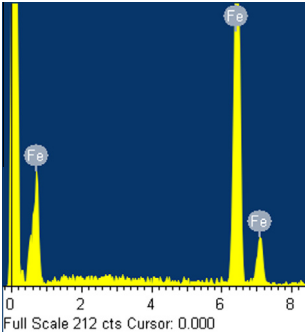
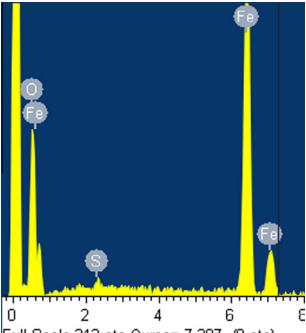
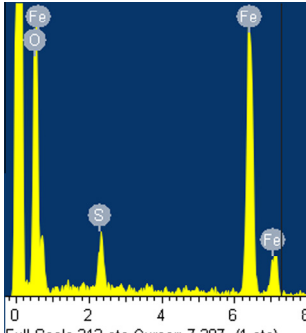
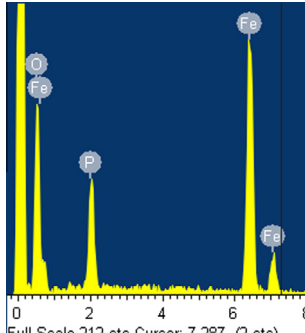
3.1. Characterization of Fe⁰ particles in different systems

SEM images and EDX analyses of acid-washed MIPs after reaction with SMX are summarized in Table 1. Four systems were compared in order to understand the role of PS in the process of iron corrosion and to evaluate the use of PB in iron-activated PS systems: System 1 (wFe/SMX), System 2 (wFe/PS), System 3 (wFe/SMX/PS) and System 4 (wFe/SMX/PS/PB). The concentrations of all reactants were as follows: [Fe⁰] = 17.85 mM, [PS]₀ = 1.0 mM, [SMX]₀ = 39.5 μM, [PB] = 1.0 mM. It can be noted that after a reaction time of 2 h, the surface of MIPs in contact with a PS free solution was composed of almost 100% Fe (Table 1, System 1). However, when MIPs were in contact with PS solution (System

2), the Fe% composition dropped to 54.6% making from O and S the other constituents of the iron particles surface (44.6% and 0.87% respectively). This trend was similar in the presence of SMX (System 3) where the iron particle surface composition also showed less iron (36.2%) and more oxygen (60.4%) and sulfur (3.55%). In the presence of PB (System 4), the analysis did not show any sulfur on the surface of MIPs. This may be due to phosphate fixation on iron oxides formed at the surface of MIPs, as previously demonstrated [39]. Accordingly, phosphate species quickly covered the surface of MIPs avoiding PS access and therefore making iron corrosion more difficult, especially at neutral pH conditions. To understand the effect of phosphate species on the reactive medium, a survey of the concentration of ICPs (as total iron [Fe]_t = [Fe^(II)] + [Fe^(III)]) in all solutions was undertaken. Without acidification, the concentration of Fe²⁺ species was below the maximum concentration limit (MCL) set by the WHO (e.g. 0.3 mg L⁻¹ or 5.4 μM) [38]. However, after acidification with concentrated HCl, the solution turned colorless after dissolution of ICPs and quantification of Fe²⁺ species became reliable. Results showed less iron concentration in the PS free system (System 1) e.g. [Fe]_t = 3.5–mg L⁻¹ compared to PS containing systems (Systems 2–4) after 2 h of reaction. For example, 20.88 and 17.75 mg L⁻¹ of ICPs were found in System 2 and System 3, respectively, while only 11.46 mg L⁻¹ was present in the phosphate containing system (System 4). These results confirmed that the surface of iron particles was more seriously affected by the presence of PS (Systems 2–4) than by its absence (System 1). A pitting trend appeared on iron particles in contact with PS containing solution. However, such an observation was absent for iron particle surfaces in PS free and PB containing solutions as seen in SEM results of Table 1. The observed pitting phenomenon is due to the direct reaction of PS with MIPs (Eq. (6)) to yield Fe²⁺.



Table 1
SEM/EDX of MIPs after reaction in different Fe⁰/H₂O systems. Experimental conditions: [Fe]₀ = 17.85 mM, [SMX]₀ = 39.5 μM, [PS]₀ = 1.0 mM, [PB] = 1.0 mM.

System 1	System 2	System 3	System 4
Fe ⁰ /SMX	Fe ⁰ /PS	Fe ⁰ /SMX/PS	Fe ⁰ /SMX/PS/PB
			
			
Fe 100%	Fe 54.6%, O 44.6%, S 0.87%	Fe 36.2%, O 60.4%, S 3.5%	Fe 31.3%, O 59.7%, P 9.0%
pH _i	5.63	5.54	7.00
pH _f	6.66	5.28	6.85
[Fe ^{2+/3+}] mg L ⁻¹	3.50	17.75	11.46

Accordingly, excess of PS might produce excess of $\text{Fe}^{2+/3+}$ and ICPs yielding more SO_4^- quenching (Eq. (2)). As a result, the concentration of PS should be rigorously optimized in order to conserve an acceptable RSE. However, phosphate species can delay or even inhibit the iron corrosion process after fixation on nascent iron oxides formed at the surface of MIPs. Furthermore, iron species can form different complexes with PB (e.g. $\text{Fe}(\text{H}_2\text{O})_4(\text{H}_2\text{PO}_4)^{2+}$, $\text{Fe}(\text{H}_2\text{O})_4(\text{H}_2\text{PO}_4)_2^+$, $\text{Fe}(\text{H}_2\text{O})_4(\text{PO}_4)_2^{3-}$, etc.) and hinder the release of Fe^{2+} /ICPs responsible for the activation of PS into SRs [37,39–41]. Phosphate concentration in solution should be well controlled so that iron species are not completely complexed, keeping some free Fe^{2+} and nascent iron oxides in solution, which play a crucial role in the production of SRs. This might present a disadvantage especially for the treatment of effluent containing phosphates species.

3.2. Effect of iron surface and phosphate buffer on the degradation of SMX

Fig. 1 shows the effect of iron particles surface (acid washed or used as received / un-washed) on the degradation yield of SMX in the presence and in the absence of PS and PB at different pH values. It can be seen that reactions with acid-washed MIPs (wFe/SMX) were more successful than those carried out with un-washed MIPs

(nwFe/SMX). For example, it was determined that 27% SMX disappeared for wFe systems, in contrast to only 7% for nwFe systems. This may be attributed to the omnipresence of aged iron oxide on the surface of commercial MIPs making the oxide scale non-porous and consequently resistant to corrosion. However, acid washed MIPs are temporary exempted from the impervious oxide scale making the latter porous, accessible to SMX molecules and more reactive toward water dissolved species [42–44]. Therefore, SMX adsorption and transformation are more likely to occur in this case, which can explain higher SMX removal extent than for nwFe system. A greater increase in the pH of the solution treated with wFe (pHi 5.63 to pHf 6.66) than with that of nwFe (pHi 5.63 to pHf 6.32) was also observed, which is likely due to the formation of additional hydroxide anions upon aqueous oxidic corrosion (Eqs. (4) and (5)).

The same systems operating in the presence of PB (wFe/SMX/PB and nwFe/SMX/PB) at pHi 7.00 did not show any significant SMX removal (7–8%). In view of this low SMX removal rate, reactors with and without PB were spiked with PS to obtain a final PS concentration of about 1 mM. Under PS spiking, the PB systems showed different results depending on the starting pH of the solution. For example, at pHi 7.00, nwFe/SMX/PS/PB and wFe/SMX/PS/PB showed only 12% and 8% SMX removal after 2 h of reaction with

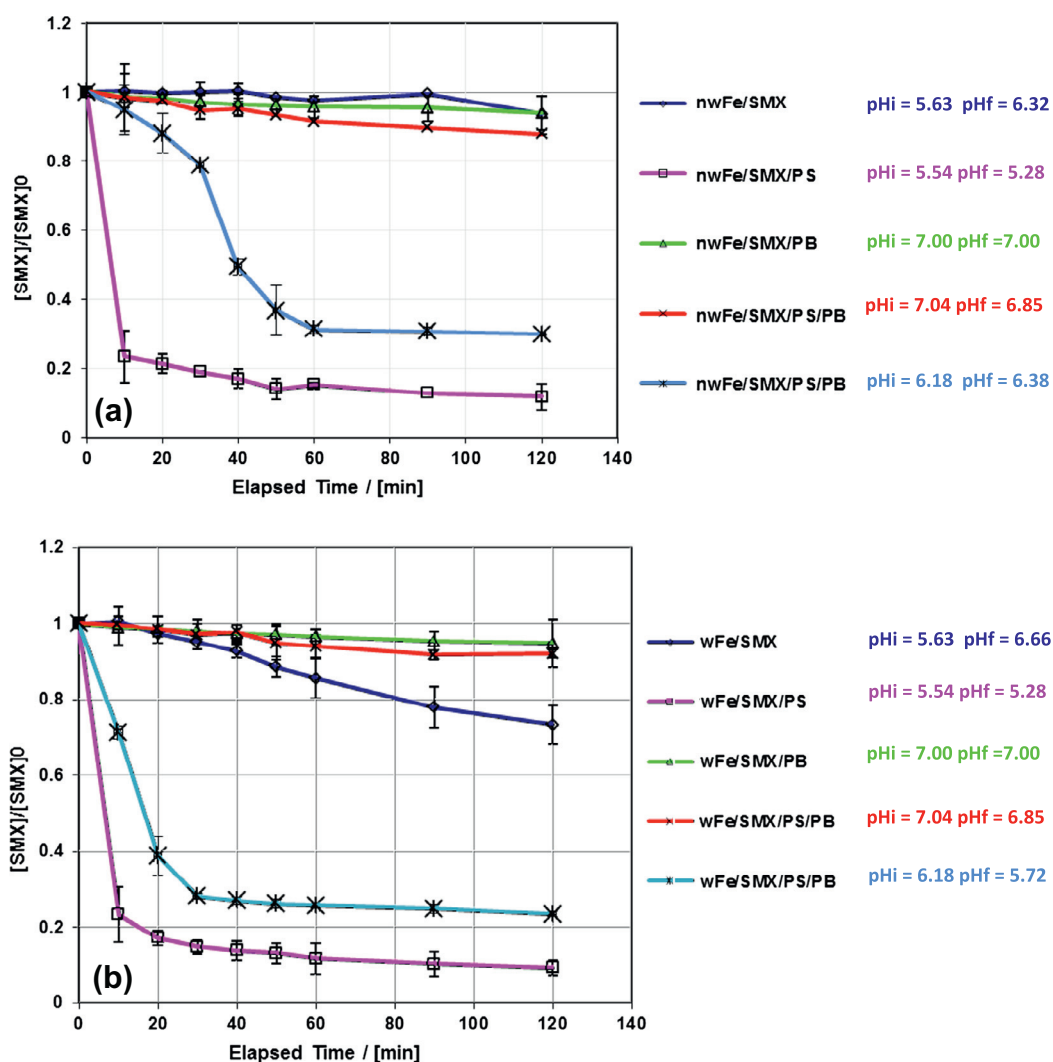


Fig. 1. Influence of MIPs surface and PB on the oxidation of SMX by PS. (a) MIPs used as received (nwFe for non-washed Fe), and (b) acid-washed MIPs (wFe for acid-washed Fe). Experimental conditions: $[\text{Fe}^0] = 17.85 \text{ mM}$, $[\text{PS}]_0 = 1.0 \text{ mM}$, $[\text{SMX}]_0 = 39.5 \text{ }\mu\text{M}$, $[\text{PB}] = 1 \text{ mM}$. Solid lines are only used to connect data. Error bars represent uncertainties at a 95% confidence interval.

a slight pH decrease (pHf 6.85). However, at a starting pH of 6.18, SMX removal reached 71% and 77% for nwFe/SMX/PS/PB and wFe/SMX/PS/PB systems, respectively, which is mostly due to more iron corrosion in acidic, compared to neutral medium. The decrease in pH is likely due to the formation of HSO_4^- (Eqs. (7) and (8)) responsible for the release of protons (Eq. (9)), even in the presence of PB.

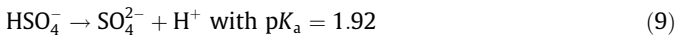


Fig. 1 also reveals the delay taken by SMX to disappear in nwFe/SMX/PS/PB and wFe/SMX/PS/PB systems compared to PB free systems. This can be attributed to different lag times taken by wFe and nwFe to corrode in the presence of phosphate species. For example, only 12% of SMX removal was recorded after 20 min of reaction in

the nwFe/SMX/PS/PB system in contrast to 72% in the wFe/SMX/PS/PB system to yield finally comparable SMX removal rates at later stage. However, the removal rates in these systems remained less than those reported for PS spiked PB free systems (e.g. wFe/SMX/PS and nwFe/SMX/PS). This can be explained by the deposition of phosphate species at the surface of MIPs hindering quick iron corrosion and sequestration/adsorption of SMX molecules into the iron oxides matrix covering the surface of iron particles. This can also be accompanied by iron complexation with phosphate species, which limits free Fe^{2+} in solution for PS activation. In fact, PB-free systems e.g. wFe/SMX/PS and nwFe/SMX/PS were most efficient towards SMX removal yielding 91% and 89%, respectively. One can also notice that for both systems pH changes were not significant. A pH decrease from 5.54 to 5.28 was observed, confirming that the choice of 1 mM PS “in excess” was reasonable for SMX degradation. On the other hand, a survey of the concentration of remaining PS in the reactors showed that full PS consumption takes place in PB free systems at an early stage of the reaction (10 min) while partial PS

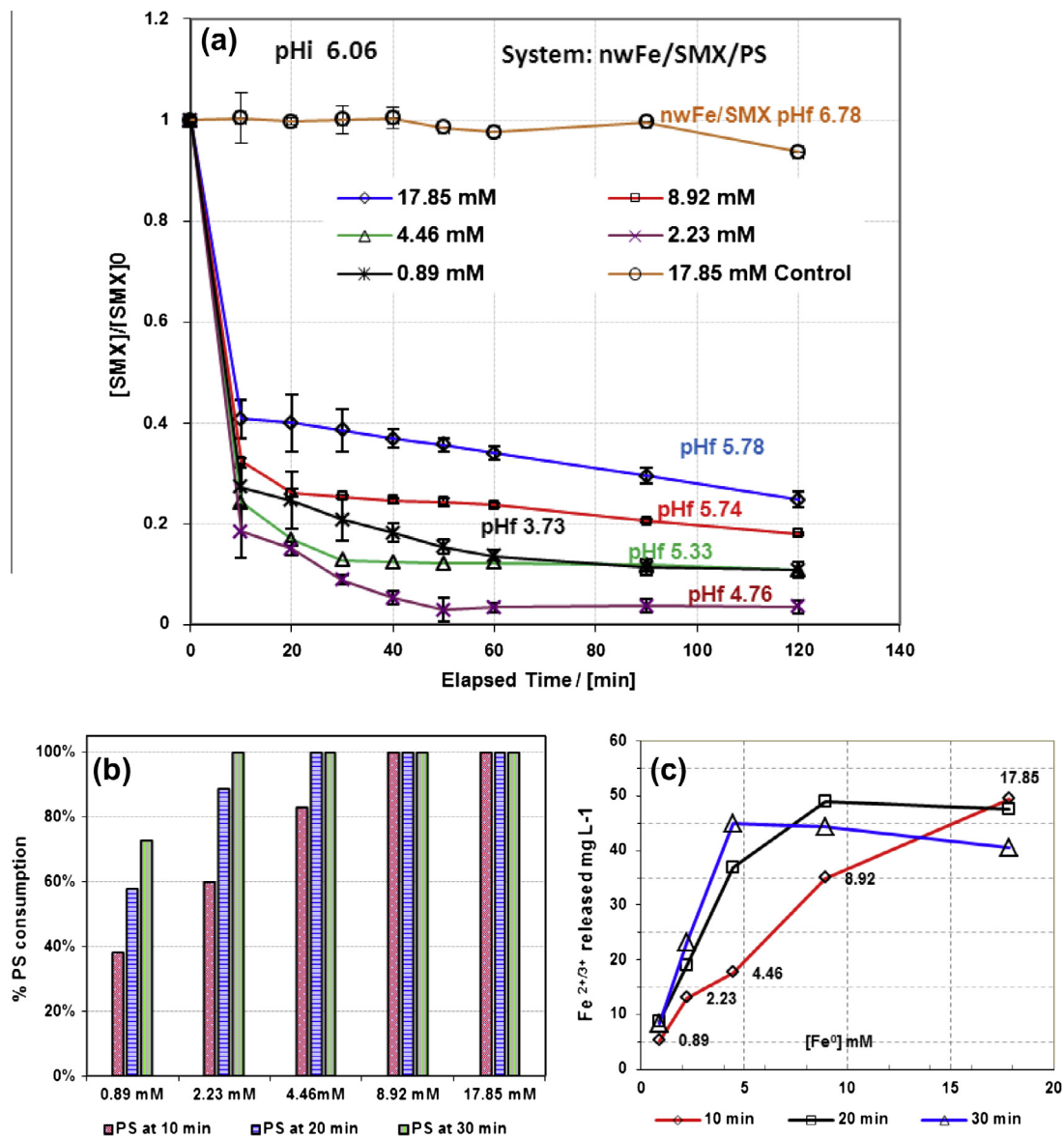


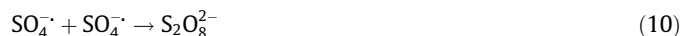
Fig. 2. (a) Influence of iron load on the oxidation yield of SMX in deionized water. (b) PS consumption at 10, 20 and 30 min of the reaction. (c) Concentration of total dissolved iron species into the reactor at 10, 20 and 30 min of the reaction. Experimental conditions: $[\text{Fe}^0] = 0.89\text{--}17.85$ mM, $[\text{PS}]_0 = 1.0$ mM and $[\text{SMX}]_0 = 39.5$ μM . Solid lines are only used to connect data. Error bars represent uncertainties at a 95% confidence interval.

consumption (~45%) was observed in PB systems even by the end of the reaction (e.g. 2 h). Accordingly, one can deduce that PS and/or derived SRs might have reacted with the iron-phosphate complexes yielding less SMX removal, probably due to SRs quenching. PS remaining clearly explains the steep decline in the SMX curves until 10 min of reaction for wFe/SMX/PS and nwFe/SMX/PS systems, followed by a very moderate degradation rate for reaction time >10 min mainly. Such a slow rate might be due to the continuous action of nascent iron oxides formed upon MIPs corrosion after PS depletion into the solution. Nascent iron oxides are very active at the surface of MIPs and present high adsorption properties toward organic and inorganic species [45–47].

Finally, these results suggest that commercial MIPs may be used “as received” without prior conditioning in the absence or presence of phosphate species whose concentration might be significant in special effluents.

3.3. Iron load effect on SMX degradation

A set of experiments was designed to optimize MIPs load for the degradation of SMX in nwFe/SMX/PS systems. The aim was to define a minimum amount of MIPs able to activate enough PS into SRs for SMX degradation without encountering radical quenching due to the presence of a high concentration of iron species released into solution (Eq. (2)). Loads ranged from 0.05 to 1.0 g L⁻¹ corresponding to a Fe⁰ concentration range of about 0.89–17.85 mM. The results are presented in Fig. 2. The upper curve shows the control experiment carried out in the nwFe/SMX system with the highest MIPs load of about 17.85 mM in the absence of PS (Fig. 2a). No significant SMX degradation was observed. However, a sudden decrease in the concentration of SMX happened at different rate depending on MIPs load in all PS containing systems. By observing all SMX decline curves, one can distinguish two different parts (Fig. 2a). The first part shows a steep decline up to 10 min, while the second part is characterized by a slow decrease at different MIPs loads with an asymptotic behavior. The first part can be explained by the oxidative action of SRs on SMX since at early stage of the reaction (<10 min) and for moderate iron loads (<4.46 mM), PS is not yet depleted (Fig. 2b) and produce upon Fe²⁺ release (Fig. 2c) a consequent number of SRs. However, if SRs are in excess, radical–radical reactions occur (Eq. (10)) decreasing the degradation rate. For example, only 59% and 68% of SMX is removed after 10 min of reaction time with 17.85 and 8.92 mM of MIPs loads, respectively, while 76%, 73% and 82% of SMX removal is noticed with lesser MIPs loads e.g. 4.46, 2.23 and 0.89 mM, respectively.



As seen in Fig. 2b, the second part of the decline curves is subjected to a depletion of the solution from PS especially at highest MIPs loads. For example, after 20 min of reaction, all PS was consumed for MIPs loads >4.46 mM. Only for MIPs loads of 0.89 and 2.23 mM, PS consumption is partial. At 10 min, 38%, 60% and 83% of PS has been consumed for 0.89, 2.23 and 4.46 mM MIPs loads, respectively. However, at 20 min, 58%, 89% and 100% of PS has been consumed for 0.89, 2.23 and 4.46 mM MIPs loads, respectively. Starting at 30 min of reaction time, all PS has been consumed and the system is only governed by the interaction of SMX molecules with MIPs surface, as well as generated ICPs. Accordingly, the additional SMX removal (16.1% and 14.3%) observed for the highest MIPs loads (17.85 and 8.92 mM) from 10 min to 2 h is only due to MIPs able to adsorb and sequester at pH >5.0 SMX molecules into nascent iron oxides formed upon iron corrosion in oxic medium. However, for lesser iron loads, some of the PS remained

unconsumed and contributed to additional SMX removal (e.g. 16.4%, 14.8% and 13.4% for MIPs loads of 0.89, 2.23 and 4.46 mM, respectively).

A survey of the concentration of the total iron species (Fe^{2+/3+}) produced in the reactors at early stages of the reaction e.g. 10, 20 and 30 min (Fig. 2c) confirmed that for higher loads, more Fe^{2+/3+} is present, which may affect the performance of the PS activated systems in terms of SRs quenching (Eq. (2)). For example, 50 mg L⁻¹ (892 μM) of Fe^{2+/3+} was noted at 10 min of the reaction for the highest MIPs load (e.g. 17.89 mM) while only 5 mg L⁻¹ (89.2 μM) were found at the lowest MIPs load (e.g. 0.89 mM). The concentration of Fe^{2+/3+} reported here at 17.89 mM of MIPs load is greater than the one reported in the previous section (Table 1, System 3) due to faster shaking. This allowed more MIPs interactions, and therefore more iron oxide cracks, which increases the total iron content in solution. Accordingly, the metallic iron load in solution should be carefully chosen based on the corrosion potential of the medium (e.g. presence of dissolve oxygen, starting pH), the ability of MIPs to dissolve (e.g. specific surface area, particle size) and the initial PS concentration. Fig. 2c also shows that a linear relationship between MIPs loading and iron in solution (ICPs) is not likely to occur, especially at later stages of the reaction and for MIPs load >4.46 mM. This can be attributed to the solubility limit of iron species and to an equilibrium reached under the experimental conditions. This clearly appears on Fe^{2+/3+} curves at 20 and 30 min where an iron concentration maximum is reached, followed by a steady state or even a slight decrease especially for iron loads greater than 4.46 mM. In the current case, the most performing system at 1 mM PS was the system initiated with 2.23 mM of MIPs load. At this concentration, SMX degradation was faster until the end of the reaction of 2 h with a removal extent up to 97%. However for 0.89 mM, it seems that Fe²⁺ was limiting and PS could not be effectively activated. One should not forget the direct reaction between PS and MIPs, which decreases the number of PS molecules available for activation by Fe²⁺ and ICPs as well. A progressive release of Fe²⁺ should be maintained in solution to maintain PS activation with a minimum of radical quenching. These conditions seem to be met under the current experimental conditions of 2.23 mM MIPs load at a starting pH around 6.0. Accordingly, PS optimization will be tested under those conditions to determine the optimum conditions for a maximum RSE.

3.4. Effect of PS content on SMX degradation

Fig. 3a shows that more SMX degradation occurs at the highest PS load. For example, 95% of SMX disappeared after 2 h of reaction for 1 mM of PS additive and only 50%, 69% and 85% of SMX degradation was obtained with PS load of 0.4, 0.6 and 0.75 mM, respectively. However, most of the SMX degradation happened at an early stage of the reaction (up to 20 min) followed by a steady state (asymptotic behavior) during which, little or insignificant additional SMX degradation occurred. Such an observation can be attributed to the excessive PS activated at an early stage of the reaction (0–20 min) into SRs as it can be seen from Fig. 3b displaying the remaining PS concentration into the solution. Complete PS consumption was observed after 20 min of reaction for almost all systems. This can clearly explain the steady state of the SMX decline curves observed after 20, 30, 40 and 50 min of reaction for 0.4, 0.6, 0.75 and 1.0 mM PS loads, respectively. In order to better understand this observation in terms of SRs selectivity, the RSE was calculated for all PS concentrations used at different reaction times (5–60 min). Fig. 3c shows that RSE averages (calculated for each PS load at all selected times 5–60 min) ranged between 3.28% and 5.03%; the highest RSE being for the lowest PS load (e.g. 0.4 mM) while the lowest RSE was noticed for the highest

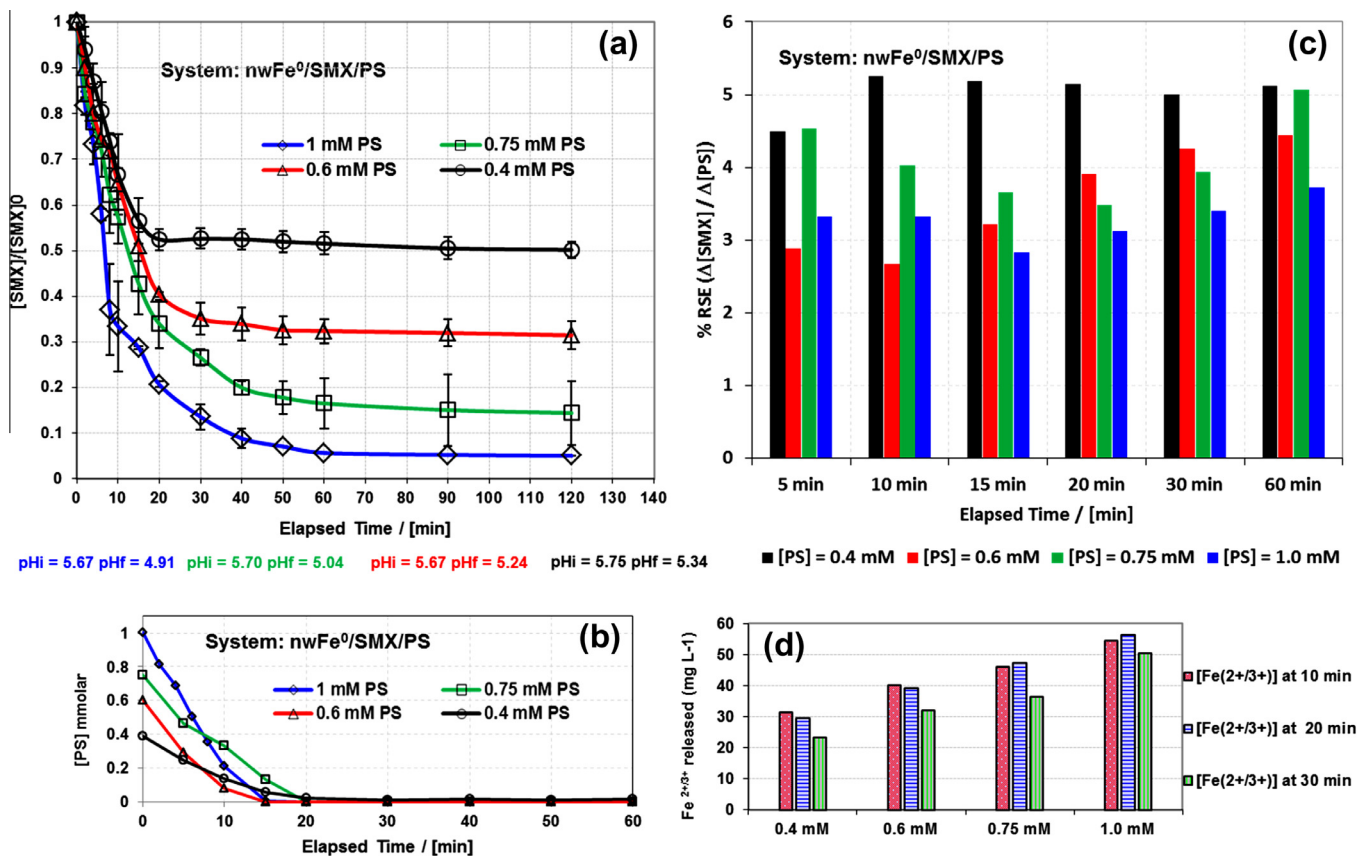


Fig. 3. (a) Influence of PS additives on the oxidative treatment of SMX in deionized water. (b) Time course of PS during the reaction. (c) The RSE relative to each PS concentration in Fig. 3a calculated at different reaction times (5–60 min). (d) Concentration of iron species (equivalent Fe²⁺) at 10, 20 and 30 min of the reaction. Experimental conditions: [nwFe⁰] = 2.23 mM, [PS]₀ = 0.40–1.00 mM, [SMX]₀ = 39.5 μM. Solid lines are only used to connect data. Error bars represent uncertainties at a 95% confidence interval.

PS load (e.g. 1 mM). For the same initial MIPs content, more ICPs were produced in systems containing more PS additives upon direct reaction of PS with MIPs (Eq. (6)). The corresponding results are presented in Fig. 3d. For example, the concentration of Fe^{2+/3+} increased linearly from 31 to 55 mg L⁻¹ after 10 min of reaction at pHi 5.65 when PS load increases from 0.4 to 1.0 mM. The same trend was also observed after 20 and 30 min of reaction time. Accordingly, more SRs are produced at higher PS loads due to the formation of more Fe²⁺ activators. This favored radical-Fe²⁺ reaction (Eq. (2)), radical-radical reaction (Eq. (10)) [48], and radical-H₂O reaction (Eq. (7)) [49]. However, for less PS content (0.4 mM), fewer iron species are produced and therefore less SRs are generated, which disfavors side reactions and increases the calculated RSE.

The RSE values found in the current work are not comparable to RSE values found in thermally activated persulfate systems (e.g. Bisoprolol, Ibuprofen) for the treatment of pharmaceuticals [29,30]. For example, the minimum and maximum RSE values reported after 1 h of 1 mM PS reaction with 50 μM bisoprolol were about 20% and 100% at 40 and 50 °C of activation temperature, respectively. However, the RSE reported in this work has a maximum of 3.7% for the same PS concentration and reaction time. The direct reaction between PS and MIPs is in part responsible for the low RSE values obtained, but also the acidic medium (5.67 < pHi < 5.75), which improves iron corrosion and results in an excess of ICPs that might quench SRs. As previously reported (Eq. (2)), most of the SRs produced are quenched with an excess of Fe²⁺ species resulting from rapid oxidation of MIPs especially under acidic conditions. This was confirmed by the final pH values

(pH_f) being more acidic for the highest PS solution load (e.g. [PS] = 1.0 mM). For example, the lowest and highest reported pH_f were 4.91 and 5.34 for SMX solutions containing initial [PS] of about 1.0 and 0.4 mM, respectively. Recall that this pH decrease is a result of bisulfate formation (Eqs. (7) and (8)) and dissociation (Eq. (9)). pH_f reported are usually greater than 2 unless an extremely high persulfate concentration (e.g. 1 M) is used [50,51]. Fig. 3c also reveals that above a certain [PS] limit (e.g. 0.4 mM), RSEs are almost comparable. Accordingly, one can conclude that MIPs content is the limiting factor and, once controlled in terms of corrosion rate, can contribute to longer PS lifetime and consequently sustainable SRs generation into the solution. This will result in continuous SMX degradation instead of reaching a steady state where no more SMX degradation occurs. Further experiments were performed to evaluate the potential of the remaining oxidized MIPs and their corresponding ICPs to activate additional PS spiked at a later stage of the reaction. This was carried out by conducting successive experiments where different water matrices were tested (Section 3.6).

3.5. Mineralization of SMX in nwFe⁰/SMX/PS system

A mineralization analysis was done on an SMX solution prepared in a 40 mL reactor in order to have enough solution to conduct TOC measurements [52]. The reactants were set at previously determined optimum concentrations e.g. [SMX] = 39.5 μM, [PS] = 1.0 mM, [Fe⁰] = 2.23 mM. The theoretical TOC value of the solution was 4.74 mg L⁻¹ and the experimental TOC value given by the instrument was about 4.79 mg L⁻¹. After 2 h of reaction,

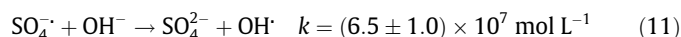
the solution was centrifuged and filtered giving a TOC content of 3.02 mg L^{-1} and a TOC removal of 37%. Such a value is comparable and even exceeds those detailed in the literature for similar oxidation experiments at room temperature. For example, the % TOC removal obtained by Vicente and collaborators [20] on $85.8 \mu\text{M}$ Diuron solution reached 27% and 45% at 20 and 50°C , respectively with $[\text{PS}] = 2.6 \text{ mM}$ and Fe^{2+} feeding (50 mg L^{-1}) instead of MIPs. Although the experimental conditions are not comparable in terms of selected probes, PS concentration, temperature, ionic strength, iron content and iron feeding, one can deduce that SMX mineralization obtained through oxidation in $\text{nwFe}^0/\text{SMX}/\text{PS}$ system at room temperature is very encouraging.

3.6. Water matrix effect on SMX degradation in successive degradation cycles

Three different cases were investigated to study the effect of the water matrix on the performance of the Fe/PS system used for the degradation of SMX using the optimized conditions previously determined. Case 1 consists of tap water ($G = 1,146 \mu\text{mhos/cm}$); Case 2 corresponds to underground water ($G = 490 \mu\text{mhos/cm}$) and Case 3 to DI water ($G = 1.96 \mu\text{mhos/cm}$). Cycles were about 1 h each for a total of three. Residual PS concentrations were monitored (see Supplementary material for details, Fig. 1S). For tap and underground water, speciation was not determined since it was assumed that the main SRs quenchers were the carbonated species.

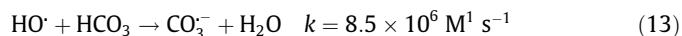
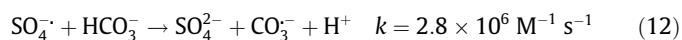
3.6.1. Case 1 (Tap water)

Fig. 4a shows that the $\text{nwFe}/\text{SMX}/\text{tap water}$ system is not efficient in removing SMX. Non-significant loss in SMX concentration was observed for all cycles. This is attributed to (i) the absence of PS as SRs precursor and (ii) the low load of MIPs (e.g. 2.23 mM) that was not sufficient to induce any reduction and/or co-precipitation of SMX. In addition, the initial pH of tap water ($\text{pHi} = 7.93$) does not favor MIPs oxidation and, therefore, the formation of ICPs responsible for SMX elimination. A slight increase in the pH of the resulting solution was detected ($\text{pHf} = 8.07$) which correlates with iron oxidation and consequently the formation of hydroxide species. However, in the $\text{nwFe}/\text{SMX}/\text{PS}/\text{tap water}$ system, SMX degradation yielded 20% for the first two cycles and about 16% for the 3rd cycle. This low% degradation may be attributed to poor release of Fe^{2+} species due to the initial basic pH of the solution (e.g. $\text{pHi} = 7.81$). While iron oxidation occurs at slightly basic pH, a sufficient amount of Fe^{2+} is released resulting in the activation of a consequent amount of PS therefore the formation of the acidic species HSO_4^- (Eqs. (7) and (8)). This explains the slight decrease in pH of the starting solution from $\text{pHi} = 7.81$ to $\text{pHf} = 7.75$. An analysis of the residual PS content into the solution showed that 70% of the initial PS was consumed by the end of the 1st and 2nd cycle and only 58% by the end of the 3rd cycle (Supplementary material, Fig. 1S). This indicates that most of the SRs interact with foreign species present in tap water including OH^- resulting in a small SMX degradation yield (Eq. (11)) [53].



To indirectly demonstrate the contribution of the basic pH of the starting solution in the small degradation yield of SMX, $5 \mu\text{L}$ of concentrated HCl was added to the reactor to obtain a pH of 5.71. The resulting $\text{nwFe}/\text{SMX}/\text{PS}/\text{acidified tap water}$ system increased SMX degradation to about 60%, 58% and 70% for the first, second and third cycle, respectively. The remaining PS present at the end of the first, second and third cycles was about 0%, 40% and 60% respectively showing faster PS consumption at acidic pH, especially during the first cycle (Supplementary material, Fig. 1S). As cycles were running, PS consumption decreased due

to less Fe^{2+} species available in solution after MIPs depletion. SMX degradation yields were less than those obtained for DI water under the same conditions. This can be attributed to some species present in tap water responsible for SRs and OH^- quenching. One of them is carbonate species known for their reaction with sulfate and hydroxyl radicals at significant reaction rate constants (Eqs. (12) and (13)) [54,55]. To confirm this hypothesis, additional experiments were carried out in DI water, however they were enriched with bicarbonate at a concentration close to the one encountered in drinking and underground water (e.g. $[\text{NaHCO}_3] = 160 \text{ mg L}^{-1}$).



3.6.2. Case 2 (DI water)

recycling experiments conducted in Case 1 were performed again, however using DI water instead of tap water. Fig. 4b shows similar behavior for the $\text{nwFe}/\text{SMX}/\text{PS}/\text{DI}/\text{Bicarbonate}$ system as reported in Case 1 (e.g. $\text{nwFe}/\text{SMX}/\text{PS}/\text{tap water}$). For example, 20%, 16% and 10% of SMX was degraded during the first, second and third cycles, respectively. The pH decreased from $\text{pHi} 8.26$ to $\text{pHf} 7.00$ confirming the activation of PS into SRs after iron corrosion even at slightly basic pH. The analysis of the remaining PS content showed 80%, 60% and 58% consumption during the first, second and third cycles, respectively (Supplementary material, Fig. 1S). However, the situation was improved in the $\text{nwFe}/\text{SMX}/\text{PS}/\text{DI}$ system where SMX degradation reached 90% for the first and second cycle and only 20% for the third cycle. The low degradation yield observed for the third cycle was mostly due to MIPs depletion from the system. This was confirmed after analysis of the remaining PS in solution. For example, 100% of PS was consumed at 20 min of the first cycle, 90% at 60 min of the second cycle and only 17% by the end of the third cycle (Supplementary material, Fig. 1S). High SMX degradation yields were due to an appropriate starting pH ($\text{pHi} = 5.67$) allowing MIP oxidation into Fe^{2+} responsible for PS activation. To confirm the role of bicarbonate in quenching SRs and OH^- as well, the $\text{nwFe}/\text{SMX}/\text{PS}/\text{DI}/\text{Bicarbonate}$ system was acidified by adding $5 \mu\text{L}$ of concentrated HCl to obtain a starting pH of $\text{pHi} = 5.66$, which is close to the pH of DI water. Results were similar to those of the $\text{nwFe}/\text{SMX}/\text{PS}/\text{DI}$ system. This pH value being less than the pK_1 of carbonic acid ($\text{pK}_1 = 6.4$ and $\text{pK}_2 = 10.3$), most of the carbonate species were in the form of H_2CO_3 that will dissociate into H_2O and CO_2 and escape from the solution. Consequently, the generated SRs react with SMX without being quenched. The last feature from this system is for the third cycle where less SMX degradation occurred (only 5%) because of the rapid depletion of MIPs by the end of the 2nd cycle. This was due to HCl addition responsible of quick MIPs dissolution.

3.6.3. Case 3 (Underground water, UGW)

Experiments similar to those conducted in Case 1 and Case 2 were undertaken, however in the presence of UGW. The latter has a pH of 8.05 and was collected from an aquifer, through a well at a depth of 300 m by means of a pump at a 313 m altitude (Position given by Google Earth: $34^\circ 08' 56.58'' \text{N}$ $35^\circ 40' 37.22'' \text{E}$). After dissolution of SMX, the new pH dropped slightly to 7.95. Two systems were tested in Case 3. The first ($\text{nwFe}/\text{SMX}/\text{PS}/\text{UGW}$) was carried out without pH adjustment, whereas the second system ($\text{nwFe}/\text{SMX}/\text{PS}/\text{acidified UGW}$) with pH lowering after adding $5 \mu\text{L}$ of concentrated HCl to the starting solution. As seen in Fig. 4c, the results of $\text{nwFe}/\text{SMX}/\text{PS}/\text{UGW}$ system showed a SMX degradation yield of about 17%, 10% and 8% for cycles 1, 2 and 3, respectively. These results are close to those obtained with the $\text{nwFe}/\text{SMX}/\text{PS}/\text{DI}/\text{Bicar}$

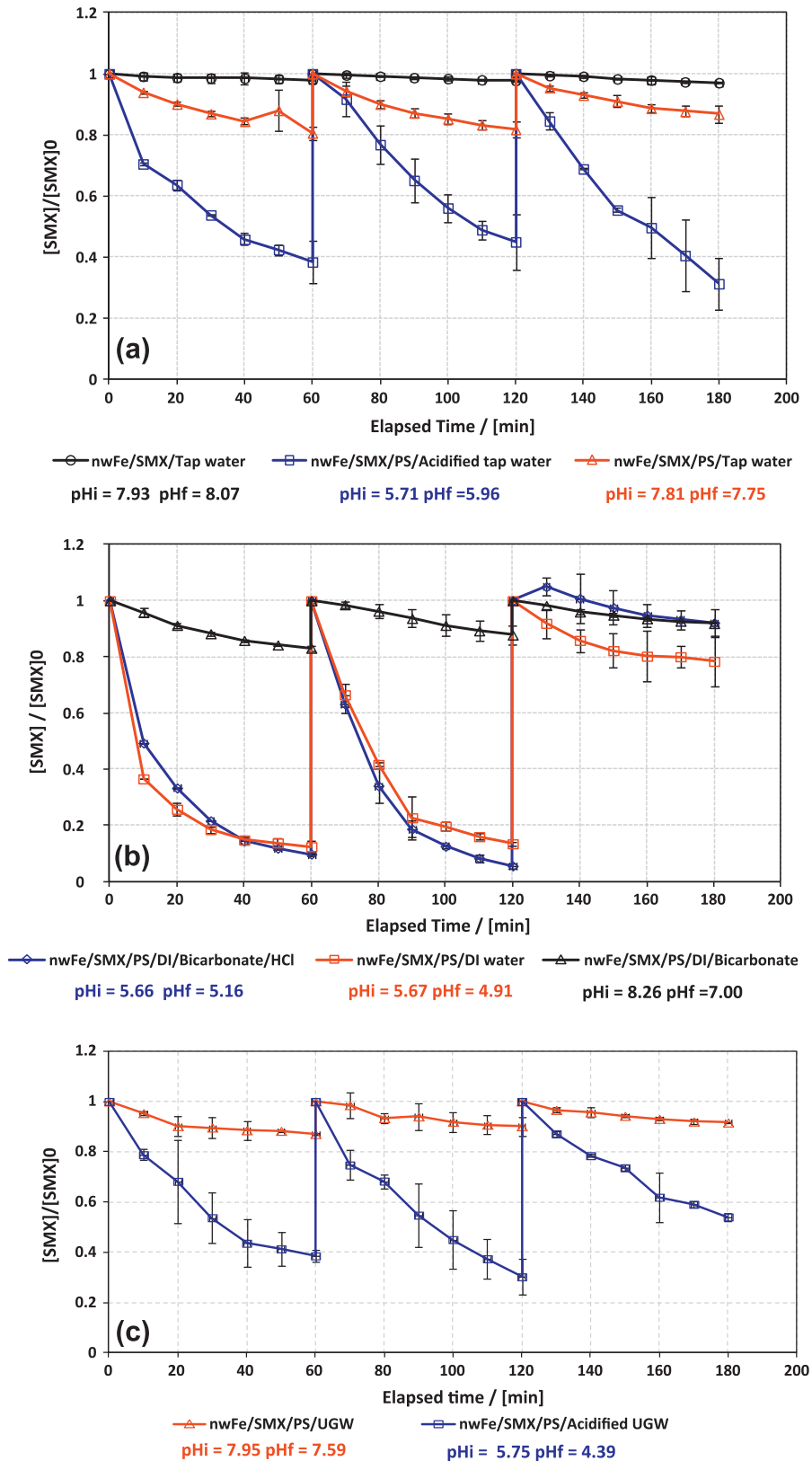


Fig. 4. Repetitive oxidation cycles with different water matrices. (a) Tap water, (b) DI water and (c) Underground water (UGW). Experimental conditions: $[\text{nwFe}^0] = 2.23 \text{ mM}$, $[\text{PS}]_0 = 1.0 \text{ mM}$, $[\text{SMX}]_0 = 39.5 \text{ }\mu\text{M}$. Solid lines are not fitting functions, they are only used to connect data. Error bars represent uncertainties at 95% confidence interval.

bonate system (Case 2). The similarity among results reveals the common content of UGW and bicarbonate enriched DI water in bicarbonate species at a slightly basic pH. However, once acidified,

the nwFe/SMX/PS/acidified UGW system shows better result with reported SMX degradation yield of about 62%, 71% and 43% by the end of cycles 1, 2 and 3 respectively. These results are close to those

obtained with the nwFe/SMX/PS/acidified tap water system (Case 1). Another feature from Fig. 4c is the continuous reactivity of PS toward SMX correlated to the omnipresence of MIPs not totally dissolved in acidified UGW during the first two cycles. This is also the case in Fig. 4a, where the nwFe/SMX/PS/acidified tap water system was efficient until the third cycle in contrast to Case 2 experiments where reduced activity of the nwFe/SMX/PS/DI system is noticed due to the consumption of MIPs by the end of the 2nd cycle. This may be advantageous in terms of application of nwFe/SMX/PS systems to natural effluents whose composition is close to the one of tap and underground waters and far away from that of DI water exempted from inorganic species.

3.7. Effect of iron ageing on the degradation of SMX and its transformation product

3.7.1. SMX case in nwFe⁰/SMX/PS system

Since Fe⁰/H₂O system was inefficient in removing SMX in a reasonable time and acceptable MIPs loads, three systems (1–3) were tested to investigate the possibility of making Fe⁰/H₂O more efficient after PS feeding. Fig. 5 shows SMX solutions for all systems treated with nwFe⁰ particles (100 mg Fe⁰/20 mL SMX solution e.g. [Fe⁰] = 89.2 mM) over 120 min (Zone A). Thereafter, the solutions were differently treated (Zone B in Fig. 5) prior to being fed by an appropriate volume of PS (e.g. [PS]₀ = 1 mM) as follows: For system 1, the resulting solution was immediately spiked with PS without prior magnetic filtration. The latter applied to systems 2 and 3 was carried out by settling the SMX reactor on a magnet for 1 min so all remaining MIPs were attracted to the bottom of the reactor. Afterwards, the solution was transferred to a new reactor using a syringe. For system 2, the resulting magnetically filtered solution was then spiked with PS and supplied at the same time with 2.5 mg of nwFe⁰ particles (2.23 mM). Finally, for system 3 the magnetically filtered solution was spiked with PS, however without any nwFe⁰ additive. The aim of this procedure was to check if: (i) used/oxidized MIPs (uFe⁰) in the original solution are able to activate PS even at high load (system 1); (ii) less fresh nwFe⁰ (e.g. 2.5 mg compared to 100 mg) can rapidly activate the PS under the same conditions (system 2) and (iii) dissolved ICPs are capable of sustaining PS activation into SRs (system 3). Results showed (Fig. 5) that at 2 h of treatment, prior to adding any PS,

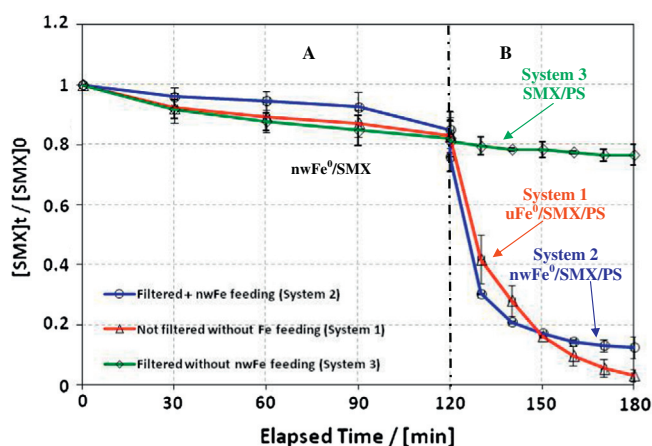


Fig. 5. Time course of SMX in Fe⁰ and Fe⁰/PS systems. Zone A is a PS free system. Zone B corresponds to PS-spiked systems. System 1 is made of the resulting solution at 120 min of reaction time to which 170 μ L of PS is added with [PS]₀ = 1 mM. System 2 is similar however after magnetic filtration of the resulting solution at 120 min of reaction time and addition of 1.6 mg of nwFe⁰ so as to obtain [Fe⁰] = 2.23 mM. System 3 is similar to system 2 however without any Fe⁰ addition.

SMX degradation only reached 18% for an iron load of 89.2 mM (Zone A). System 1 showed almost complete disappearance of SMX (97%) after adding PS; most of which occurred during the first 10 min (60%) of spiking. System 2 whose PS spiking was done after magnetic filtration followed by nwFe⁰ supply exhibited almost similar behavior regarding SMX degradation yielding 88% removal by the end of the treatment (at 180 min). However, system 3 was less reactive toward SMX whose degradation only reached 24% after 180 min of reaction time. This can be explained by the non-activation of PS into SRs due to the absence of Fe²⁺ species and other ICPs.

In both systems 1 and 2, it is expected that SRs are produced and most of them are involved in SMX degradation however, self-quenching reactions are likely to occur especially if excess of dissolved Fe(II) species are present into the solution (system 1). This was accompanied by the appearance of a transformation product at 5.7 min, which can be seen in the chromatograms presented in Fig. 6. The difference between systems 1 and 2 in terms of SMX removal is not significant, however the chromatograms revealed the following: In system 1, one can notice the appearance of a transformation product whose concentration increased as long as the treatment duration continued (up to 180 min, Fig. 6b). However, system 2 did not reveal the presence of any transformation product at the same time as SMX degraded (chromatograms not shown). This can be explained as follows: in system 1, PS additives reacted with a large excess of Fe⁰ particles after activation into SRs. During the first 2 h of Fe⁰ treatment, the surface of iron particles is mostly oxidized and covered by an imperious layer (non-diffusive). However, after reaction with PS, MIPs surface became clean with lesser oxide layer. This makes the oxide scale diffusive thereby allowing SMX adsorption and transformation into SMX derivative compound before being released again into solution. This observation is clearly observed in Fig. 6b, where all SMX disappeared in favor of the transformation product eluted at 5.7 min. In contrast, for system 2, MIPs load was much less (2.5 mg). Accordingly, SRs are not quenched by an excess of Fe²⁺ in solution but directly reacted with SMX molecules. These are converted into a non-stable intermediate that also undergoes oxidative reaction by SRs as well. The intermediate was not even detected in system 2 while in system 1, its presence yielding maximum concentration was observed. As for system 3, the relative chromatograms (not shown) revealed the presence of SMX transformation product at 5.7 min however with lesser extent as for system 1.

3.7.2. SMX transformation product case in nwFe⁰/SMX/PS system

To determine whether PS additive destroyed the SMX transformation product or if Fe⁰ alone was involved, two experiments (systems 4 and 5) were performed in parallel with an extended reaction time of up to 240 min. At the early stages, the experimental procedure was similar to that of system 1 described in Section 3.7.1. However, in system 4 and at 180 min of reaction time (end of zone B) the resulting solution was magnetically filtered, spiked with PS and supplied with nwFe⁰ particles at 2.23 mM. In system 5, the resulting solution was filtered and spiked with PS without the addition of nwFe⁰ particles at 180 min. The results summarized in Fig. 7 show that the SMX transformation product, stable in Fe⁰ solution, was completely degraded after PS addition. This occurred in the first 10 min of spiking, which can be seen in Fig. 7 between 180 and 200 min of reaction time and on Fig. 6c where a rapid vanishing of the corresponding chromatographic peak at Rt = 5.7 min occurred. As for system 5, SMX transformation products exhibited partial disappearance to an extent of 58% of its maximum at 180 min. This can be explained by the action of some SRs produced after activation of PS by some residual Fe²⁺ remaining in solution. The final chromatogram reveals the appearance of two small peaks between 4.2 and 5.6 min. Those peaks are almost

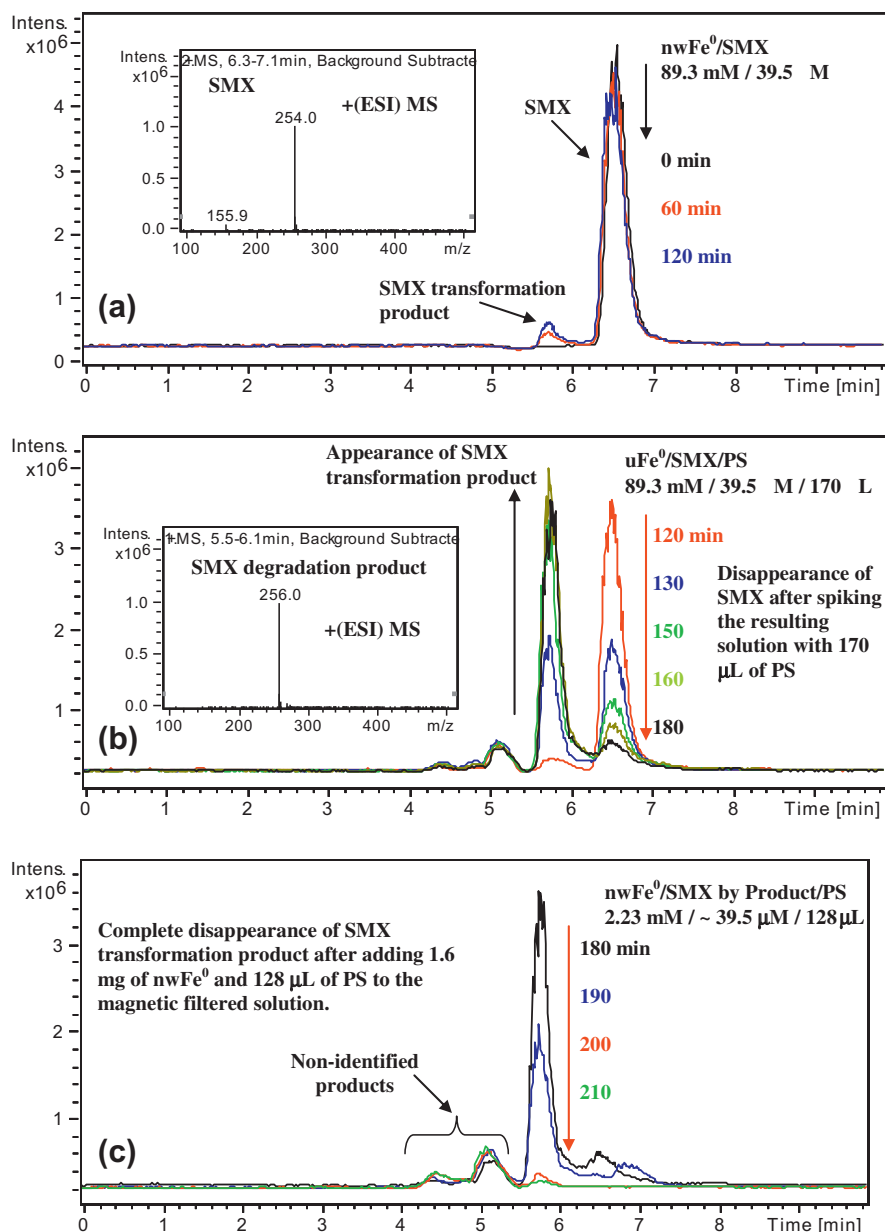


Fig. 6. LC-MS total ion chromatograms of SMX solution (20 mL) treated with $nwFe^0$ and PS. (a) $nwFe^0/SMX$ system, $[Fe^0] = 89.2$ mM, $[SMX]_0 = 39.5$ μM . The inset is the MS spectrum of SMX obtained in (+)ESI. (b) $uFe^0/SMX/PS$ system: the resulting solution was spiked with 170 μL PS at 120 min. The inset is the MS spectrum of SMX transformation product obtained in (+)ESI and eluted at 5.8 min. (c) $nwFe^0/SMX/PS$ system: the resulting solution (17 mL) was magnetically filtered, spiked with 128 μL PS and supplied with 1.6 mg of $nwFe^0$ (2.23 mM).

stable in terms of chromatographic areas and not clearly resolved. In addition their UV/Vis and MS spectra was not clear for further investigation. Accordingly, additional efforts were done in order to understand the way SMX disappeared. This was carried out by studying the MS spectra of the main SMX transformation product.

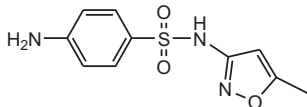
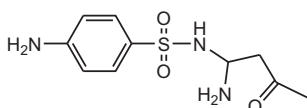
3.8. Identification of transformation product, structure elucidation and proposed reaction pathway

LC-MS and LC-MSⁿ analysis was done on SMX and its transformation product. As seen in Fig. 6 and Table 2, the MS spectrum of SMX presented a molecular ion $[M+H]^+$ at 254 m/z in positive ionization and a molecular ion $[M-H]^-$ at 251.8 m/z in negative ionization mode. Both modes showed a fragment at 155.9 m/z that corresponds to the loss of the $C_4H_6N_2O^+$ moiety. These results cor-

roborated those obtained in previous investigations on the removal of SMX via microbially mediated abiotic transformation under iron-reducing soil conditions [15]. Different fragments were also identified after MS² and MS³ analyses as reported in Table 2 (see Supplementary material for more details, Figs. 2S and 3S).

The transformation product eluted at 5.7 min was determined to be the β -aminoenone SMX derivative after studying its MS spectrum. This transformation product showed a molecular ion $[M+H]^+$ at 256 m/z in positive ionization and a molecular ion $[M-H]^-$ at 253.8 m/z in negative ionization mode. The increase by 2 amu in the mass of an organic compound upon chemical reaction in an aqueous acidic environment is an indicator of hydrogenation. However, in an oxidative medium (e.g. PS/H₂O system) hydrogenation is not likely to occur in contrast to reductive medium (e.g. Fe^0/H_2O system) where hydrogenation is plausible [56]. Accordingly,

Table 2
MS and chromatographic characteristics of SMX and its transformation product after reaction in Fe⁰/SMX/PS system.

Product	Rt (min)	λ_{\max} (nm)	[M+H] ⁺ (m/z) ^a	[M-H] ⁻ (m/z) ^b	+MS/MS (m/z)	-MS/MS (m/z)	+MS ³	-MS ³	Difference with SMX	Proposed structure ^d
SMX	6.7	200, 262	254	251.8	188, 155.9 ^c , 147, 108, 92.2	155.6 ^c , 91.9	254 → 155.8	251.8 → 155.9	-	
SMX transformation product	5.3	200, 270	256	253.8	214 ^c , 173, 155.9, 101.2, 83.8	170.8 ^c , 82.1	256 → 214	253.8 → 170.8	+2H	
							108, 92.1, 80.3	107.8, 91.9, 64.2		
							196.9, 155.9 ^c , 140, 121, 106, 75.4	106.8, 79.9 ^c , 64.3		

^a Mass for pseudomolecular ion formed by protonation of the neutral molecule shown in the structure.

^b Mass for pseudomolecular ion formed by deprotonation of the neutral molecule shown in the structure.

^c Indicate most abundant fragment ion in MS² and/or MS³ spectrum.

^d Structural interpretations of MS² and MS³ fragments provided in Table 1S.

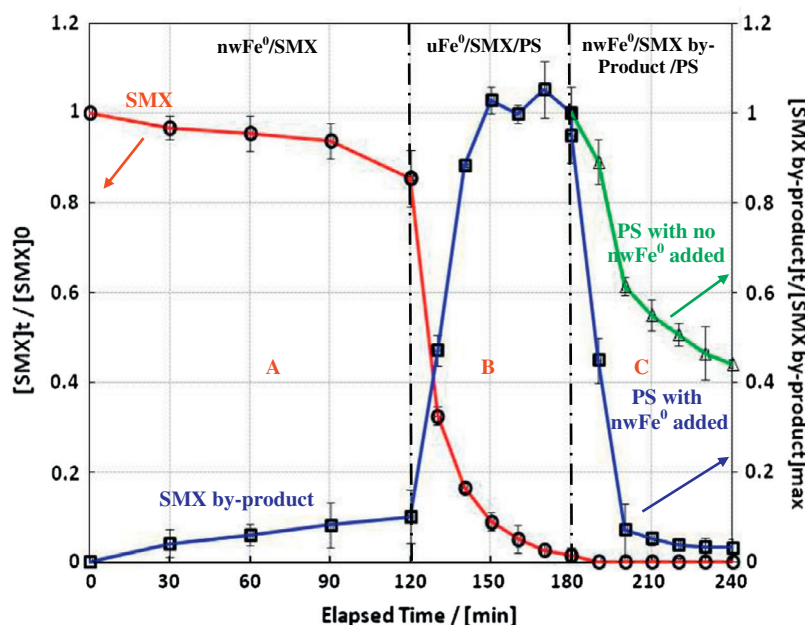


Fig. 7. Time course of SMX and its transformation product during treatment in Fe⁰/SMX/PS system. Zone A corresponds to wFe⁰/SMX system. Zone B corresponds to uFe⁰/SMX/PS (u: used) system in which PS was added to the resulting solution of Zone A; Zone C corresponds to SMX by-product/PS system in which the resulting solution of Zone B was magnetically filtered, spiked with PS and supplied or not with nwFe⁰. Experimental conditions: Zone A [nwFe⁰] = 5 g L⁻¹, [SMX]₀ = 39.5 μM; Zone B: [PS]₀ = 1.0 mM; Zone C: [nwFe⁰] = 0.1 g L⁻¹ for the upper curve, [nwFe⁰] = 0 g L⁻¹ for the lower curve, [PS]₀ = 1.0 mM.

one might expect isoxazole ring opening yielding 4-amino-N-(1-amino-3-oxobut-1-enyl)benzenesulfonamide through two different routes: (1) by electron abstraction upon SRs attack [18] and the formation of an unstable radical cation (SMX⁺) followed by electron acceptance from MIPs in acidic medium; (2) by electron addition originated from Fe⁰ surface yielding the formation of an unstable radical anion (SMX⁻) that will be converted into the same transformation product upon protonation as shown in the mechanism of Fig. 8. MS² and MS³ analyses in (-) and (+) ionization mode

confirmed the loss of respective moieties yielding fragments for which significant abundances were present (see Supplementary material for more details, Figs. 4S and 5S). Our findings were also confirmed by UV/Vis absorbance of the SMX transformation product. The latter showed a bathochromic shift from 262 to 270 nm corresponding to a lesser transition energy of the transformation product that may be explained by the formation of a carbonyl and primary ammonium groups [52] (see Supplementary material for more details, Fig. 6S).

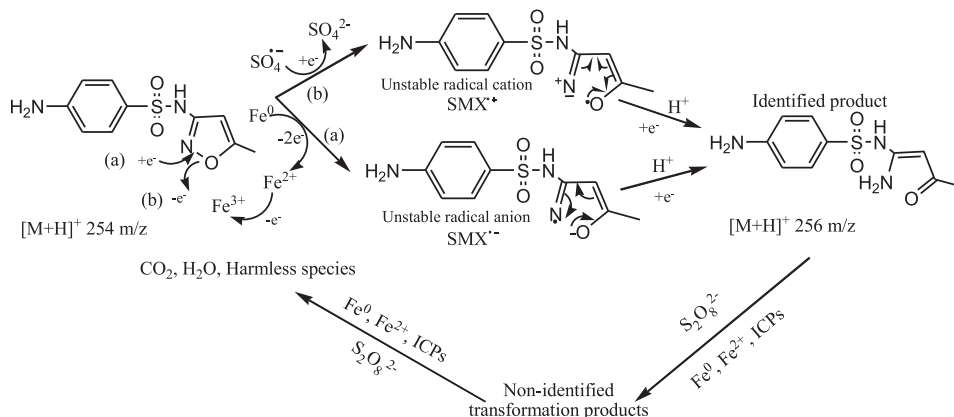


Fig. 8. Proposed degradation mechanism of SMX in (a) Fe^0/H_2O and (b) $Fe^0/PS/H_2O$ systems at room temperature.

4. Conclusions

This work demonstrated that PS chemical activation is a reliable method for the treatment of water contaminated with recalcitrant SMX (39.5 μM) in less than 2 h. Fe^0/H_2O systems were efficient in activating PS progressively minimizing therefore under optimized conditions SRs quenching. A small load of commercial MIPs (e.g. 2.23 mM) was sufficient to completely degrade SMX over a 60 min reaction time. The application of PS in different water-based matrices revealed that initial pH is important to consider, especially in the context of initiating iron corrosion responsible for the release of Fe^{2+} species for PS activation. Results using DI, tap and UG water revealed similarities between the last two water types where SMX degradation efficiency was directly affected by bicarbonate content. In contrast, after its elimination through acidification, all solutions showed similar behavior toward SMX degradation over 3 cycles of 1 h until complete MIPs depletion. SMX degradation in Fe^0/H_2O systems showed the presence of a stable transformation product. However, in Fe^0/H_2O PS-spiked systems, complete disappearance of SMX and its transformation product occurred; the mineralization extent reached 37% under smooth conditions making PS oxidation technology an excellent method for the treatment of organic micro-contaminants. Additional investigations into the long-term use of PS activators like bimetallics, trimetallics and natural iron oxide-based systems (e.g. ferrihydrite, lemonite, etc.) might be useful in order to improve the RSE that reached a maximum of 5.2% in the current work. Compared to thermal activation, PS chemical activation could present an economical advantage in terms of energy consumption and long term application if natural minerals could demonstrate their effectiveness for sustainable solution toward PS activation. Research in this direction is in progress in our laboratory for a comprehensive optimization of PS/Activators in aqueous systems using natural minerals.

Acknowledgements

This research was funded in part by the University Research Board of the American University of Beirut (Award Number 102542) and USAID-Lebanon through The National Academy of Sciences under PEER Grant (Award Number AID-OAA-A-11-00012). AG is thankful to Prof. David Sedlak (UC Berkeley), Dr. Tarek Ghaddar (AUB) and Prof. Makhlof Haddadin (AUB). Technical assistance was provided by the personnel of the Kamal Al Shair Central Research Scientific Laboratory (KAS CRSL). English corrections provided by Dr. Marinella Sandros (JSNN, North Carolina) on the revised manuscript are gratefully acknowledged.

Appendix A. Supplementary material

Supplementary data associated with this article can be found, in the online version, at <http://dx.doi.org/10.1016/j.cej.2013.05.045>.

References

- [1] National Research Council, The use of Drugs in Food Animals, National Academy Press, Washington, DC, 1999.
- [2] A. Białk-Bielińska, J. Maszkowska, W. Mroziak, A. Bielawska, M. Kołodziejska, R. Palavinskas, P. Stepnowski, J. Kumirska, Sulfadimethoxine and sulfaguanidine: their sorption potential on natural soils, *Chemosphere* 86 (2012) 1059–1065.
- [3] T.A. Ternes, N. Herrmann, M. Bonerz, T. Knacker, H. Siegrist, A. Joss, A rapid method to measure the solid-water distribution coefficient (K-d) for pharmaceuticals and musk fragrances in sewage sludge, *Water Res.* 38 (2004) 4075–4084.
- [4] D.W. Kolpin, E.T. Furlong, M.T. Meyer, E.M. Thurman, S.D. Zaugg, L.B. Barber, H.T. Buxton, Pharmaceuticals, hormones, and other organic wastewater contaminants in US streams, 1999–2000: a national reconnaissance, *Environ. Sci. Technol.* 36 (2002) 1202–1211.
- [5] B.A. Wilson, V.H. Smith, F. Denoyelles, C.K. Larive, Effects of three pharmaceuticals and personal care products on natural freshwater algal assemblages, *Environ. Sci. Technol.* 37 (2003) 1713–1719.
- [6] J.C. Underwood, R.W. Harvey, D.W. Metge, D.A. Repert, L.K. Baumgartner, R.L. Smith, T.M. Roane, L.B. Barber, Effects of the antimicrobial sulfamethoxazole on groundwater bacterial enrichment, *Environ. Sci. Technol.* 45 (2011) 3096–3101.
- [7] C.W. Knapp, C.A. Engemann, M.L. Hanson, P.L. Keen, K.J. Hall, D.W. Graham, Indirect evidence of transposon-mediated selection of antibiotic resistance genes in aquatic systems at low-level oxytetracycline exposures, *Environ. Sci. Technol.* 42 (2008) 5348–5353.
- [8] M.C. Dodd, C.H. Huang, Transformation of the antibacterial agent sulfamethoxazole in reactions with chlorine: kinetics, mechanisms, and pathways, *Environ. Sci. Technol.* 21 (2009) 5607–5615.
- [9] M. Petrovic, D. Barceló, LC-MS for identifying photodegradation products of pharmaceuticals in the environment, *TrAC – Trends Anal. Chem.* 6 (2007) 486–493.
- [10] A.G. Trovó, R.F.P. Nogueira, A. Agüera, C. Sirtori, A.R. Fernández-Alba, Photodegradation of sulfamethoxazole in various aqueous media: persistence, toxicity and photoproducts assessment, *Chemosphere* 10 (2009) 1292–1298.
- [11] R.F. Dantas, S. Contreras, C. Sans, S. Esplugas, Sulfamethoxazole abatement by means of ozonation, *J. Hazard. Mater.* 150 (2008) 790–794.
- [12] M.N. Abellán, B. Bayarri, J. Giménez, J. Costa, Photocatalytic degradation of sulfamethoxazole in aqueous suspension of TiO_2 , *Appl. Catal. B: Environ.* 74 (2007) 233–241.
- [13] M.N. Abellán, J. Giménez, S. Esplugas, Photocatalytic degradation of antibiotics: the case of sulfamethoxazole and trimethoprim, *Catal. Today* 144 (2009) 131–136.
- [14] D.M. Klauson, M. Krichevskaya, M. Borissova, S. Preis, Aqueous photocatalytic oxidation of sulfamethazole, *Environ. Technol.* 31 (2010) 1547–1555.
- [15] J.L. Mohatt, L. Hu, K.T. Finneran, T.J. Strathmann, Microbially mediated abiotic transformation of the antimicrobial agent sulfamethoxazole under iron-reducing soil conditions, *Environ. Sci. Technol.* 45 (2011) 4793–4801.
- [16] A.D. Anderson, J.M. Nelson, S. Rossiter, F.J. Angulo, Public health consequences of use of antimicrobial agents in food animals in the United States, *Microb. Drug Resist.* 9 (2003) 373–379.
- [17] O.A. Travina, Y.N. Kozlov, A.P. Purmal, I.Y. Rod'ko, Synergism of the action of the sulfite oxidation initiators, iron and peroxydisulfate ions, *Russ. J. Phys. Chem.* 73 (1999) 1215–1219.

- [18] G.P. Anipsitakis, D.D. Dionysiou, Radical generation by the interaction of transition metals with common oxidants, *Environ. Sci. Technol.* 38 (2004) 3705–3712.
- [19] C. Liang, Y.Y. Guo, Mass transfer and chemical oxidation of naphthalene particles with zerovalent iron activated persulfate, *Environ. Sci. Technol.* 44 (2010) 8203–8208.
- [20] F. Vicente, A. Santos, A. Romero, S. Rodriguez, Kinetic study of diuron oxidation and mineralization by persulphate: effects of temperature, oxidant concentration and iron dosage method, *Chem. Eng. J.* 170 (2012) 127–135.
- [21] C. Liang, M.C. Lai, Trichloroethylene degradation by zero valent iron activated persulfate oxidation, *Environ. Eng. Sci.* 25 (2008) 1071–1077.
- [22] X.R. Xu, X.Z. Li, Degradation of azo dye Orange G in aqueous solutions by persulfate with ferrous ion, *Sep. Purif. Technol.* 72 (2010) 105–111.
- [23] H. Kusic, I. Peternel, S. Ukic, N. Koprivanac, T. Bolanca, S. Papic, A.L. Bozic, Modeling of iron activated persulfate oxidation treating reactive azo dye in water matrix, *Chem. Eng. J.* 172 (2011) 109–121.
- [24] J. Yan, M. Lei, L. Zhu, M.N. Anjum, J. Zou, H. Tang, Degradation of sulfamonomethoxine with Fe₃O₄ magnetic nanoparticles as heterogeneous activator of persulfate, *J. Hazard. Mater.* 186 (2011) 1398–1404.
- [25] M. Usman, P. Faure, C. Ruby, K. Hanna, Application of magnetite-activated persulfate oxidation for the degradation of PAHs in contaminated soils, *Chemosphere* 87 (2012) 234–240.
- [26] H. Lucida, J.E. Parkin, V.B. Sunderland, Kinetic study of the reaction of sulfamethoxazole and glucose under acidic conditions. I. Effect of pH and temperature, *Int. J. Pharm.* 202 (2000) 47–61.
- [27] C. Liang, C.J. Bruell, M.C. Marley, K.L. Sperry, Thermally activated persulfate oxidation of trichloroethylene (TCE) and 1,1,1-trichloroethane (TCA) in aqueous systems and soil slurries, *Soil Sediment Contam.* 12 (2003) 207–228.
- [28] C. Liang, C.J. Bruell, Thermally activated persulfate oxidation of trichloroethylene: experimental investigation of reaction orders, *Ind. Eng. Chem. Res.* 47 (2008) 2912–2918.
- [29] A. Ghauch, A. Tuqan, Oxidation of bisoprolol in heated persulfate/H₂O systems: kinetics and products, *Chem. Eng. J.* 183 (2012) 162–171.
- [30] A. Ghauch, A. Tuqan, N. Kibbi, Ibuprofen removal by heated persulfate in aqueous solution: a kinetics study, *Chem. Eng. J.* 197 (2012) 483–492.
- [31] A. Ghauch, H. Baydoun, P. Dermesropian, Degradation of aqueous carbamazepine in ultrasonic/Fe⁰/H₂O₂ systems, *Chem. Eng. J.* 172 (2011) 18–27.
- [32] A. Ghauch, A. Tuqan, Catalytic degradation of chlorothalonil in water using bimetallic iron-based systems, *Chemosphere* 73 (2008) 751–759.
- [33] A. Ghauch, A. Tuqan, H. Abou Assi, Antibiotic removal from water: elimination of amoxicillin and ampicillin by microscale and nanoscale iron particles, *Environ. Pollut.* 157 (2009) 1626–1635.
- [34] C. Liang, C.F. Huang, N. Mohant, R.M. Kurakalva, A rapid spectrophotometric determination of persulfate anion in ISCO, *Chemosphere* 73 (2008) 1540–1543.
- [35] APHA, Standard Methods for the Examination of Water and Wastewater, 20th ed., American Public Health Association, Washington, DC, 1998.
- [36] A. Ghauch, H. Abou Assi, H. Baydoun, A. Tuqan, A. Bejjani, Fe⁰-based trimetallic systems for the removal of aqueous diclofenac: mechanism and kinetics, *Chem. Eng. J.* 172 (2011) 1033–1044.
- [37] R.L. Parfitt, R.J. Atkinson, R.C. Smart, The mechanism of phosphate fixation by iron oxide, *Soil Sci. Soc. Am. J.* 39 (1975) 837–841.
- [38] <<http://water.epa.gov/drink/contaminants/index.cfm>>.
- [39] G. Lente, M.E.A. Magalhães, I. Fábrián, Kinetics and mechanism of complex formation reactions in the iron(III)-phosphate ion system at large iron(III) excess. Formation of a tetranuclear complex, *Inorg. Chem.* 39 (2000) 1950–1954.
- [40] A. Ghauch, Rapid removal of flutriaol from water by zero valent iron powder, *Chemosphere* 71 (2008) 816–826.
- [41] F. Al-Soghair, H.M. Marafie, N.M. Shuaib, H. Ben Youngo, M.S. El-Ezaby, Interaction of phosphate with iron(III) in acidic medium, equilibrium and kinetic studies, *J. Coord. Chem.* 55 (2002) 1097–1109.
- [42] C. Noubactep, Processes of contaminant removal in Fe⁰/H₂O systems revisited: the importance of co-precipitation, *Open Environ. J.* 1 (2007) 9–13.
- [43] C. Noubactep, A critical review on the process of contaminant removal in Fe⁰-H₂O systems, *Environ. Technol.* 29 (2008) 909–920.
- [44] A. Ghauch, H. Abou Assi, A. Tuqan, Investigating the mechanism of clofibrac acid removal in Fe⁰/H₂O systems, *J. Hazard. Mater.* 176 (2010) 48–55.
- [45] A. Ghauch, H. Abou Assi, H. Baydoun, A.M. Tuqan, A. Bejjani, Fe⁰-based trimetallic systems for the removal of aqueous diclofenac: mechanism and kinetics, *Chem. Eng. J.* 172 (2001) 1033–1044.
- [46] C. Noubactep, Characterizing the discoloration of methylene blue in Fe⁰/H₂O systems, *J. Hazard. Mater.* 166 (2009) 79–87.
- [47] R.J. Crawford, I.H. Harding, D.E. Mainwaring, Adsorption and coprecipitation of single heavy metal ions onto the hydrated oxides of iron and chromium, *Langmuir* 9 (1993) 3050–3056.
- [48] R.H. Waldemer, P.G. Tratnyek, R.L. Johnson, J.T. Nurmi, Oxidation of chlorinated ethenes by heat-activated persulfate: kinetics and products, *Environ. Sci. Technol.* 41 (2007) 1010–1015.
- [49] D.E. Pennington, A. Haim, Stoichiometry and mechanism of the chromium (11)-peroxydisulfate reaction, *J. Am. Chem. Soc.* 90 (1968) 3700–3704.
- [50] C. Liang, C.J. Bruell, M.F. Albert, P.E. Cross, D.K. Ryan, Evaluation of reverse osmosis and nanofiltration for in situ persulfate remediated groundwater, *Desalination* 208 (2007) 238–259.
- [51] R. van Eldik, G.M. Harris, Kinetics and mechanism of the formation, acid-catalyzed decomposition, and intramolecular redox reaction of oxygen-bonded (sulfito)pentaamminecobalt(III) ions in aqueous solution, *Inorg. Chem.* 19 (1980) 880.
- [52] F. Rouessac, A. Rouessac, *Chemical Analysis: Modern Instrumentation Methods and Techniques*, second ed., Wiley, England, 2008.
- [53] C. Liang, Z.S. Wang, C.J. Bruell, Influence of pH on persulfate oxidation of TCE at ambient temperatures, *Chemosphere* 66 (2007) 106–113.
- [54] R.E. Huie, C.L. Clifton, Temperature dependence of the rate constants of reactions of the sulfate radical, SO₄^{•-} with anions, *J. Phys. Chem.* 94 (1990) 8561–8567.
- [55] G.V. Buxton, T.N. Malone, G.A. Salmon, Pulse radiolysis study of the reaction of SO₃^{•-} with HO₂, *J. Chem. Soc. Faraday Trans.* 92 (1996) 1287–1289.
- [56] A. Ghauch, A. Tuqan, Reductive destruction and decontamination of aqueous solutions of chlorinated antimicrobial agent using bimetallic systems, *J. Hazard. Mater.* 169 (2009) 665–674.

REFERRED PUBLICATION II: SUBMICROMETRIC IRON
PARTICLES FOR THE REMOVAL OF PHARMACEUTICALS IN
WATER: APPLICATION TO B-LACTAM ANTIBIOTICS

Submicrometric iron particles for the removal of pharmaceuticals from water: Application to b-lactam antibiotics

Antoine Ghauch^{1,a}, Habib Baydoun^{1,b}, Al Muthanna Tuqan^{1,c},
Ghada Ayoub^{2,d}, Sahar Naim^{2,e}

¹ American University of Beirut, FAS, Chemistry Dept. P.O. Box 11-0236 Riad El Solh, Lebanon

² Lebanese University, Faculty of Sciences, Chemistry Dept. Hadath, Lebanon

^aag32@aub.edu.lb, ^bhbb08@aub.edu.lb, ^caff01@aub.edu.lb

Keywords: antibiotics, decontamination, Fe⁰/H₂O systems, water treatment

Abstract: Sub-micrometric iron particles (Fe⁰) and amended Fe⁰ (Cu⁰Fe⁰) were tested for the aqueous removal of b-lactam antibiotics. Comparative batch experiments were performed separately on aqueous solutions of dicloxacillin (DCX), cloxacillin (CLX) and oxacillin (OXA). Three different initial concentrations (1, 5 and 10 mg L⁻¹) and four different iron loads (r = 10, 20, 40 and 53 g L⁻¹) were tested. Furthermore, two different mixing regimes were tested: (i) non-disturbed conditions, and (ii) vortex mixing. This experimental design enabled the confirmation of the crucial role of in-situ formed iron corrosion products (Fe oxides) on the removal process. The dynamic process of Fe oxides formation induces adsorption and enmeshment (sequestration or co-precipitation) of dissolved antibiotics. Results clearly delineated the superiority of Cu⁰Fe⁰ bimetallics compared to Fe⁰. For example, after 4 h of contact with iron particles at r = 40 g L⁻¹, OXA, CLX and DCX (10 mg L⁻¹ each) disappeared to an extent of 31, 46 and 71%. However, quantitative antibiotic removal (~90%) was noticed when Cu⁰Fe⁰ bimetallic was used at lesser load (r = 20 g L⁻¹) under vortex mixing. On the other hand, non-disturbed systems showed partial removal (~ 25%) of antibiotics over 7 h of reaction at r = 10 g L⁻¹ (Fe⁰) while almost complete removals were noticed for the Cu⁰Fe⁰ bimetallic system for the same metal load and period e.g. 75, 79 and 86% removal for OXA, CLX and DCX respectively.

Introduction

Pharmaceuticals are an important subgroup of emergent contaminants that are commonly released into the environment through waste water treatment plants (WWTPs) [1, 2]. A major class of pharmaceuticals is antibiotics that have been detected in surface water and WWTPs effluents at trace levels (from ng L⁻¹ to mg L⁻¹) [3-5]. Antibiotics are Oxacillin (OXA - C₁₉H₁₉N₃O₅S: 401.436 g/mol), Cloxacillin (CLX - C₁₉H₁₈ClN₃O₅S: 435.880 g/mol) and Dicloxacillin (DCX - C₁₉H₁₇Cl₂N₃O₅S: 470.327 g/mol) are antibiotics of the penicillin's family and of great concern due to their extensive use [6, 7]. The WHO recommended that antibiotics used to treat human should not be used to promote animal growth in order to reduce antibiotic resistance. However, such antibiotics could still be used to treat ill animals [8]. In 1994, the Commission of the European Community established the MRLs of 30 mg/kg for each of OXA, CLX and DCX in milk [9]. Consequently, penicillin residues are an important aspect of milk quality but also water safety [10]. Their monitoring in milk as well as their elimination from water becomes a necessity. Recently, different methods are conventionally used for the aqueous removal of antibiotics including ozonation, Fenton's reagent, filtration and adsorption [11-15]. In recent years metallic iron (Fe⁰) has been discussed in the literature as an affordable and efficient technology for water treatment. Here contaminant removal occurs fundamentally by adsorption and co-precipitation [16].

The aim of this work was to investigate the efficiency of Fe⁰ and plated Fe⁰ (Cu⁰Fe⁰) for aqueous removal of OXA, CLX and DCX. An attempt was made to assess the long-term use of submicrometric Fe⁰ for environmental remediation.

Experimental methods

Micrometric iron particles were purchased from Fluka (USA), OXA, CLX and DCX from Sigma. All other reagents are similar to those used in previous work [17]. The detailed procedure of Fe^0 pre-treatment and Fe^0 plating to Cu^0Fe^0 is described in previous works [18, 19]. Experiments were done under disturbed (Vortex agitation) and non-disturbed (shelves-experiments) conditions. SEM/EDX technique was used to characterize metallic particles however HPLC/MS for the monitoring of probes and their transformation products.

Results and discussion

Antibiotics removal by Fe^0 under disturbed conditions

Fig. 1a summarizes the results of antibiotics removal under vortex mixing for $t \leq 4$ h. The increasing order of reactivity with Fe^0 after 4 hours is: OXA (31 %) < CLX (45 %) < DCX (71 %) and coincides with the increasing order of molecular weights. These results suggest that the functional groups are of minor importance in the removal process and in concordance with the view that adsorption and co-precipitation are the fundamental removal mechanisms through iron corrosion products (ICP). ICP are able to sequester and co-precipitate organic contaminants. This observation is supported by the pH (see inset Fig. 1b) of the reactive medium being within the domain of precipitation of ICP. Accordingly antibiotics are progressively enmeshed in the structure of nascent adsorbents. At lesser Fe^0 load e.g. 10 g L^{-1} (Fig. 1b), less nascent adsorbent are produced and a smaller removal is achieved for the same experimental duration (< 20% removal). These results are further supported by the absence of transformation products under oxic conditions. Parent contaminant and transformation products are removed via adsorption and co-precipitation.

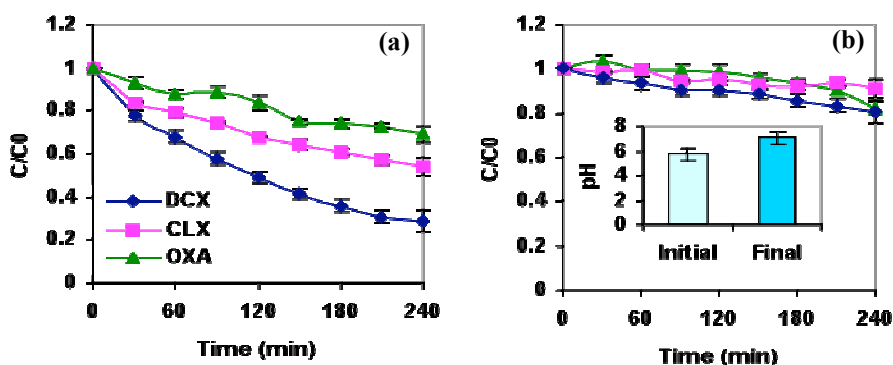


Fig. 1: Graphs showing the decline curves of OXA, CLX and DCX after contact with (a) 0.6 g and (b) 0.15 g Fe^0 under oxic conditions. Experimental conditions: Room Temperature, non buffered solutions: [OXA] = [CLX] = [DCX] = 10 ppm, V = 15 mL.

Antibiotics removal by Cu^0Fe^0

Cu^0Fe^0 characterization

Fig. 2 shows SEM images of iron particles (a) before and (b) after washing with 0.1 M HCl. Iron particles showed more brightness and clustering after acid washing demonstrating thereby the clearness of their surface covered earlier with iron oxide layers. The average particle diameter is ranging from 1.5 to 2.8 μm . Fig. 2c shows clearly after plating the deposition of Cu (yellow square) as metallic foam or needles (yellow circle) on the surface of iron particles. One can also notice another form grow of copper on iron surface. This may be due to the kinetics however this issue is beyond the scope of this paper. EDX elemental maps of Fe and Cu are shown in Fig. 3 a-c. The Cu distribution is heterogeneous since many iron particles are devoid from any trace of Cu. This is in agreement with previous studies [20].

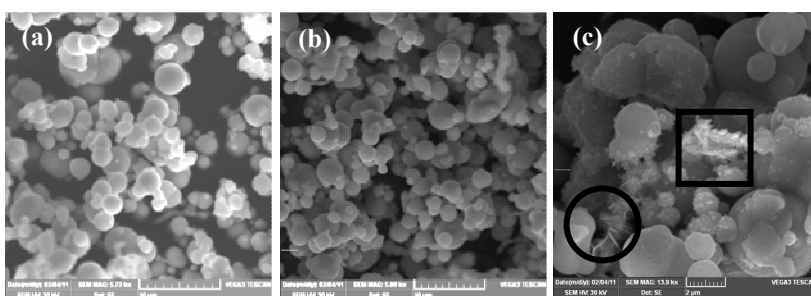


Fig. 2: SEM of iron particles (a) before acid wash, (b) after acid wash and (c) after being plated with Cu (47 Omol Cu/g Fe).

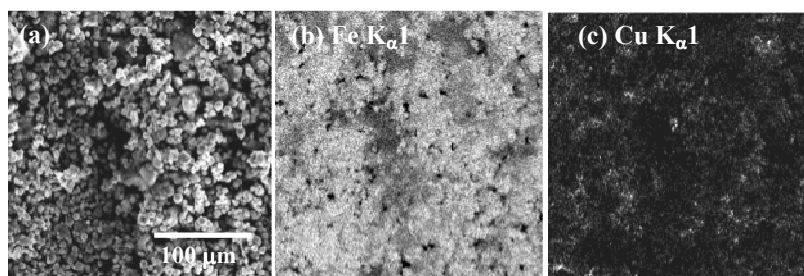


Fig. 3: (a) Secondary electron image of iron grains plated with 47 μmol Cu/g Fe and the corresponding maps of (b) Fe and (c) Cu obtained from the same CuFe bimetallic system in (a). Areas of relatively high Fe concentrations are shown as bright regions in (b). In (c) bright regions indicate areas of relatively high Cu surface concentration.

Antibiotics removal by Cu^0Fe^0 under disturbed conditions

Fig. 4a clearly shows that at an iron load of 10 g L^{-1} the antibiotic's removal reaches 58, 77 and 93% for OXA, CLX and DCX respectively. Increasing the iron load to 20 g L^{-1} positively affects antibiotics removal to an extent of 88, 91 and 82% for OXA, CLX and DCX respectively (Fig. 4b). This result confirms the superiority of bimetallic systems upon Fe^0 for contaminant removal. For the same metal load and antibiotics concentrations Cu^0Fe^0 is found to be 3.22, 7.70 and 4.65 times more efficient in term of OXA, CLX and DCX elimination over 4 h of reaction respectively. The elimination reaction is very fast. It is interesting to notice that the other reactivity as observed in $\text{Fe}^0/\text{H}_2\text{O}$ system is no more strictly the same. The inversion observed for DCX in particular can be attributed to combined effects of hydrodynamics, increased production of nascent adsorbents and steric hindrance due to the large size of DCX. In fact, as adsorbents progressively covered the surface of Fe^0 , the potency to co-precipitation decreases while the importance of pure adsorption increased. Unlike co-precipitation, adsorption portends to evolutes to an equilibrium state.

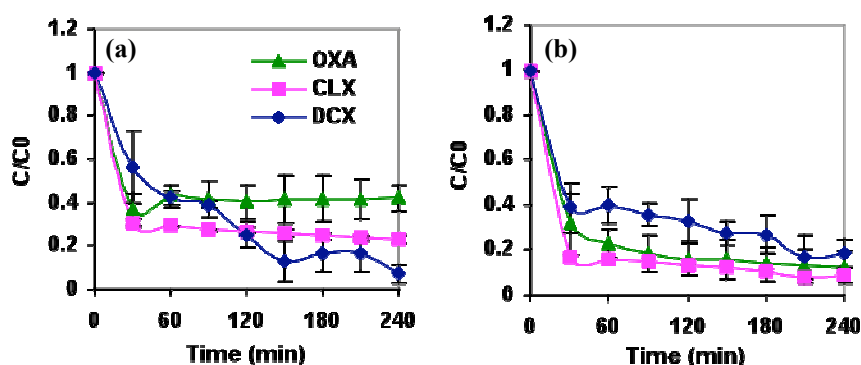


Fig. 4: Graphs showing the decline curves of OXA, CLX and DCX after contact with (a) 0.15 g and (b) 0.30 g Cu^0Fe^0 under oxic conditions. Experimental conditions: Room Temperature, non buffered solutions: $[\text{OXA}] = [\text{CLX}] = [\text{DCX}] = 10 \text{ ppm}$, $V = 15 \text{ mL}$.

Antibiotics removal by Fe^0 vs Cu^0Fe^0 under non-disturbed conditions

In contrary to vortex mixed systems, the curves obtained under non-disturbed conditions did not show any pseudo-steady state. This relates the fact that no steady state (pseudo-equilibrium) could be expected before Fe^0 depletion. In other words, the pseudo-equilibrium observed for vortex mixing does not have any physical significance, moreover it should be regarded as experimental bias. Real world situations allow the continuous formation of porous iron oxide layers able to sequester antibiotics molecules after being diffused into the interstices of the porous oxide scale on Fe^0 [20-21]. These results support the view that iron technology is better applied to non disturbed conditions including Fe^0 filtration beds, Fe^0 reactive barriers or column technology where particles are immobilized and create a diffusive environment able to enmesh (organic) contaminants.

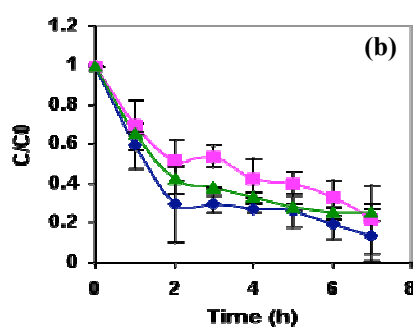
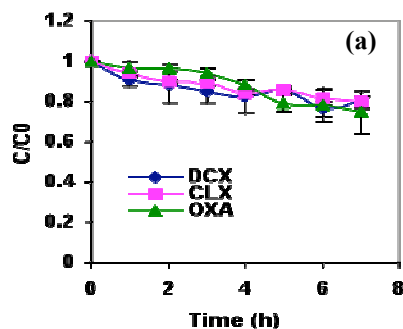


Fig. 5: Graphs showing the decline curves of OXA, CLX and DCX after contact with 0.15 g (a) Fe^0 and (b) Cu^0Fe^0 under oxidic and non-disturbed conditions. Experimental conditions: Room Temperature, non buffered solutions: $[\text{OXA}] = [\text{CLX}] = [\text{DCX}] = 5$ ppm, $V = 15$ mL.

Concluding remarks

This work acknowledged that the use of iron particles and bimetallic systems e.g. Cu^0Fe^0 is successful in removing β -lactam antibiotics from water. The experimental design played an important role in maintaining the long term efficiency of the metallic systems. Non-disturbed reactions have proven to be a more appropriate technique for sustaining iron corrosion after showing a constant reactivity toward antibiotics over 7 h of reaction. In contrast, a steady state has quickly occurred when reactions were undertaken under disturbed conditions over 4 h of reaction. This was ascribed to the mechanical stress applied to the iron oxide scale being responsible of the diffusion of antibiotics toward the reactive interstices of the spider-like iron oxide network. The more this network is disturbed, the more contaminants' diffusion vanished while in-situ formed iron oxide material exhibits serious crack and consequently will break up from the iron core matrix. Finally, non-disturbed reactions have to be tested for different contaminants to be closer to field applications for more realistic long term applications.

References

- [1] E. Eljarrat and D. Barcelo: Trends Anal. Chem. 22 (2003), p. 655.
- [2] T. Smital, T. Luckenbach, R. Sauerborn, M.A. Hamdounb, R.L. Vega and D. Epel: Mutat. Res. 552 (2004), p. 101.
- [3] T.A. Ternes: Water Res. 32 (1998), p. 3245.
- [4] R. Hirsch, T. Ternes, K. Haberer and K. Kratz: Sci. Tot. Environ. 225 (1999), p. 109.
- [5] D.W. Kopin, E.T. Furlong, M.T. Meyer and E.M. Thurman: Environ. Sci. Technol. 36 (2002), p. 1202.
- [6] M.A. Gilliver, M. Bennett, M. Begon, S.M. Hazel and C.A. Hart: Nature 401 (1999), p. 233.
- [7] P. Kubalec, E. Brandsteterová and A. Bednáriková: Unters.-Forsch. A (1997) p. 85.
- [8] A. Woolfsen, R. Huebner, A. Wasas, S. Chola, P. Godfrey-Faussett and K. Klugmann: Bulletin of the World Health Organization (1997), p 75.
- [9] Commission Regulation (EG) No. 2701/94, Off. J. Eur. Commun. L. (1994), 287 p.7.
- [10] M. Marchetti, I. Schwaiger, E.R. Schmid: Fresenius' J. Anal. Chem. (2001), 371 p. 64.
- [11] R.F. Dantas, S. Contreras, C. Sans and S. Esplugas : J. Hazard. Mater. Vol. 150 (2008) p. 790.
- [12] A.G. Trovo, R.F.P. Nogueira, A. Aguera, A.R. Fernandez-Alba, C. Sirtori and S. Malato: Wat. Res. Vol. 43 p. 3922.
- [13] F. Ay and F. Kargi: J. Hazard. Mater. Vol. 179, (2010) p. 622.
- [14] E. Hapeshi, A. Achilleos, A. Papaioannou, L. Valanidou, N.P. Xekoukoulotakis, D. Mantzavinos and D. Fatta-Kassinos: Wat. Sci. Technol. Vol. 61 (2010) p. 3141.
- [15] J. Radjenović, M. Petrović, F. Ventura and D. Barceló: Wat. Res. Vol. 42 (2008) p. 3601.
- [16] C. Noubactep: Water SA Vol. 36 (2010) p. 663.
- [17] A. Ghauch, A. Tuqan and H. Abou Assi: Environ. Pollut. Vol. 157 (2009) p. 1626.
- [18] A. Ghauch and A. Tuqan: Chemosphere Vol. 73 (2008), p. 751.
- [19] A. Ghauch and A. Tuqan: J. Hazard.Mater. Vol. 164 (2009), p. 665.
- [20] S. Bransfield, D. Cwiertny, A. Lynn Robert and D. Howard Fairbrother: Environ. Sci. Technol. Vol. 40 (2006) p. 1485.
- [21] C. Noubactep: Chem. Eng. J. Vol. 162 (2010) p. 656.